Department of Mechanical Engineering

Division of Mechanics

ISRN LUTFD2/TFME – 19/5041– SE(1-85)

Simulation of a Rotational Brake System Regulated by Change in Angular Deceleration

Degree Project by
Marko Sarajärvi
Dennis Stenson

Supervisors:
Prof. Aylin Ahadi, Division of Mechanics
Prof. Solveig Melin, Division of Mechanics
Patrik Zander, Brillianze Sweden AB

Printed by Media-Tryck, Lund, Sweden

For information address:
Division of Mechanics, Lund University, Box 118, SE-211 00 Lund, Sweden
Homepage: http://www.mek.lth.se

Preface

This project was carried out at the Division of Mechanics, Faculty of Engineering, Lund University from October 2018 until May 2019 as part of our master thesis. We wish to thank our supervisors, Aylin Ahadi and Solveig Melin, as well as our contacts at Brillianze Sweden AB, Patrik and Sten-Thore Zander, for their support and our thoughtful discussions with them.

Abstract

A fully mechanical rotational brake system activated and regulated by rate of change in angular velocity has been developed by Brillianze Sweden AB. Its field of usage is currently limited and is to be expanded upon. Therefore new models were made to perform multibody dynamics simulations in Adams/View. This is the first time any research or simulations have been made on this specific brake system.

Validating and further exploring the theory behind the brake system was the main objective of this thesis. This was fulfilled by observing how different parameters, such as body mass and friction, influence two already existing prototypes and one untested model implementing a spring.

From the results, the following conclusions can be drawn. Lower friction coefficients, but rather not too low, are preferred. Although these coefficients lead to longer brake times, they give smoother behaviour which is more desired. The optimal spring stiffness values are system dependent. No conclusions can be drawn as to which are the best in general and must be altered for different applications. A trade-off between keeping the brake arm activated and slowing down steadily has to be made. When the equilibrium of the brake arm is changed, another trade-off emerges. If the angular velocity needed to avoid activation due to gravity increases the deceleration, or force, needed for activation of the brake arm decreases.

By comparing the results Brillianze Sweden AB already had with those presented in this report, they seem to be consistent with each other. None of the results in this thesis were found to disprove the theory and sequence of events assumed by the company.

Sammanfattning

Ett fullt mekaniskt rotationsbromssystem aktiverat och reglerat av vinkelacceleration har utvecklats av Brillianze Sweden AB. Bromsens användningsområde ska utökas och därför skapades modeller för flerkroppsdynamiska simuleringar i Adams/View. Det är första gången forskning eller simulationer har gjorts på systemet.

Det huvudsakliga målet med avhandlingen var att bekräfta och fortsatt undersöka bromssystemets teori. Observation av olika parametrars påverkan, så som pendelviktens och friktionskoefficienternas, gjordes för att uppnå detta mål. Två befintliga prototyper och en ny experimentell modell som implementerar en fjäder undersöktes.

Lägre, men ej för låga, friktionskoefficienter föredras. Även om dessa koefficienter leder till längre bromstid, är det mjukare beteendet mer önskvärt. Den optimala fjäderstyvheten beror på systemets användning. En avvägning måste göras gällande en aktiv bromsarm och en stadig nedsaktning. När bromsarmens jämnvikt ändras uppstår en annan avvägning. Om rotationsfrekvensen som krävs för att undvika aktivering på grund av gravitation ökar kommer kraften som krävs för aktivering av armen att minska.

Resultaten som Brillianze Sweden AB har försett och de som presenteras i rapporten tycks stämma överens. Inga resultat i avhandlingen motbevisar teorin och det händelseförlopp antaget av företaget.

Contents

1 Introduction

1.1 Background

Brillianze Sweden AB is a small startup company with great ambitions. The company has developed a fully mechanical rotational brake system, known as the Alphabrake^{TM}, which is activated and regulated by rate of change in angular velocity. The idea is that it is activated and deactivated due to its own inertia when the velocity at the pendulum axle and on the rest of the brake arm differ. Subsequently, the pendulum swings out from or in towards the zero reference line. The mentioned parts are defined in subsection 2.2, figure 1.

The brake system has previously been implemented with a type of casting reel called multiplier reel. Such reels are difficult to master, often leading to entanglement of fishing lines in spools. This is also known as backlash. Fishing reels currently use several types of brake systems, including centrifugal brakes and magnetic brakes, at the same time to solve this problem. While solving it, the casting distance is greatly reduced. Brillianze Sweden AB aims to replace these systems with the more efficient Alphabrake. The purpose of the brake system is preventing entanglement, as well as increasing casting distance. A model of this brake system is referred to as the *universal brake system for multiplier reels*.

When increasing the scale of the universal brake system, Brillianze Sweden AB decided to modify it. In larger scale the company needed to eliminate certain effects that became apparent. This system turned out to be a very effective emergency brake, and is the current focus of research and development. The report refers to a model of it as the *emergency brake for winch*.

More information on the company and its fishing brand can be acquired by visiting these web pages found among the references. [1] [10]

1.2 Objective

Since the field of usage of the brake system is currently limited, Brillianze Sweden AB wants to expand upon its field of usage. Models should be made to enable multibody dynamics simulations because building and testing prototypes demands a lot of money and time.

Validating and further exploring the theory behind the brake system is the main objective of this thesis by looking into how it is influenced by different parameters. This should be done for the two already existing models mentioned above. A new model currently without a prototype is also to be examined. It is referred to as the *web tension control for spools*.

The focus of this project is on activation due to deceleration, but by changing the design, activation may be caused by acceleration instead.

Depending on the progress made during this thesis work, optimisation of whole running sequences can be performed to allow for quicker testing of different scenarios. Furthermore, finite element calculations may be carried out using the engineering simulation software ANSYS which will help optimising shape and materials by analysing forces and deformations.

1.3 Resources

The thesis took place at the Division of Mechanics. It consists of one part multibody simulations and one part post-processing data from said simulations.

MSC Adams, further denoted as Adams, is a multibody dynamics simulation software widely used among engineers and companies. A base module of the software, Adams/View, is used in the project. [4] The software is provided by the Division of Mechanics.

MATLAB is a numerical computing software used to analyse data and create mathematical models, among other things. It is used in the post-processing phase. [2]

2 Theory

In order to understand the reasoning behind what was done for the first part of the thesis, one must know mechanics, the composition of the brake system, how Adams works and how it all ties together. In the multibody dynamics software there are several integration methods available. GSTIFF is a backward differentiation formula, or BDF, integrator. In it, Newton-Raphson iterations are used to solve non-linear differential equations of motion. The equations are derived from definitions of kinetic energy, virtual work and non-linear algebraic constraints together with Lagrange's equation. [3]

2.1 Multibody Dynamics and Mechanics

The centre of mass, G, for a body can be calculated individually for each dimension i with

$$r_{G_i} = \frac{\int_V \Big(\rho(\boldsymbol{r}) \cdot r_i\Big) dV}{\int_V \rho(\boldsymbol{r}) dV} \tag{1}$$

which for homogeneous bodies in three dimensions may be simplified with

$$\boldsymbol{r}_G = \frac{\rho}{m} \int_V \boldsymbol{r} dV \tag{2}$$

In the above equations, $\boldsymbol{r}$ is the position tensor, V is the volume, ρ is the density and m is the total mass of the body.

For a rigid body rotating around a fixed z-axis, *moment of inertia* is denoted I_{zz} and defined with the equation

$$M_z = I_{zz}\ddot{\theta} \tag{3}$$

where M_z is momentum and θ is the angle around the z-axis.
Moment of inertia for a body depends on its geometry. Adams automatically calculates it for each body in a model. As an example, moment of inertia for a sphere is given by

$$I_{xx} = I_{yy} = I_{zz} = \frac{2}{5} m r^2 \tag{4}$$

where r is the radius of the sphere. [5]
Moment of inertia is an additive property. To get the relation between moment of inertia for an axis and a mass at a distance, *Steiner's theorem* is used

$$I_{zz} = I_{zz}^G + md^2 \tag{5}$$

where I_{zz} is the inertia for an axis z, with a distance d from a parallel axis through the centre of mass. [5, p.103]

Friction coefficient dependence is a vital part of this project. In general, the friction condition is

$$\frac{|\boldsymbol{f}|}{|\boldsymbol{N}|} \leq \mu \tag{6}$$

where $\boldsymbol{f}$ is the friction force, $\boldsymbol{N}$ the normal force and μ the friction coefficient. Equality is only achieved when the bodies are on the cusp of or are sliding. Whatever force that overcomes the friction, for example pulling force, needs to be greater than the maximum friction force, determined by the static friction coefficient, μ_s. During motion the pulling force would only need to be greater than the friction force determined by the dynamic friction coefficient, μ_d.

This is why the dynamic friction coefficients always are said to be less than or equal to the static ones, $\mu_d \leq \mu_s$.

For linear springs, *Hooke's law* applies. Force F, elongation x and stiffness coefficient k gives

$$F = kx \tag{7}$$

A related constitutive equation for linear elastic materials using the stress tensor σ and strain tensor ε, sometimes called *Hooke's generalised law*, is

$$\sigma_{ij} = D_{ijkl}\varepsilon_{kl} \tag{8}$$

where D is composed of elastic constants dependent on Young's modulus, E, and Poisson's ratio, ν, for the material. Without speculating about how Adams might be calculating the behaviour of its finite element bodies, this might give a little insight into how the software implements flexible material. [6, p.248-254]

Most of the bodies in the observed brake systems are set as solid. Which ones that are made flexible and why is further discussed in section 3.1.

For a multibody system consisting of n_b number of bodies, the kinetic energy T^i for a rigid body i is defined as

$$T^i = \frac{1}{2}\dot{\boldsymbol{R}}^{iT}\boldsymbol{m}^i_{RR}\dot{\boldsymbol{R}}^i + \frac{1}{2}\dot{\boldsymbol{\theta}}^{iT}\boldsymbol{m}^i_{\theta\theta}\dot{\boldsymbol{\theta}}^i \tag{9}$$

where $\boldsymbol{R}^i$ is the set of coordinates that represents the translation of the origin of the body reference, and $\boldsymbol{\theta}^i$ represents the orientation of this reference with respect to the inertial frame. Furthermore, the rigid body's mass matrix, $\boldsymbol{M}^i$, is

$$\boldsymbol{M}^i = \begin{bmatrix} \boldsymbol{m}^i_{RR} & 0 \\ 0 & \boldsymbol{m}^i_{\theta\theta} \end{bmatrix} \tag{10}$$

The virtual work, δW^i, of externally applied forces acting on the body is

$$\delta W^i = \boldsymbol{Q}^{iT}_e \delta \boldsymbol{q}^i \tag{11}$$

where $\boldsymbol{Q}^i_e$ is the vector of generalised forces and $\delta\boldsymbol{q}^i$ is the virtual change in that vector. To describe kinematic constraints between different components in the multibody system, the vector $\boldsymbol{C}$ is introduced. It contains linearly independent constraint equations and is defined as

$$\boldsymbol{C}(\boldsymbol{q}, t) = \boldsymbol{0} \tag{12}$$

where t is time and $\boldsymbol{q}$ is a vector of the generalised coordinates of the system defined as

$$\boldsymbol{q} = \begin{bmatrix} \boldsymbol{q}^{1T}_r & \boldsymbol{q}^{2T}_r & \dots & \boldsymbol{q}^{n_bT}_r \end{bmatrix}^T \tag{13}$$

For a set of q_j with dimension n, Lagrange's equation is defined as

$$\frac{d}{dt}\left(\frac{\partial T}{\partial \dot{q}_j}\right) - \frac{\partial T}{\partial q_j} - Q_j = 0 \quad , j = 1, 2..., n \tag{14}$$

Now, equations (9)-(14) can be used to write the equations of motion for a rigid body in a multibody system with

$$\boldsymbol{M}^i\ddot{\boldsymbol{q}}^i_r + \boldsymbol{C}^T_{\boldsymbol{q}^i_r}\boldsymbol{\lambda} = \boldsymbol{Q}^i_e + \boldsymbol{Q}^i_v \tag{15}$$

where $\boldsymbol{C}_{\boldsymbol{q}^i_r}$ is the Jacobian matrix with constraints, $\boldsymbol{\lambda}$ is the vector of Lagrange multipliers and $\boldsymbol{Q}^i_v$ is a quadratic velocity vector that is acquired when the kinetic energy is differentiated. [9, p.122-155]

The equations of motion may be expressed in matrix form, giving

$$\boldsymbol{M}\ddot{\boldsymbol{q}} + \boldsymbol{C}^T_{\boldsymbol{q}}\lambda = \boldsymbol{Q}_e + \boldsymbol{Q}_v \tag{16}$$

2.2 The Anatomy of the Brake Systems

An idea of a general design of the brake system is displayed in figure 1. Each of the three models differs a bit from this design. The emergency brake for winch and web tension control for spools are similar in size, while the universal brake system for multiplier reels is smaller.

As previously mentioned, prototypes of the universal brake system for multiplier reels and the emergency brake for winch have already been constructed, while the web tension control for spools is based on theories and mechanisms used in multiplier reels.

The *brake axle* is connected to an external system that has forces acting on the brake axle. It is also connected to the *pendulum axle*, via the *brake hub*. In turn, the pendulum axle is connected to the *pendulum*. As the two bodies are connected with ball bearings, the pendulum may rotate about the pendulum axle. Movement of the pendulum is constrained by the *pendulum zero limiter*. The *brake pad* is considered a part of the pendulum, and has friction material at the top. The pendulum is also referred to as the brake arm.

A *pendulum bob* is located at the bottom of the pendulum and is versatile. This can be used to alter the position of the mass centre of the entire brake arm. It may also be replaced, changing the total weight of the pendulum.

The *brake drum* does not rotate. It is composed of two parts, one of them replaceable. At activation of the pendulum, a contact between the brake pad and brake drum is established when the rotated angle of the pendulum is high enough. How large this angle needs to be differs for each of the models. All parts but the brake drum are considered rotating parts.

Connecting many of the bodies, the brake hub is an important part of the brake system. All rotating parts but the pendulum obtain the same angular velocity.

What material each part should be assigned was obtained from Brillianze Sweden AB. These materials corresponds to the ones used in their prototypes. Every part except the pendulum bob and brake pad is initially made of aluminium. The pendulum bob is brass, except when altering its weight during mass body dependence simulations.

Figure 2 depicts the brake arm at activated and deactivated positions. Rotational direction and movement of the pendulum is defined. The zero reference line is depicted in figure 2a. It is defined as the line through the centre of the brake and pendulum axles. Negative and positive sides of the zero reference line are defined. If the mass is distributed evenly between the two sides, the pendulum is in equilibrium.

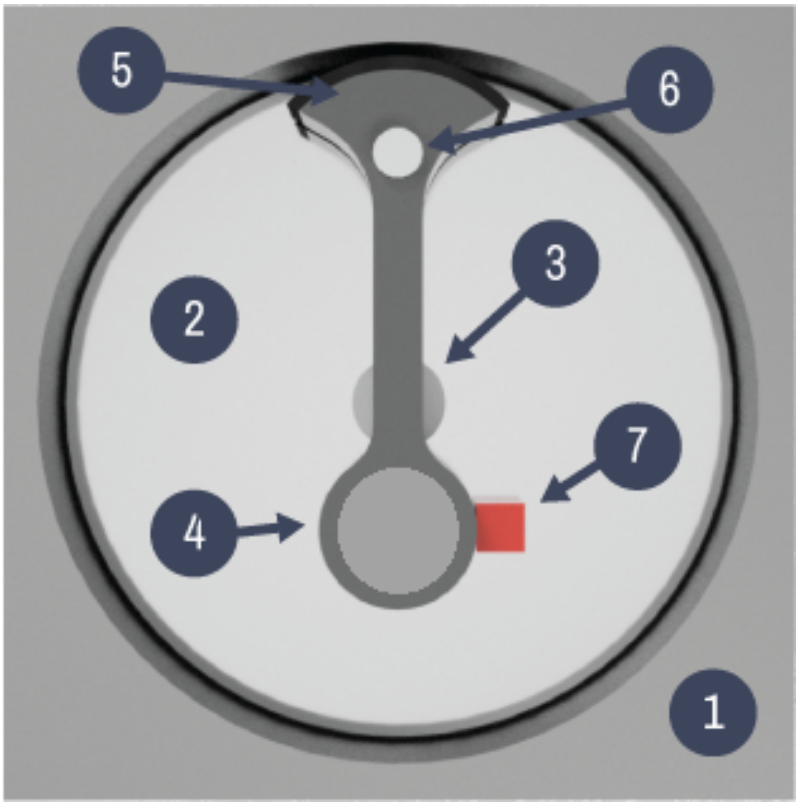

1. Brake drum
2. Brake hub
3. Brake axle
4. Pendulum with pendulum bob
5. Brake pad
6. Pendulum axle
7. Pendulum zero limiter

Figure 1: Parts of the brake system.

(a) Deactivated brake arm with zero reference line defined.

(b) Activated brake arm.

Figure 2: Different positions for the brake arm. 1: Rotational direction. 2: Pendulum movement.

2.2.1 Universal Brake System for Multiplier Reels

An image of the universal brake system for multiplier reels as represented in Adams is shown in figure 3.

Figure 4 depicts only certain parts of the system. The image is captured at the moment in time when the brake drum and brake pad first make contact. Red force arrows are displayed. The inner diameter of the brake drum is 29.4 mm.

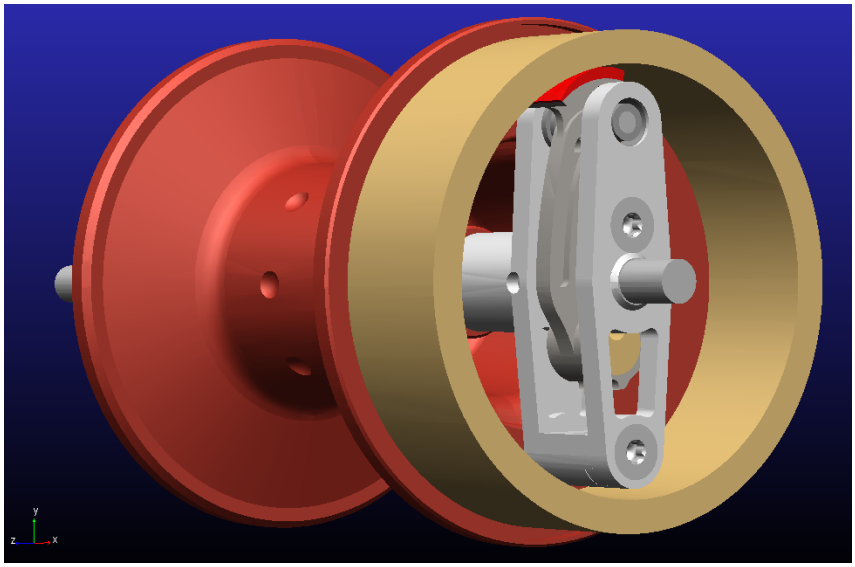

Figure 3: Graphic of the brake system and its spool.

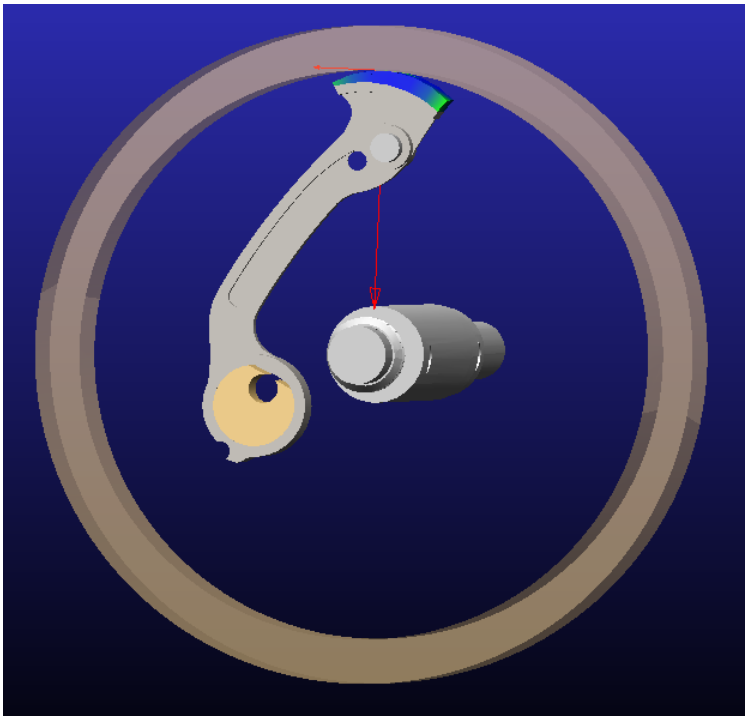

Figure 4: Graphic for part of the brake system.

2.2.2 Emergency Brake for Winch

An image of the emergency brake for winch as represented in Adams is shown in figure 5.

Figure 6 depicts only certain parts of the system. The image is captured at the moment in time when the brake drum and brake pad first make contact. Red force arrows are displayed. The inner diameter of the brake drum is 150.0 mm.

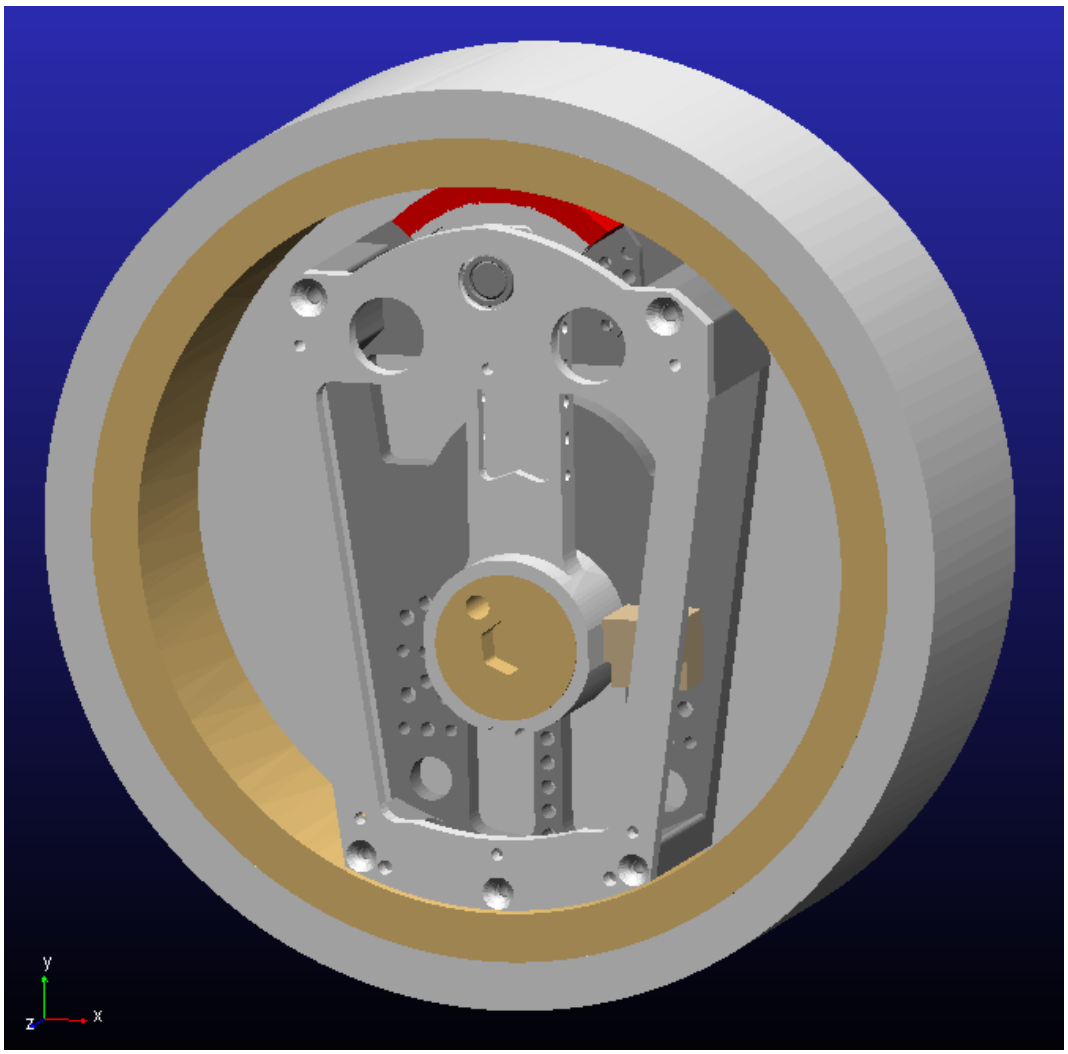

Figure 5: Graphic of the brake system.

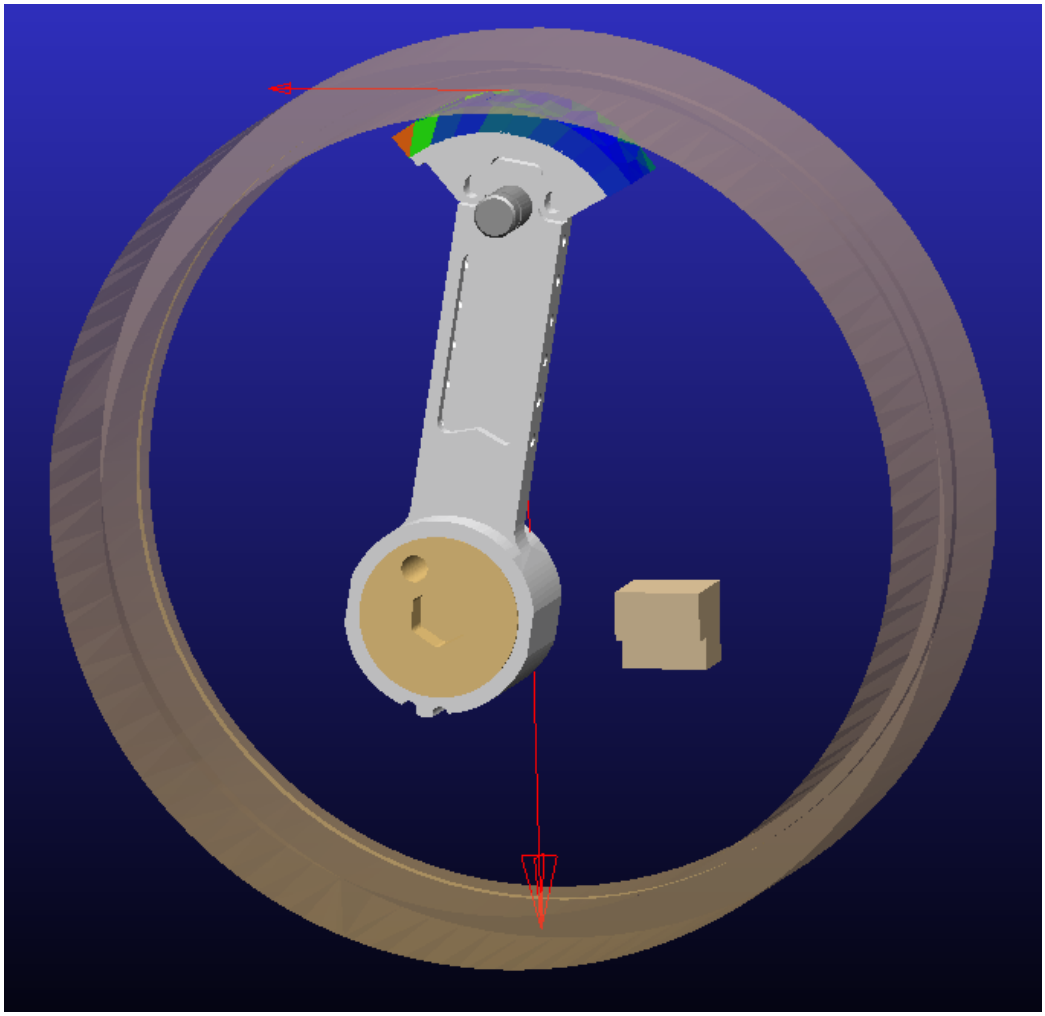

Figure 6: Graphic for part of the brake system.

An example of the difference between two flexible bodies is displayed in figure 7. They are created from the same solid body but are composed of a different number of nodes. This number determines the number of elements in the flexible body. During the introduction phase the number was experimented with to get a close enough approximation of the roundness of the material. Figure 7b is used in the simulation phase. It is the brake pad friction material that is made flexible.

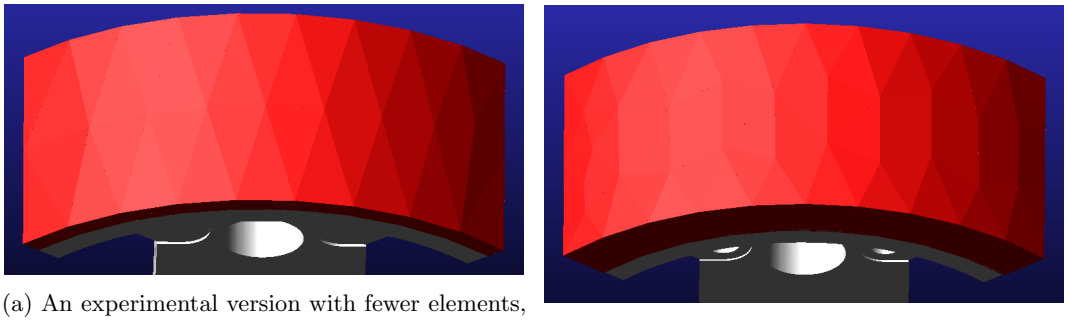

(a) An experimental version with fewer elements, not used in the simulation phase.

(b) Version with more elements.

Figure 7: Flexible brake pad friction materials.

2.2.3 Web Tension Control for Spools

An image of the web tension control for spools as represented in Adams is shown in figure 8. Its design is similar to the emergency brake system. The big difference is a modified brake pad with a spring attached between it and the pendulum. The spring is meant to act as a substitution to the flexible friction material with similar flexibility properties.

Figure 9 depicts only certain parts of the system. The image is captured at the moment in time when the brake drum and brake pad first make contact. Red force arrows are displayed. The spring is also represented in red. The inner diameter of the brake drum is 150.0 mm.

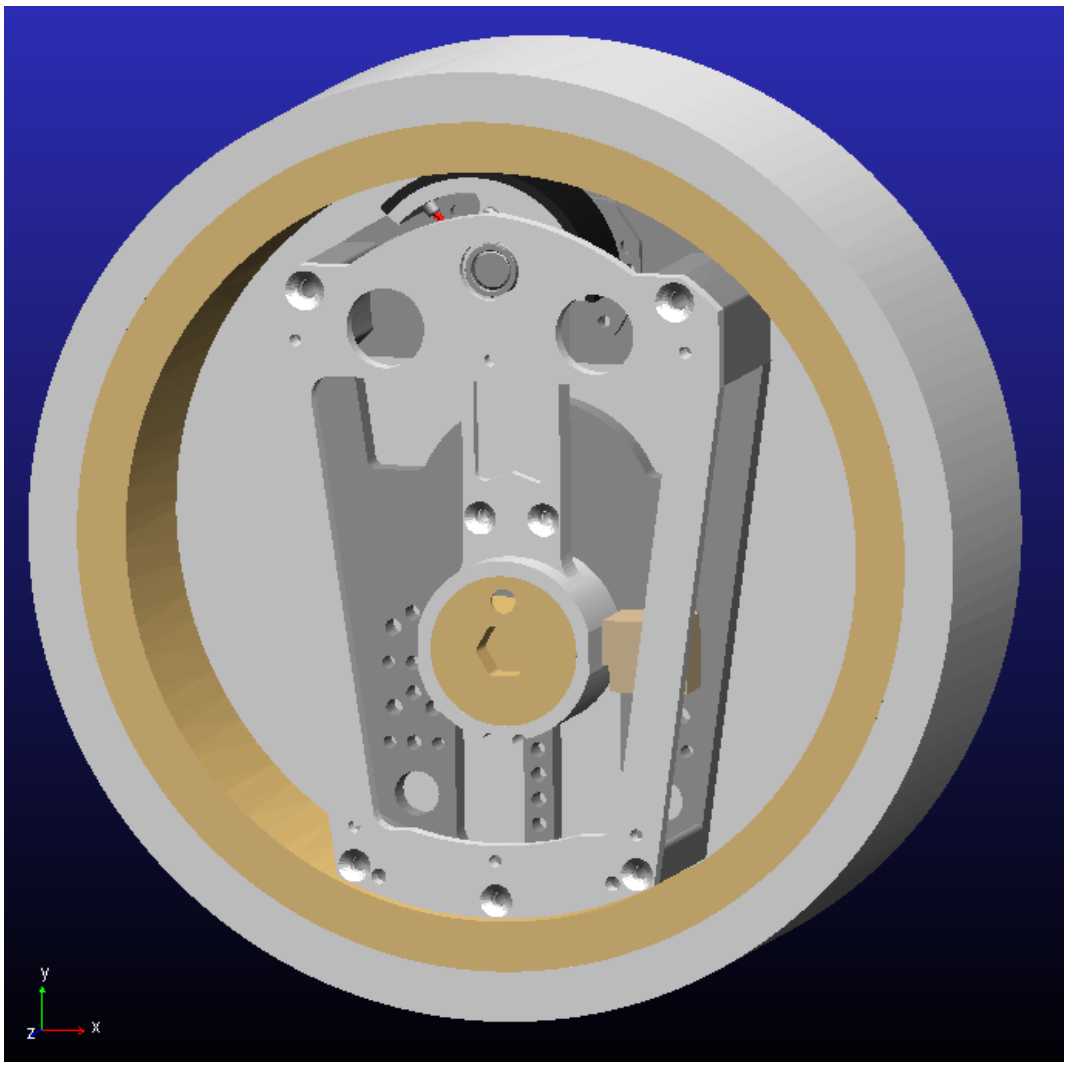

Figure 8: Graphic of the brake system.

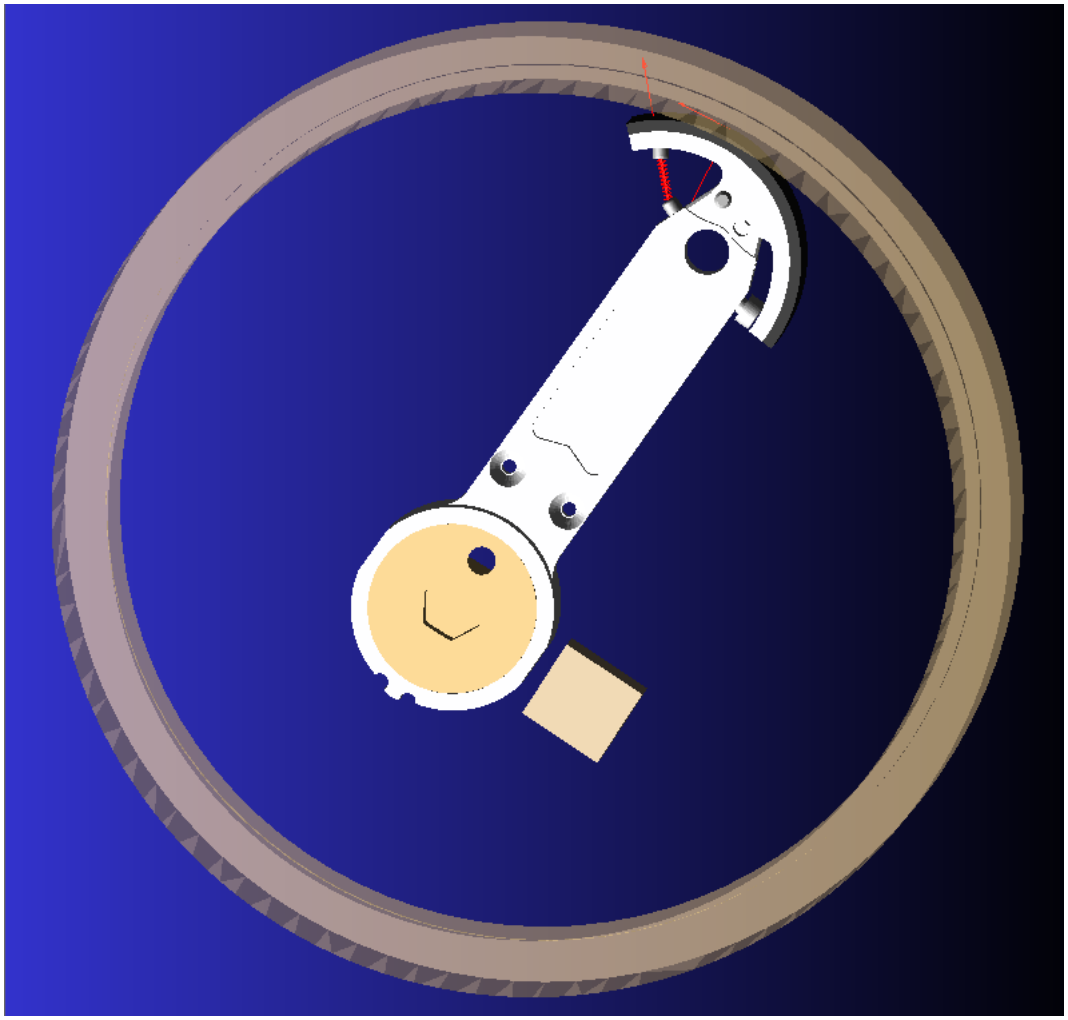

Figure 9: Graphic for part of the brake system.

2.2.4 Mass Added on the Brake Axle

A brake system only has its own weight and moment of inertia to counteract. These increase if an external mass body is attached to the brake axle. For a constant angular velocity, this gives an angular momentum greater in magnitude, see equation (3). The stopping time, as defined in section 2.3.1, consequently increases with added external mass.

Two simulations regarding activation of the brake system are seen in figure 10. It is accelerated to a certain velocity and then activated. The magnitude of the contact force between the brake drum and the brake pad is plotted versus time on the right axis. Angular velocity of the brake axle is plotted versus time on the left axis. When the contact force first is non-zero, the brake system is activated. For the simulation in figure 10a, the brake system only has the weight and moment of inertia of the rotating parts to counteract. An external mass body, approximately ten times as large as the weight of the brake system, is connected to the brake axle. The result of this similar simulation is found in figure 10b. By comparing the two figures, the influence of added mass is found.

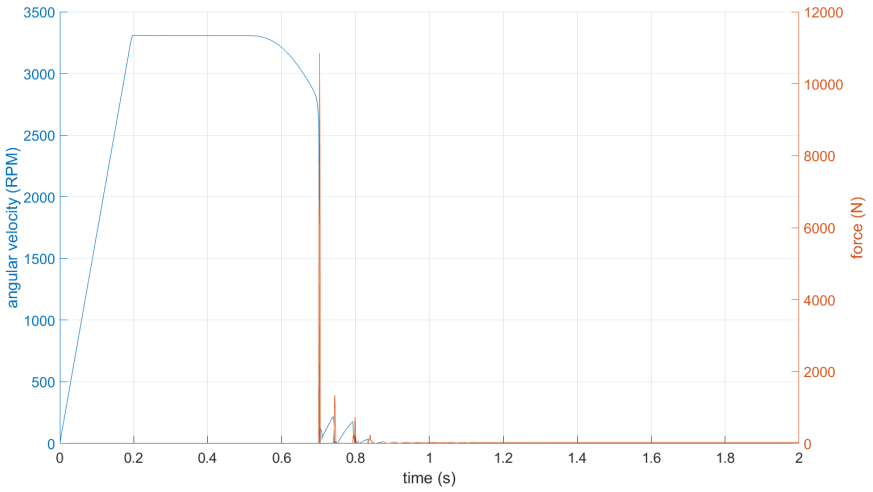

(a) Braking without an added mass body.

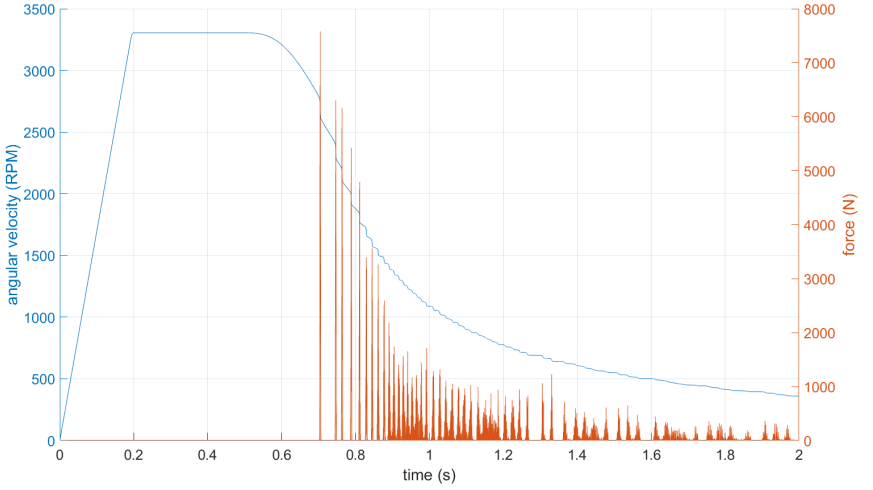

(b) Braking with an added mass body.

Figure 10: The influence of an added mass body.

2.3 Theory Behind the Brake System

2.3.1 Key Characteristics

If the pendulum mass centre is located at the negative side of the zero reference line, the brake arm will be activated by deceleration. Activation will thereby not be possible during acceleration. By moving the mass centre to the positive side of the zero reference line, rotation will instead activate the brake arm. Because the brake system is placed in the vertical plane, the brake arm will be activated due to gravity for a constant rotational speed below a certain value.

To help understanding the results of the simulations by making comparisons easier, a couple of parameters are introduced. The *reaction time* is defined as the moment in time the contact force first is non-zero. Likewise, the *swing out time* is the time the brake arm starts moving away from the pendulum zero limiter, toward the brake drum. *Stopping time* is defined as the moment in time when the rotational speed for the brake axle reaches zero. All times are defined from when the simulation starts.

The *contact force*, or the brake force, is defined as the magnitude of force between the brake pad and drum that is active when the two bodies are in contact. The brake force is dependent on the friction coefficients between the brake pad and brake drum, torque caused by moment of inertia and centrifugal force of the pendulum bob. The friction coefficients decide how great the brake force will be. It can be influenced in several other ways. Changing the position of the pendulum axle, pendulum bob mass or distance between the brake drum and brake pad are some of them.

Unless the rate of change of the angular velocity becomes positive or zero, the brake arm will not deactivate until the angular velocity of the brake axle is zero. For implementations feeding out material, such as the spool in a fishing reel, it is important to have an easy deactivation.

2.3.2 Parameters Influencing the Brake System

Several parameters influence the key characteristics of the brake system.

By translating the position of the pendulum bob mass centre, the moment of inertia of the brake arm is changed. Depending on how far the mass centre is translated to the negative side of the zero reference line, activation of the brake arm is affected to different degrees. Only the x-coordinate of the pendulum bob mass centre is assumed to affect the activation. Because of this, a translation of the mass centre is considered equal to a rotation of the pendulum bob, regarding activation of the brake arm. Changing the material of the pendulum bob will influence the brake system in a similar way.

The further away the brake pad is from the brake drum, the more the pendulum has to swing until the pad and drum establish contact. That is, for larger gaps the brake axle will need a larger deceleration applied to activate at the same reaction time. The goal is to have the brake pad as close to the brake drum as possible, but not so close as to impede the free movement of the arm.

Exposing materials to friction forces will certainly cause wear and tear over time. For the friction material this will lead to a larger distance between the brake pad and brake drum. The wear and tear should for economical and practical reasons be concentrated at parts that are cheaper and easier to replace.

For small centrifugal forces on the pendulum bob, the spring stiffness should be smaller, allowing the brake arm to rotate at larger angles. On the other hand, the spring stiffness should be larger for big centrifugal and inertial forces on the pendulum bob, so the brake arm does not rotate too much. This can be obtained by using a non-linear spring in the web tension control for spools model.

The brake pad and drum materials affect the friction coefficient at the contact between them, which in turn affects the brake force. A higher friction coefficient will give a brake force greater in magnitude, as seen in equation (6). The brake pad material used in this project is either *AlSiC* or *Ceramic Low*. AlSiC is a metal matrix composite, consisting of aluminium and silicon carbide. [7]

Ceramic Low is an approximation of the type of material that is used in carbon-ceramic brake discs. Density and Young's modulus were chosen in the range of expected values from a table found on the now changed SGL GROUP website. An archived version of the page is found among the references. Poisson's ratio was chosen the same as for AlSiC. [8]

As the difference in weight between the two brake pad materials is small compared to the total weight of all rotating parts, this difference was disregarded for all models. Table 1 displays the material parameters for both materials.

Table 1: Material parameters for the brake pad materials.

Material parameter	AlSiC	Ceramic Low
Density	3000 kg/m^3	2800 kg/m^3
Young's modulus	192 GPa	100 GPa
Poisson's ratio	0.25	0.25

3 Methodology

All simulations were carried out in Adams. Design- and simulation parameters in all tables are derived from the software. Post processing was done in MATLAB.

3.1 Introduction Phase

Schematics of the models were provided by Brillianze Sweden AB in the form of CAD files. These files were imported to Adams. Each model consists of a number of solid bodies. Only the geometry of the bodies were included in the files. Each body was assigned a material and connections to other bodies if applicable. Prototypes were provided to give further understanding of their structure. The connections are either fixed or revolute, depending on the prototype.

The geometry of the brake pad was modified before moving on to the simulation phase. A number of friction materials were experimented with. Because the differences in results between different friction materials on the brake pad were near unnoticeable, the values for AlSiC and Ceramic Low were kept during the simulation phase. Also, the brake pad friction material was converted from a solid body to a flexible body for two of the models. This process required, among other parameters, the number of finite element nodes to be set. The difference between two flexible bodies can be seen in section 2.2.2, figure 7.

For web tension control for spools, the conversion was not considered necessary as a spring attached between the brake pad and pendulum is meant to act as a substitution with similar flexibility properties. This should help moving the wear and tear issue away from the material and onto the brake drum. It also has more customisable behaviour. For example, the spring can easily be made non-linear. In Adams, this was done using spline functions. To simplify the attachment of the spring, the brake pad was modified. Also, a new pendulum bob was obtained for the model. The new mass body's weight is lower compared to the one previously used.

Different approaches were explored to changing angular velocity and its rate of change. Implementing a force at a point of a mass body is the most common method in this project. However, in part of section 3.2.6, a torque driven model was used to same effect by implementing the torque directly on the external mass body.

Lastly, the three different models were set up in Adams. The following paragraphs describe the design parameters used.

Several of them, such as weight and moment of inertia for different parts of the universal brake system for multiplier reels, are displayed in table 2. These parameters are used in all of the brake system simulations unless otherwise stated. For the moment of inertia of the rotating parts, the pendulum bob mass centre is not altered. Rotation of the spool will occur around the z-axis. The weight of the spool is included in the brake system's weight.

Table 2: Design parameters and their values for the universal brake system for multiplier reels.

Design parameter	Value
Distance between brake pad and brake drum	0.388 mm
Weight of the brake system	23.091 g
Weight of rotating parts	5.485 g
Weight of brake arm	0.741 g
Weight of spool	11.644 g
Moment of inertia of spool	$I_{xx} = 2152.642$ g $\cdot$ mm^2 $I_{yy} = 2150.765$ g $\cdot$ mm^2 $I_{zz} = 1484.931$ g $\cdot$ mm^2

Different design parameters for the emergency brake for winch, such as weight for different parts, are displayed in table 3. These parameters are used in all of the brake system simulations unless otherwise stated. Brass was chosen as the material of the pendulum bob.

Table 3: Parameters and their values for the emergency brake for winch.

Design parameter	Value
Distance between brake pad and brake drum	0.503 mm
Weight of the brake system	2.524 kg
Weight of rotating parts	0.441 kg
Weight of brake arm	0.169 kg

Different design parameters for the web tension control system, such as weight and moment of inertia for different parts, are displayed in table 4. The weight and moment of inertia of the spring are considered very small. The parameters are used in all of the brake system simulations unless otherwise stated. Brass was chosen as the material of the pendulum bob.

Table 4: Parameters and their values for the web tension control for spools.

Design parameter	Value
Distance between brake pad and brake drum	0.288 mm
Weight of the brake system	2.506 kg
Weight of rotating parts	0.423 kg
Weight of brake arm	0.150 kg

3.2 Simulation Phase

To alter the angular velocity of the brake axle, applied forces and motions were modified with the function builder in Adams. Inside the function builder, the *step* function was used. It is a cubic spline of a Heaviside function which enables a smoother transition between two values compared to a Heaviside function. Two points in time, when the transition should start and end, are used to control the rate of change of a parameter. An example of the step function is displayed and compared to a Heaviside function in figure 11.

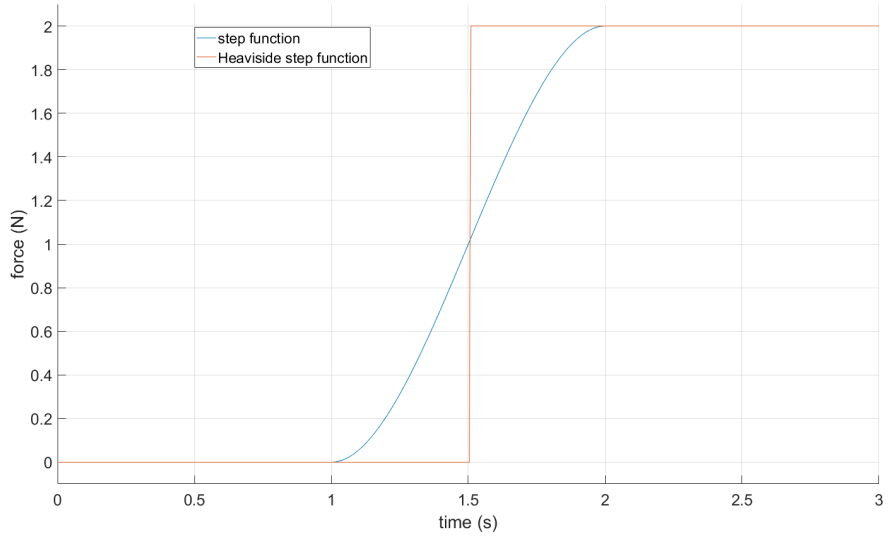

Figure 11: Comparison of a step function and a Heaviside step function.

AlSiC was used in all mass body dependence simulations, that is subsections 4.1.1, 4.2.1 and 4.3.1. In all other simulations made in section 4, Ceramic Low was used.

If not otherwise stated, an external mass body is attached with a fixed joint to the brake axle. In the case of the universal brake system, the external mass was a torus representing the thread wired around the spool in a fishing rod. For the other brake systems, a generic sphere was used.

In all simulations, GSTIFF was the integrator used. The most suitable step size and integrator tolerance were chosen for each model.

3.2.1 Mass Body Dependence

If the rotational speed is too low, activation of the brake arm due to gravity will occur. To measure the lowest rotational speed possible without activation, the brake axle was accelerated to a certain angular velocity. The applied force was turned off and observations were made whether or not the brake arm was activated due to gravity. Activation implies the need of a higher angular velocity. The procedure was repeated until arrival at the lowest rotational speed possible without activation of the brake.

The needed deceleration to activate the brake was measured by first accelerating the brake axle to a constant angular velocity. This velocity was set high enough to avoid activation due to gravity. A force was applied in the opposite direction to the original accelerating force in order to achieve a deceleration. At a certain point in time when the activation of the brake is desired to take place was chosen. The magnitude of the newly applied deceleration was varied until the activation happened at the desired time. This magnitude of this force is considered the needed deceleration for activation of the brake.

Both the weight of the pendulum bob and the position of the body's mass centre were studied separately using this approach. By altering the density of the mass body its weight was varied. Some densities correspond to known materials. The position of the body's mass centre was only moved in the negative direction of the zero reference line. These approaches were carried out for all models. For the universal brake system for multiplier reels, simulations which alternated the position of the pendulum bob's mass centre were not performed.

To examine the influence of the y-coordinate of the pendulum bob's mass centre regarding activation of the brake arm, simulations were made where the mass centre was only translated in the y-direction. The coordinate was found to not affect the activation. This topic is further discussed in subsection 5.1.

For the web tension control model, the mass centre of the pendulum bob was altered to find the equilibrium point of the brake arm.

Table 5 contains the parameters used in all mass body dependence simulations for the universal brake system for multiplier reels. Regarding needed deceleration for activation of the brake, the constant angular velocity was 3000 revolutions per minute. The location of the mass centre for the pendulum bob was not altered. No external mass was added.

Table 5: Parameters and their values used in the mass body dependence simulations, universal brake system for multiplier reels.

Simulation parameter	Value
Friction coefficient between brake drum and brake pad	$\mu_s = 0.3$ $\mu_d = 0.3$
Step size	10^{-04} s
Integrator tolerance	10^{-03}

Table 6 contains the parameters used in all mass body dependence simulations for the emergency brake for winch. Regarding needed deceleration for activation of the brake, the constant angular velocity was 3000 revolutions per minute.

When different weights of the pendulum bob were studied, the location of the body's mass centre was translated 1.25 millimetres from the zero reference line, in the negative direction. The material of the pendulum bob was brass when the position of the body's mass centre was studied. Its weight was 99.912 grams.

Table 6: Parameters and their values used in the mass body dependence simulations, emergency brake for winch.

Simulation parameter	Value
Friction coefficient between brake drum and brake pad	$\mu_s = 0.3$ $\mu_d = 0.3$
Weight of the added mass body	20.910 kg
Moment of inertia of the added mass body	$I_{xx} = 13382.682 \text{ kg} \cdot \text{mm}^2$ $I_{yy} = 13382.682 \text{ kg} \cdot \text{mm}^2$ $I_{zz} = 13382.682 \text{ kg} \cdot \text{mm}^2$
Step size	10^{-04} s
Integrator tolerance	10^{-05}

Table 7 contains the parameters used in all mass body simulations for the web tension control for spools.
Regarding needed deceleration for activation of the brake, the constant angular velocity was 3000 revolutions per minute.

The location of the mass centre for the pendulum bob was translated 1.0 millimetres from the zero reference line, in the negative direction. Brass was the material of the pendulum bob. Its weight was 86.438 grams.

Table 7: Parameters and their values used in the mass body dependence simulations, web tension control for spools.

Simulation parameter	Value
Friction coefficient between brake drum and brake pad	$\mu_s = 0.3$ $\mu_d = 0.3$
Stiffness of the spring	1000 N/mm
Weight of the added mass body	20.910 kg
Moment of inertia of the added mass body	$I_{xx} = 13382.682\ \text{kg} \cdot \text{mm}^2$ $I_{yy} = 13382.682\ \text{kg} \cdot \text{mm}^2$ $I_{xx} = 13382.682\ \text{kg} \cdot \text{mm}^2$
Step size	10^{-04} s
Integrator tolerance	10^{-04}

3.2.2 Friction Coefficient Dependence

In order to find out how the friction coefficients for the contact force between the brake pad and brake drum affect the behaviour of the brake models, a number of runs were made according to the combinations in table 8. The other parameters can be seen in table 9.

The simulation was performed by accelerating the brake axle to a velocity relatively unaffected by gravity, the same for each run. Thereafter a deceleration was applied, activating the brake arm and kept active until the system stopped. Because the same deceleration was applied each time, comparisons between the coefficients were made with the assumption that a baseline is the situation when no friction force is applied.

Three values were extrapolated each run: Stopping, reaction and swing out times. Along with them, the angular velocity of the brake arm, contact force, and the angle at which the brake arm rotates were also exported.

Table 8: The friction coefficient combinations that were simulated.

μ_s	μ_d												
0.3	0.0		0.05		0.1	0.125	0.15	0.175	0.2	0.225	0.25	0.275	0.3
0.325													0.325
0.35													0.35
0.375													0.375
0.4	0.1	0.125	0.15	0.175	0.2	0.225	0.25	0.275	0.3	0.325	0.35	0.375	0.4
0.425	0.125												0.425
0.45	0.15												0.45
0.475	0.175												0.475
0.5	0.2	0.225	0.25	0.275	0.3	0.325	0.35	0.375	0.4	0.425	0.45	0.475	0.5
0.525	0.225												0.525
0.55	0.25												0.55
0.575	0.275												0.575
0.6	0.3	0.325	0.35	0.375	0.4				0.5				0.6
0.7	0.4				0.5				0.6				0.7

Table 9: Parameters and their values used for friction tests.

(a) Universal brake system for multiplier reels.

Simulation parameter	Value
Weight of the added mass body	1.419 g
Moment of inertia of the added mass body	$I_{xx} = 148.525\ \text{g} \cdot \text{mm}^2$ $I_{yy} = 76.480\ \text{g} \cdot \text{mm}^2$ $I_{zz} = 76.480\ \text{g} \cdot \text{mm}^2$
Initial velocity	$\approx$ 2400 RPM
Deceleration applied	0.1864 N
End time	1.0 s
Step size	10^{-4} s
Integrator tolerance	10^{-3}

(b) Emergency brake for winch and web tension control for spools. Spring stiffness and damping only applies to the web tension control system.

Simulation parameter	Value
Weight of the added mass body	2.091 kg
Moment of inertia of the added mass body	$I_{xx} = 1338.440\ \text{kg} \cdot \text{mm}^2$ $I_{yy} = 1338.440\ \text{kg} \cdot \text{mm}^2$ $I_{zz} = 1338.440\ \text{kg} \cdot \text{mm}^2$
Pendulum bob mass centre on negative side	1.0 mm
Initial velocity	$\approx$ 2400 RPM
Deceleration applied	700 N
End time	1.25 s
Step size	10^{-04} s
Integrator tolerance	10^{-04}
Spring stiffness	500 N/mm
Spring damping	$1.9 \cdot 10^{-7}$ Ns/mm

3.2.3 Spring Stiffness Dependence

For all spring stiffness dependence simulations, brass was the material of the pendulum bob. Its weight was 86.438 grams. Table 10 contains the parameters used in all spring stiffness dependence simulations.

The dependence on the stiffness of a linear spring in the brake system was evaluated similarly to the friction comparisons. Spring stiffness coefficients used were in the range of 0 - 7000 N/mm. Specific values can be found in the appendix, table A.3.1. The applied deceleration was at a maximum 700 newton and slowed down the system from an initial velocity of approximately 2400 revolutions per minute.

Stopping, reaction and swing out times were extrapolated, as well as the angular velocity of the brake arm, contact force and the angle at which the brake arm rotates. A couple of simulations where the brake arm was activated and deactivated for different stiffness coefficients were compared to see the angle the arm swings out.

Two different concepts regarding non-linear springs were examined. First, simulations were performed where the brake axle was accelerated to a constant velocity. A deceleration was then applied to activate the brake arm. At a certain time an acceleration was applied to deactivate it. This was done for one exponential, one logarithmic and one linear spring and their general behaviours were evaluated.

To evaluate the stopping time for a number of springs, the acceleration to deactivate the brake was not applied.

The mathematical formulas for springs used in these simulations are found in table A.3.2.

Table 10: Parameters and their values used in the spring stiffness simulations.

Simulation parameter	Value
Friction coefficient between brake drum and brake pad	$\mu_s = 0.3$ $\mu_d = 0.3$
Weight of the added mass body	2.091 kg
Moment of inertia of the added mass body	$I_{xx} = 1338.440 \text{ kg} \cdot \text{mm}^2$ $I_{yy} = 1338.440 \text{ kg} \cdot \text{mm}^2$ $I_{zz} = 1338.440 \text{ kg} \cdot \text{mm}^2$
Pendulum bob mass centre location on negative side	1.0 mm
Spring damping	$1.9 \cdot 10^{-7}$ Ns/mm
Step size	10^{-04} s
Integrator tolerance	10^{-04}

3.2.4 Distance Between Brake Drum and Brake Pad

To get a general idea of how large the distance between the brake pad and drum should be, besides closer meaning a shorter reaction time, a couple of measurements were made on the emergency brake system comparing these as well. Specifically which values can be found in the appendix, table A.4.1, and the simulation parameters are included in table 11. No external mass body was added.

Table 11: Parameters and their values used for distance tests.

Simulation parameter	Value
Pendulum bob mass centre location on negative side	0.6 mm
Initial velocity	3000 RPM
Deceleration applied	400 N
End time	1.0 s
Step size	10^{-04} s
Integrator tolerance	10^{-04}

3.2.5 Comparison Between Models and Integrator Settings

Taking advantage of the available data, obtained from calculations made in section 3.2.2 that used similar enough conditions for the web tension control and emergency brake systems, some comparisons were made. Seeing the difference between the stopping times gives an idea of for which friction coefficients each brake system is best suited.

In the same vein, the accuracy of the simulations was evaluated on the universal brake system. Two runs with different integration settings, one *cruder* and one *finer*, were compared. The crude one used step size 10^{-04} s and integrator tolerance 10^{-03}. This is in the ball park of the standard values. Correspondingly, the finer settings were step size 10^{-06} s and integrator tolerance 10^{-05}. These were the smallest values achievable to keep the simulation from failing and without taking too much time.

3.2.6 Building Sequences

With the objective of using the brake system models in sequences simulating practical applications, the following case was considered. A sheet is stretched between two rollers. One of the rollers slows down so the sheet can be split. The other roller should now also slow down, making sure the velocity difference is at a minimum and avoiding backlash.

Limitations with the Adams software as it was available meant that the sheet couldn't be represented as a body or force like the spring. Instead, two approaches to controlling the first roller are presented below.

The so called *torque driven model* is an altered form of the standard web tension control for spools. The main difference lies in that the connection between the external mass and the brake axle now is a revolute joint instead of fixed. A friction force is applied to simulate ball bearings. This lets the brake speed be dependent on the speed of the external mass, but not necessarily the same. It also works the other way around. The brake can slow down the external mass. The brake and the external mass now act as stand ins for the rollers

Two simulation runs were done on the torque driven model. Mainly, the difference sought between the two that would matter was the alternation between lower and higher speeds. In addition to changing the parameters and arriving at the values in table 12, getting the ideal performance out of these depended on the duration of the acceleration and deceleration applied as well as making sure the velocities were of sizes not visibly affected by the gravitation.

The simulations themselves were performed by accelerating up to the desired higher velocity of the mass, staying there, then decelerating to the lower velocity, staying there and repeating. The system applied torque to the external mass as needed, and automatically changed torque direction to rectify overshooting the target.

The results obtained were the angular velocity of both the brake and external mass, the angle the brake arm has swung and the sum of applied torques.

Table 12: Parameters and their values used for the torque driven sequences.

Simulation parameter	Low speed version	High speed version.
Friction coefficient between brake drum and brake pad	$\mu_s = 0.3$ $\mu_d = 0.1$	
Ball bearing friction	$\mu_s = 0.3$ $\mu_d = 0.3$	$\mu_s = 0.4$ $\mu_d = 0.4$
Weight of the added mass body	2.091 kg	
Moment of inertia of the added mass body	$I_{xx} = 1338.440\ \text{kg} \cdot \text{mm}^2$ $I_{yy} = 1338.440\ \text{kg} \cdot \text{mm}^2$ $I_{zz} = 1338.440\ \text{kg} \cdot \text{mm}^2$	
Pendulum bob mass centre location on negative side	0.55 mm	0.4 mm
Alternating velocities	1500 RPM 2000 RPM	2000 RPM 3000 RPM
Maximum torque allowed	1000 N mm	
Spring stiffness	1500 N/mm	2500 N/mm
Spring damping	$1.9 \cdot 10^{-7}$ Ns/mm	
End time	2.0 s	3.5 s
Step size	10^{-04} s	10^{-05} s
Integrator tolerance	10^{-04}	10^{-05}

For the *angular velocity driven model*, an external mass body is attached to the brake axle. The mass body is connected with a revolute joint to another, identical, mass body, denoted the driving mass. Friction is present in the joint, representing ball bearings. The driving mass was set to alter between two, or more, desired angular velocities.

Table 13 contains the parameters used in all simulations for the angular velocity driven model. The velocity was alternated between 2000 and 1500 revolutions per minute.

Table 13: Parameters and their values used in the sequence simulations.

Simulation parameter	Value
Friction coefficient between brake drum and brake pad	$\mu_s = 0.3$ $\mu_d = 0.1$
Weight of the added mass body	3.921 kg
Weight of the driving mass body	3.921 kg
Moment of inertia of the added mass body	$I_{xx} = 4836.160\ \text{kg} \cdot \text{mm}^2$ $I_{yy} = 4836.160\ \text{kg} \cdot \text{mm}^2$ $I_{zz} = 3136.968\ \text{kg} \cdot \text{mm}^2$
Moment of inertia of the driving mass body	$I_{xx} = 4836.160\ \text{kg} \cdot \text{mm}^2$ $I_{yy} = 4836.160\ \text{kg} \cdot \text{mm}^2$ $I_{zz} = 3136.968\ \text{kg} \cdot \text{mm}^2$
Step size	10^{-04} s
Integrator tolerance	10^{-04}

3.3 Post-Processing Phase

For some parameters, such as stopping time, values were extrapolated from the post-processor in Adams. In other instances, the simulation data was exported from Adams and imported to MATLAB where plots were created.

In order to visualise the difference in behaviour of the models, stopping times were plotted in MATLAB using the built-in *mesh* and *surf* functions. Using colour to differentiate between the values, these 3D surface plots work by filling in the gaps between the measured points. However, due to the nature of them using the closest points, the end result did not always represent the actual behaviour.

Therefore, so called *pseudo values* were introduced in the surf methods when they were shown from a three-dimensional angle. In figure 12 the improvement after adding the pseudo values is shown, represented by circles while the actual measurements are crosses. Before the values were introduced, as in figure 12a, the surface was rougher and afterwards, in figure 12b, smoother. The values were chosen as the average between the two closest actual points along the static friction coefficient axis. Results show that the measured values along this axis comparatively do not differ much.

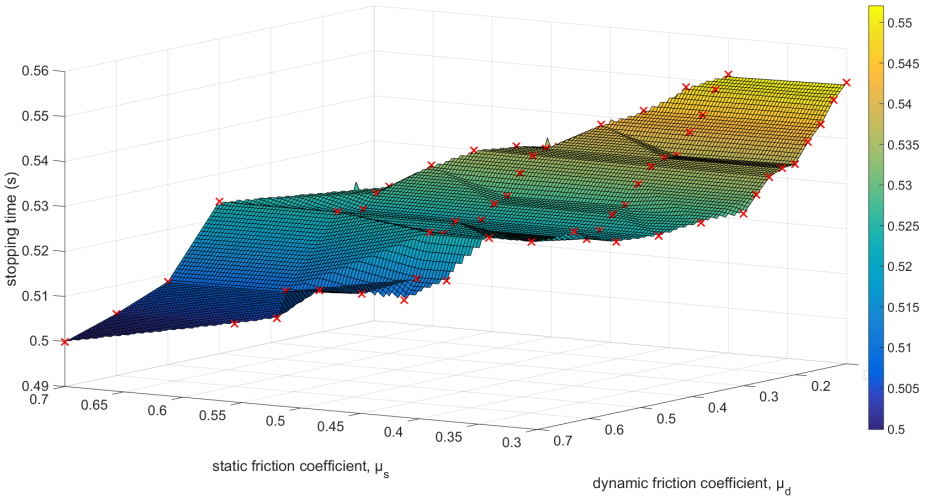

(a) Without pseudo values.

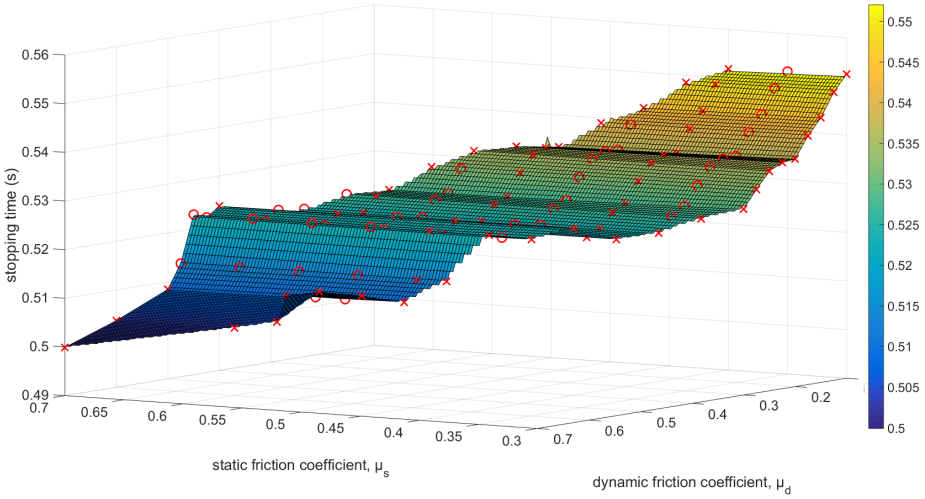

(b) With pseudo values.

Figure 12: Stopping times plotted in MATLAB using the surf function. These results are again presented with pseudo values as (b) in figure 33b.

4 Results

4.1 Universal Brake System for Multiplier Reels

The brake arm rotates to a distance of approximately 4.327 millimetres from the pendulum zero limiter before the brake pad makes contact with the brake drum. This corresponds to 23.225 degrees, or 0.405 radians.

4.1.1 Mass Body Dependence

In figure 13, the lowest constant rotational speed possible to avoid activation and magnitude of applied decelerating force needed for activation of the brake arm is plotted against the weight of the pendulum bob. The angular velocity ranges from 2850.84 to 1138.44 revolutions per minute. The force ranges from 0.164 to 1.256 newtons. Data from the simulations is found in table A.1.1.

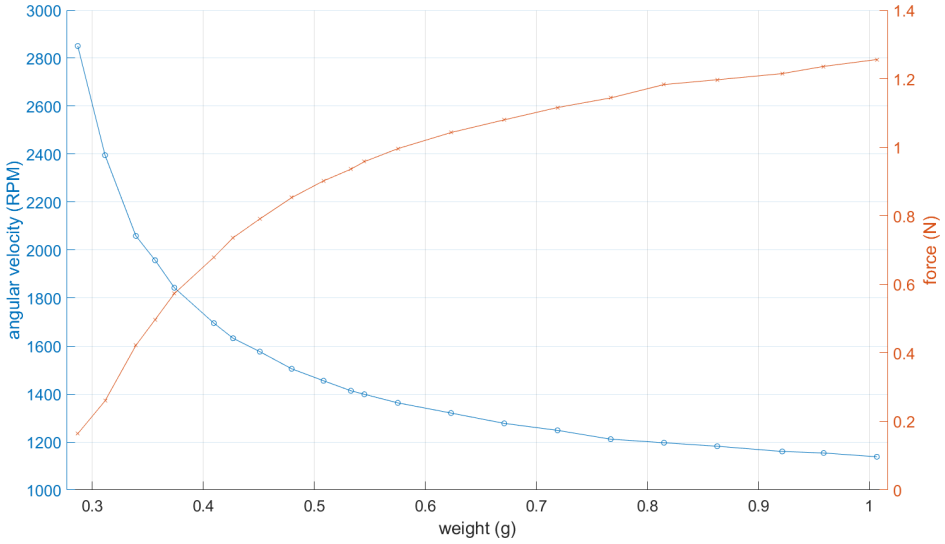

Figure 13: The influence of an alternating pendulum bob weight.

4.1.2 Friction Coefficient Dependence

The behaviour of this model of the brake system depending on the static and dynamic friction coefficients, μ_s and μ_d respectively, between the brake drum and pad is presented below in figures 14 to 16. Additionally, figures 17 and 18 show the results of the stopping time measurements.

Figure 14 shows the general behaviour of the brake system after activation by deceleration until it reaches a full stop. Presented are the angular velocity in revolutions per minute and the contact force in newton.

Figure 15 then shows the differences between a wide range of coefficients. Of special note is $\mu_s = 0.3$, $\mu_d = 0$ which is close to the same as if the brake did not activate. For easier interpretation, the dynamic friction has been indicated adjacent to each of the lines in the zoomed-in view, figure 15b.

Figure 16 is a number of runs with $\mu_s = 0.3$. The difference in μ_d is here smaller in order to compare the distribution of lines to figure 15.

The dynamic friction coefficient has a bigger influence on the stopping time than the static, as seen when comparing figures 17a and 17b. Figure 17c is the stopping times for the cases when the coefficients are equal.

Do recall that figure 18b implements pseudo values to show the expected behaviour while 18a does not. The reaction and swing out times were the same for all runs. A detailed table of all measured results can be found in the appendix, table A.2.1.

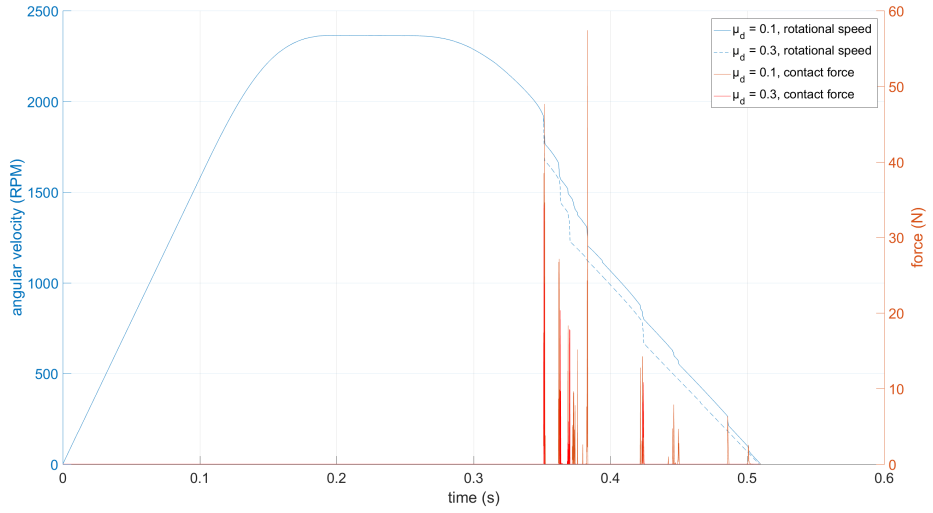

Figure 14: General behaviour of the brake system for static friction coefficient $\mu_s = 0.3$.

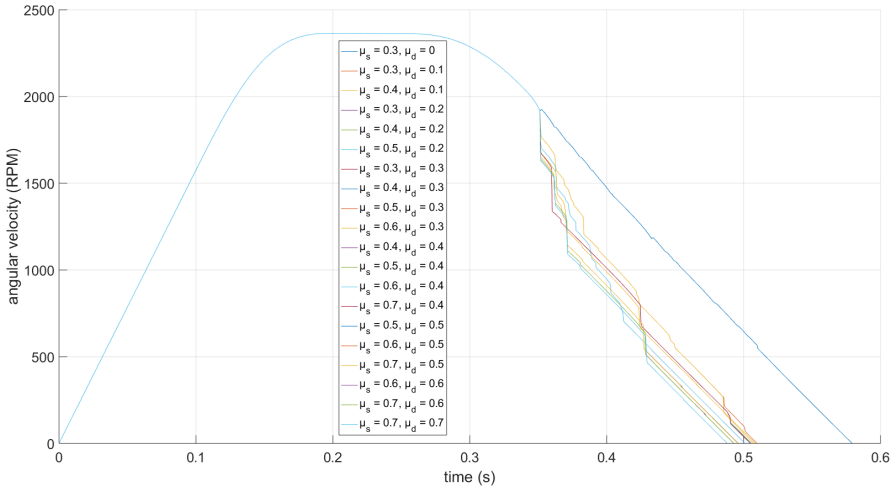

(a) Complete run.

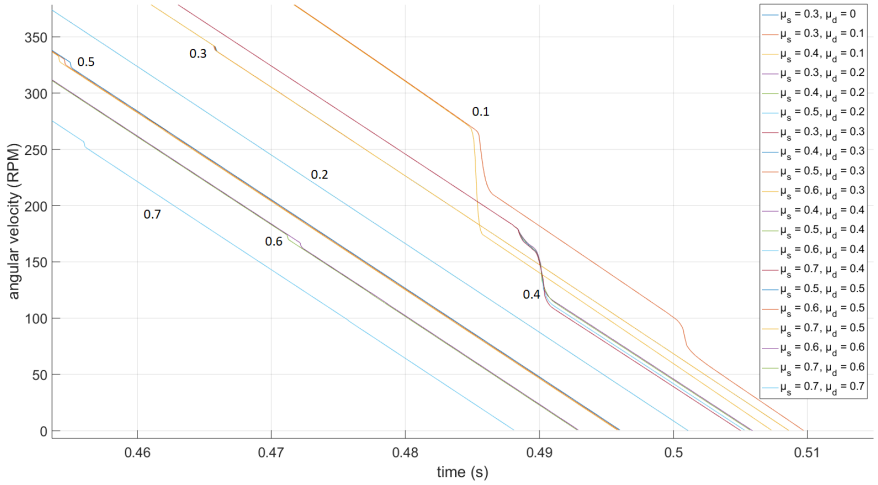

(b) Zoomed-in view.

Figure 15: Behaviour of the brake system for different friction coefficients.

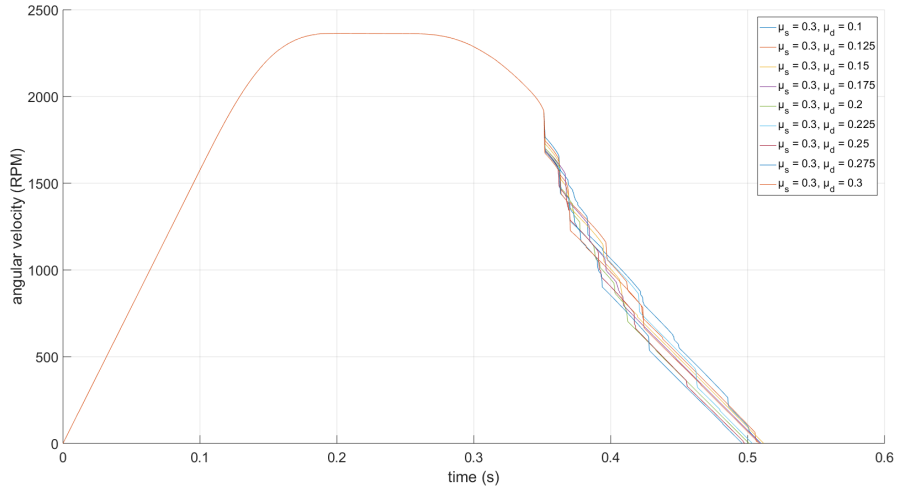

(a) Complete run.

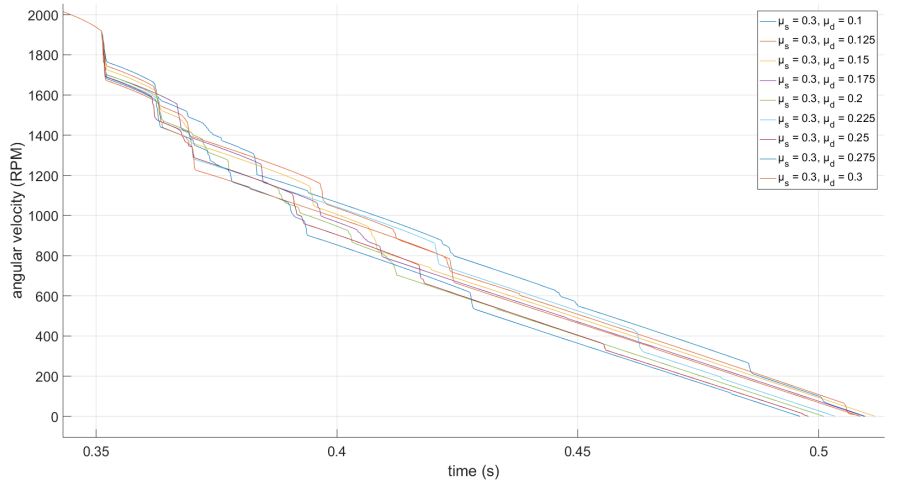

(b) Zoomed-in view.

Figure 16: Behaviour of the brake system for different dynamic friction coefficients with $\mu_s = 0.3$.

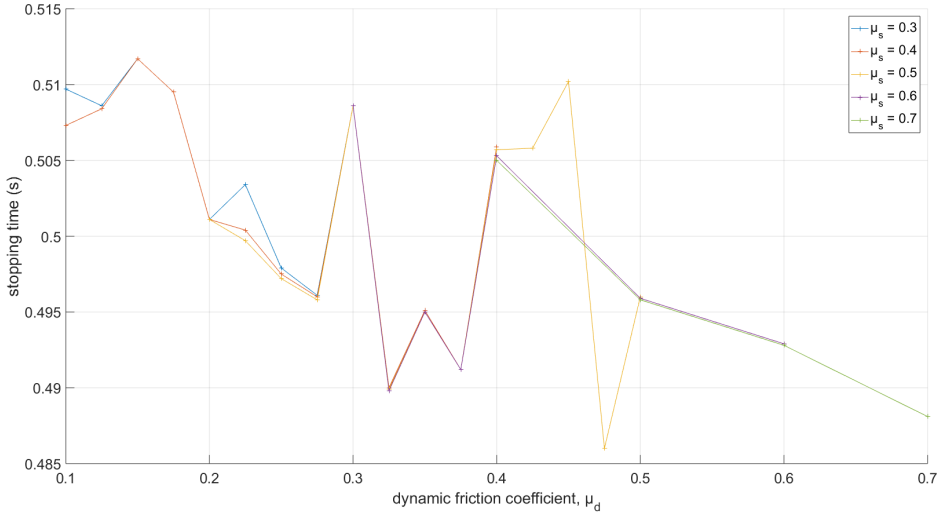

(a) μ = dynamic friction coefficient, μ_d

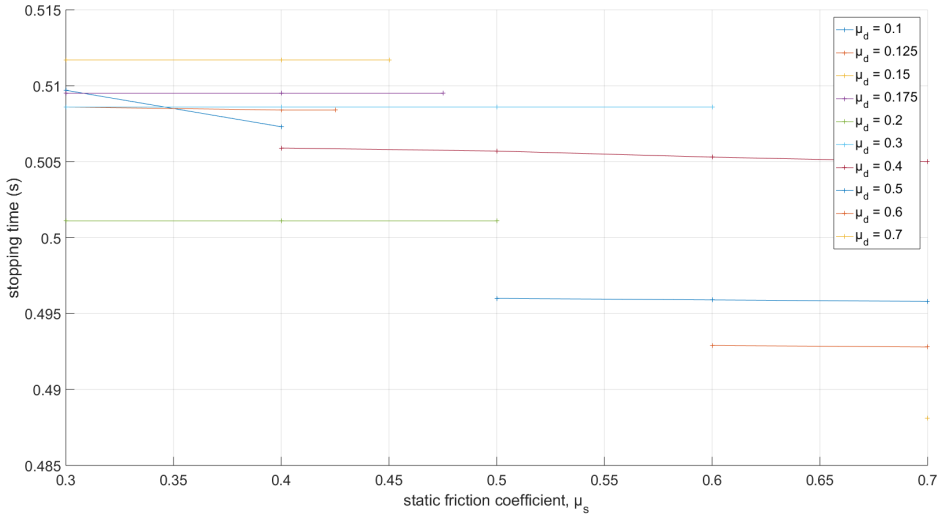

(b) μ = static friction coefficient, μ_s

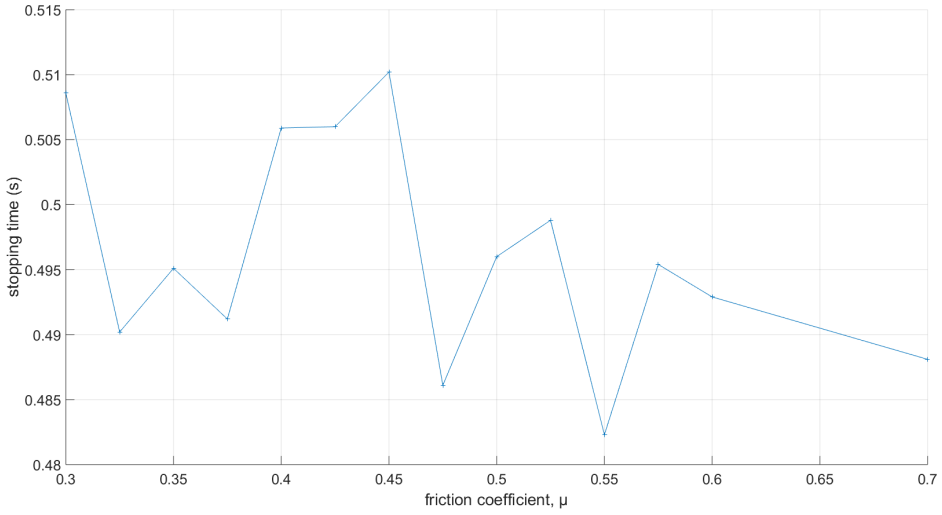

(c) When the static and dynamic friction coefficients are equal, $\mu = \mu_s = \mu_d$.

Figure 17: Stopping time as a function of friction coefficient, μ.

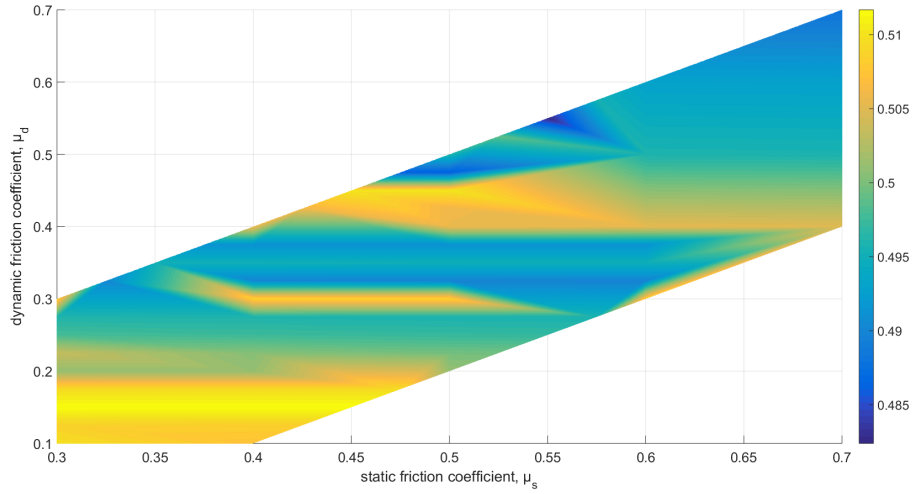

(a) Two-dimensional mesh function graph.

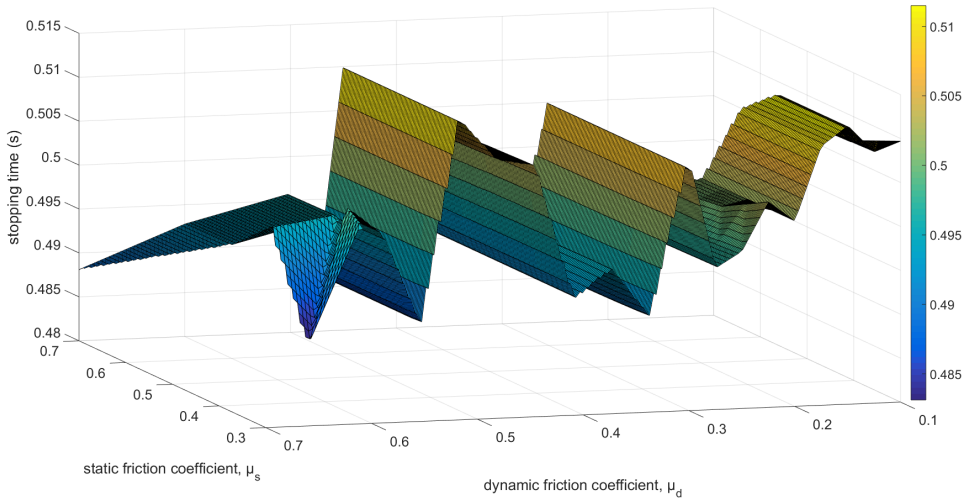

(b) Three-dimensional surf function graph.

Figure 18: Distribution of stopping times depending on the friction coefficients.

4.2 Emergency Brake for Winch

The brake arm rotates to a distance of approximately 14.116 millimetres from the pendulum zero limiter before the brake pad makes contact with the brake drum. This corresponds to 10.014 degrees, or 0.175 radians.

4.2.1 Mass Body Dependence

In figure 19, the lowest constant rotational speed possible to avoid activation and magnitude of applied decelerating force needed for activation of the brake arm is plotted against weight of the pendulum bob. The angular velocity ranges from 1281.63 revolutions per minute to 905.36 revolutions per minute. The force ranges from 12100 newtons to 26300 newtons. Data from the simulations is found in table A.1.2.

In figure 20, the lowest constant rotational speed possible to avoid activation and magnitude of applied decelerating force needed for activation of the brake arm is plotted against the position of the pendulum bob's mass centre. The angular velocity ranges from 3545.99 revolutions per minute to 515.94 revolutions per minute. The force ranges from 2800 newtons to 54500 newtons. Data from the simulations is found in table A.1.3.

Note for both figures, the magnitude of force is a lot larger compared to the universal brake system for multiplier reels.

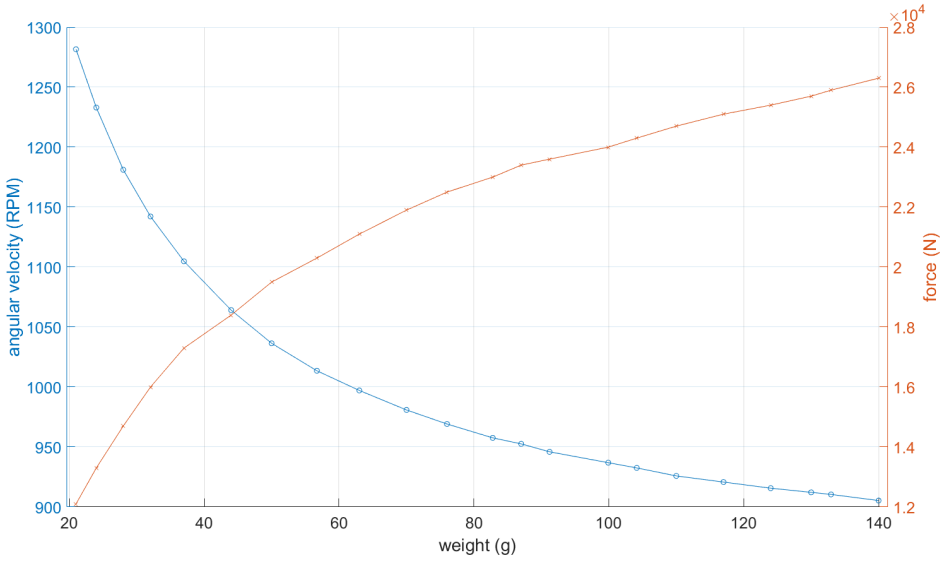

Figure 19: The influence of an alternating pendulum bob weight.

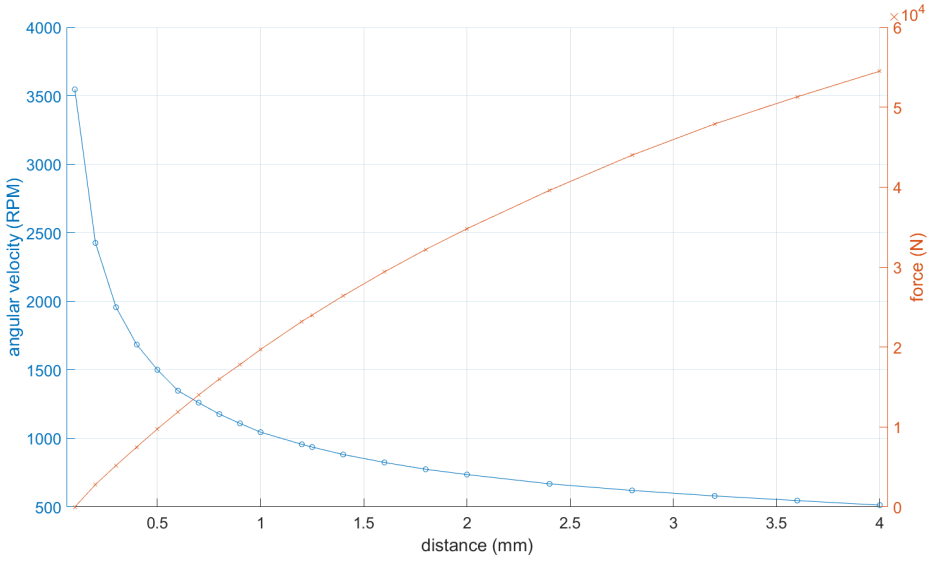

Figure 20: The influence of an alternating mass centre location for the pendulum bob.

4.2.2 Friction Coefficient Dependence

The behaviour of this model of the brake system depending on the static and dynamic friction coefficients, μ_s and μ_d respectively, between the brake drum and pad is presented below in figures 21 to 23. Additionally, figures 24 and 25 show the results of the stopping time measurements.

As was the case for the universal brake system in section 4.1.2, figure 21 shows the general behaviour of the brake system after activation by deceleration until it reaches a full stop. Presented are the angular velocity in revolutions per minute and the contact force in newton.

The following graph, figure 22 shows the differences between a wide range of coefficients. Again, note the case $\mu_s = 0.3$, $\mu_d = 0$ which is close to the same as if the brake pad had no effect on the speed. For easier interpretation, the dynamic friction has once more been indicated adjacent to each of the lines in the zoomed-in view, figure 22b.

Figure 23 is a number of runs with μ_s always set to 0.3. The difference in μ_d is here smaller in order to compare the distribution of lines to figure 22.

This model as well is more influenced by the dynamic friction coefficient than the static, as seen when comparing figure 24a to figure 24b. Figure 24c is the stopping times for the cases when the coefficients are equal.

Remember the implementation of the pseudo values in figure 25b, making it show the expected behaviour while 25a only presents the raw data according to how close each point is to the measured values. The reaction and swing out times did not change for different friction coefficients. A detailed table of all measured results can be found in the appendix, table A.2.2.

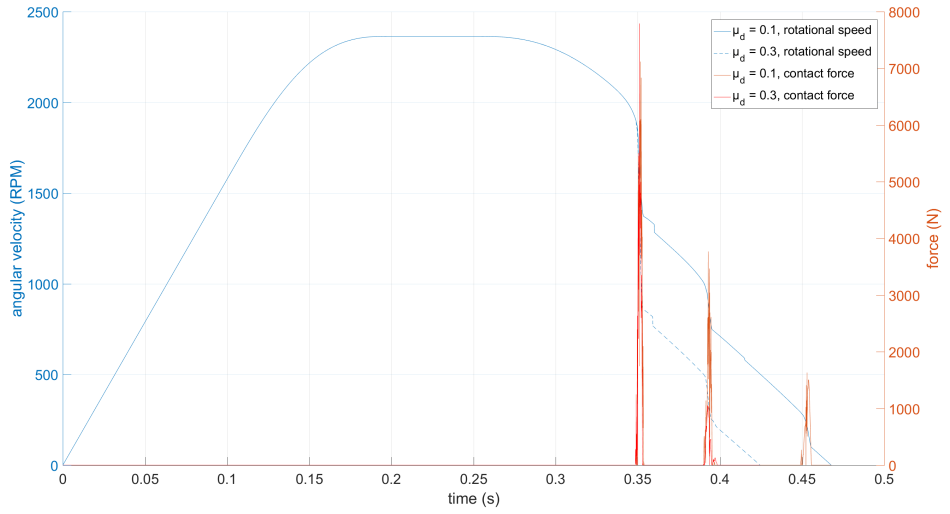

Figure 21: General behaviour of the brake system for static friction coefficient $\mu_s = 0.3$.

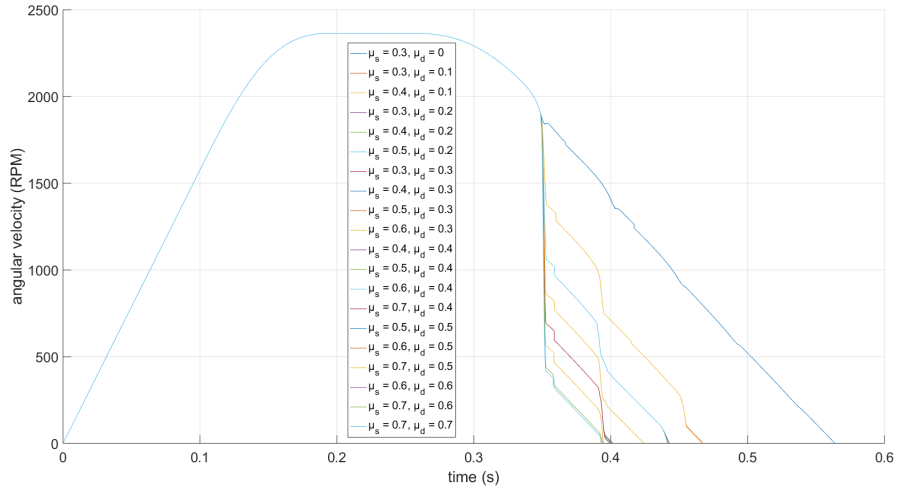

(a) Complete run.

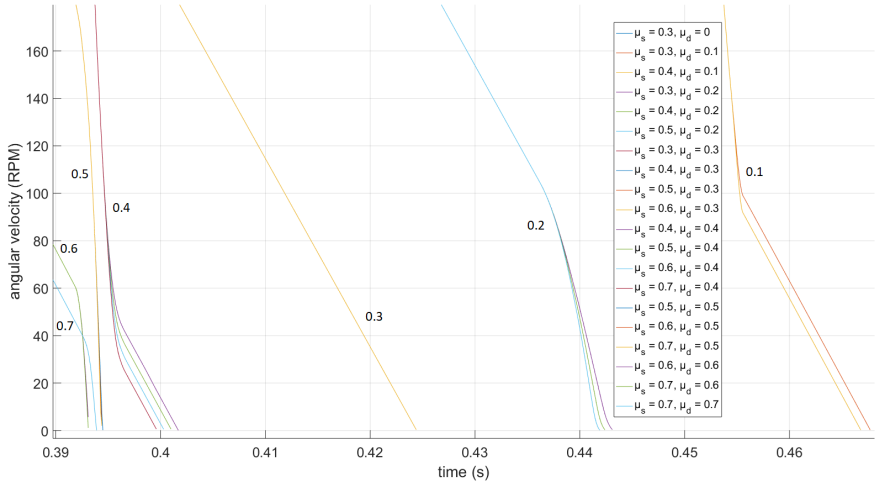

(b) Zoomed-in view.

Figure 22: Behaviour of the brake system for different friction coefficients.

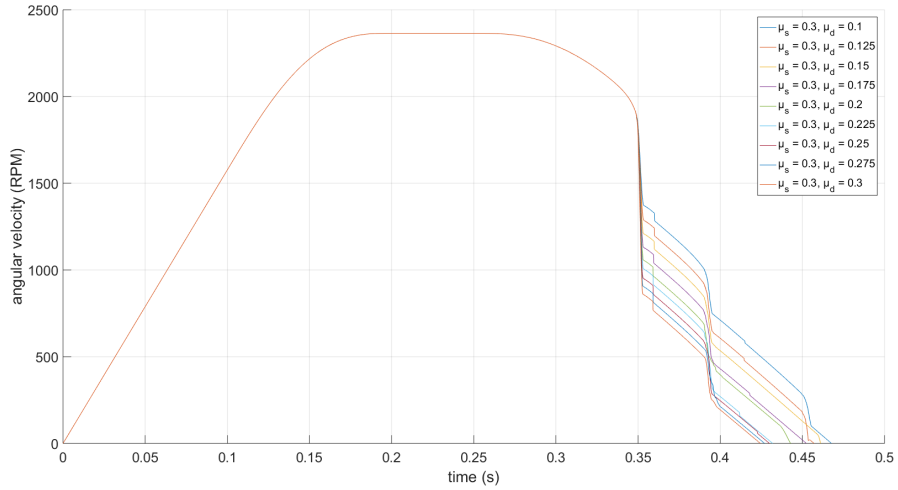

(a) Complete run.

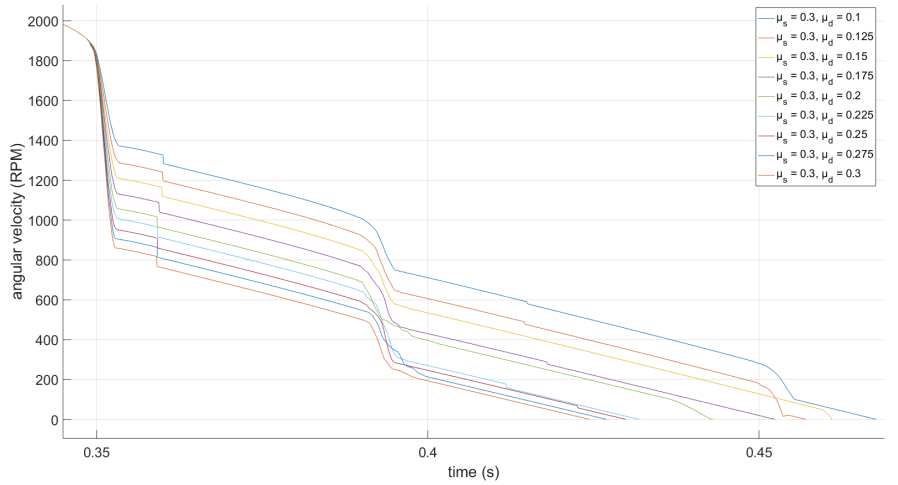

(b) Zoomed-in view.

Figure 23: Behaviour of the brake system for different dynamic friction coefficients with $\mu_s = 0.3$.

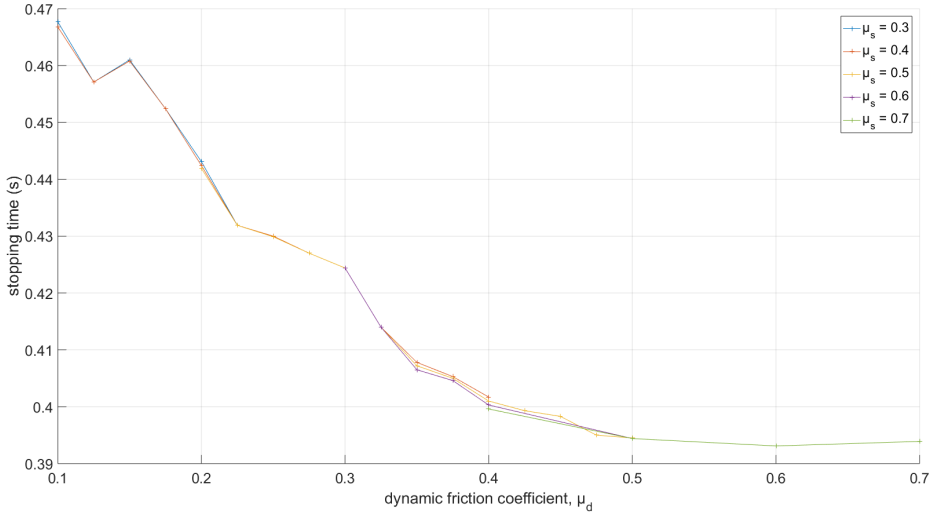

(a) μ = dynamic friction coefficient, μ_d

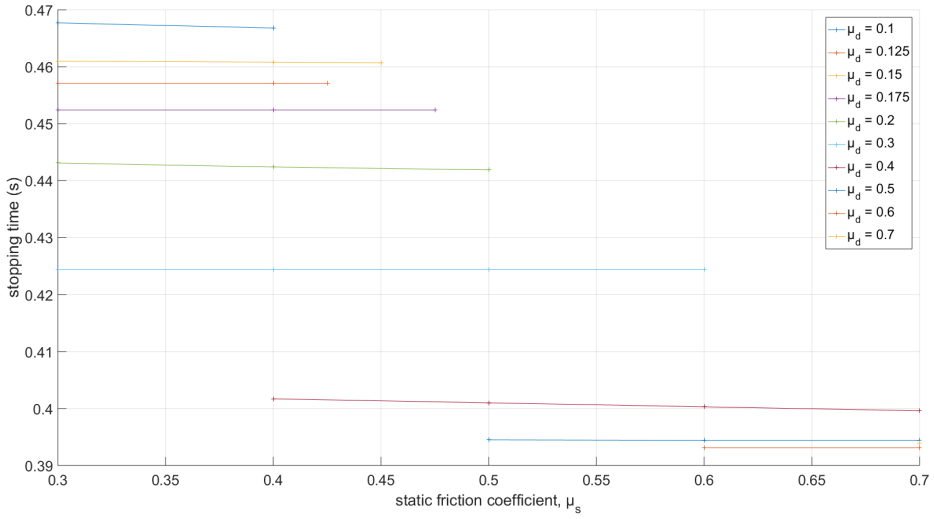

(b) μ = static friction coefficient, μ_s

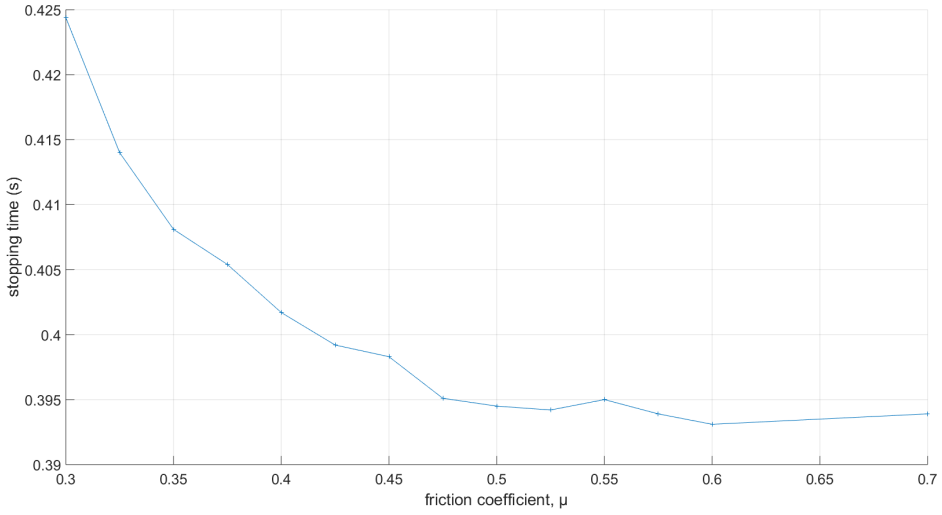

(c) When the static and dynamic friction coefficients are equal, $\mu = \mu_s = \mu_d$.

Figure 24: Stopping time as a function of friction coefficient, μ.

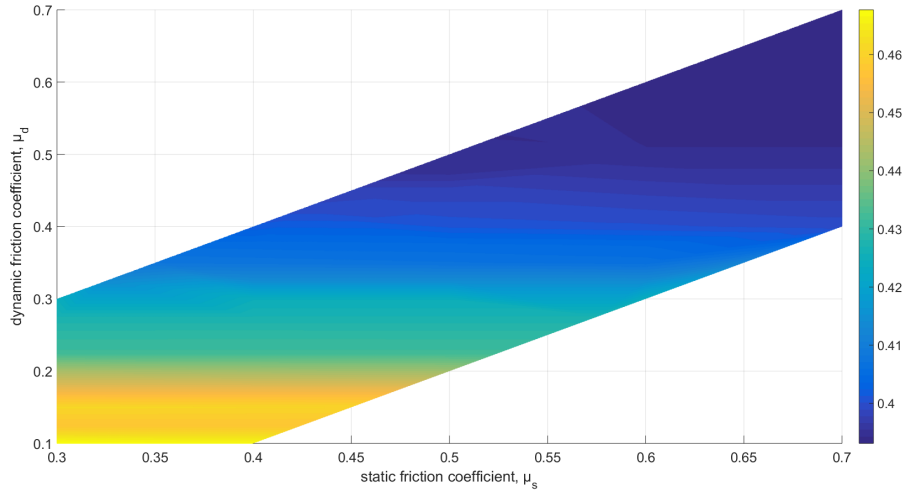

(a) Two-dimensional mesh function graph.

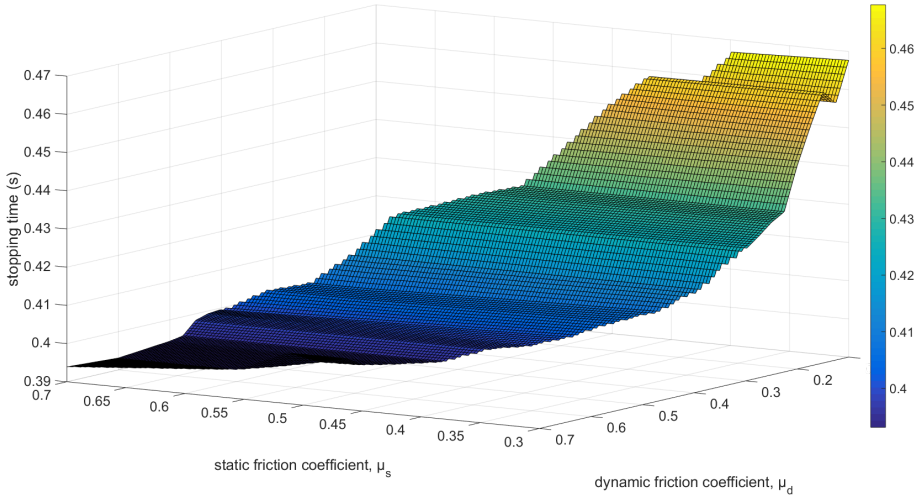

(b) Three-dimensional surf function graph.

Figure 25: Distribution of stopping times depending on the friction coefficients.

4.2.3 Distance Between Brake Drum and Brake Pad

A general idea of how the braking is affected by the distance between the brake drum and brake pad can be seen in figure 26. A polynomial curve had been fitted to the values in order to show the correlation between reaction time and the distance. The assumption is made that for the lower distances the curve will be more incorrect, as the time should approach zero.

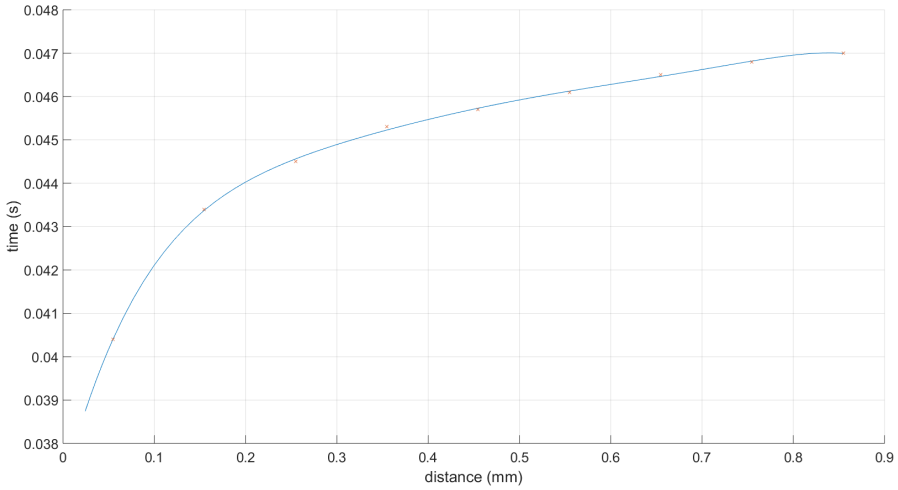

Figure 26: Reaction time plotted against the distance between the brake drum and brake pad.

4.3 Web Tension Control for Spools

The brake arm rotates to a distance of approximately 3.685 millimetres from the pendulum zero limiter before the brake pad makes contact with the brake drum. This corresponds to 2.670 degrees, or 0.047 radians.

It is noted that if the added mass body is too large, deactivation of the brake is hard to obtain.

4.3.1 Mass Body Dependence

In figure 27, the lowest constant rotational speed possible to avoid activation and magnitude of applied decelerating force needed for activation of the brake arm is plotted against weight of the pendulum bob. The angular velocity ranges from 1234.06 revolutions per minute to 1003.96 revolutions per minute. The force ranges from 10600 newtons to 15550 newtons. Data from the simulations is found in table A.1.4

In figure 28, lowest constant rotational speed possible to avoid and magnitude of applied decelerating force needed for activation of the brake arm is plotted against the position of the pendulum bob's mass centre. The angular velocity ranges from 2423.94 revolutions per minute to 542.84 revolutions per minute. The force ranges from 1700 newtons to 32500 newtons. Data from the simulations is found in table A.1.5.

A translation of the mass centre for the pendulum bob in the positive direction from the zero reference line locates the equilibrium of the brake arm. The magnitude of the translation is approximately 0.5 millimetres.

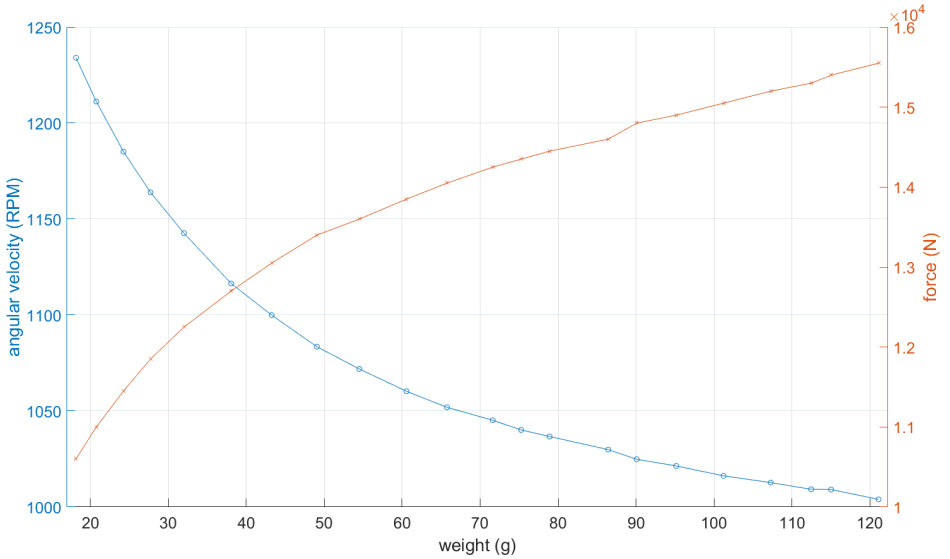

Figure 27: The influence of an alternating pendulum bob weight.

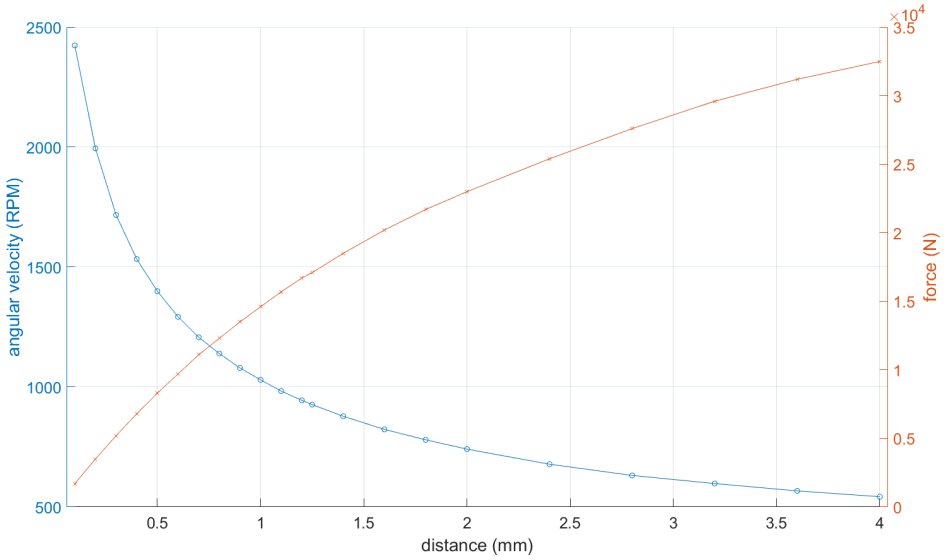

Figure 28: The influence of an alternating mass centre location for the pendulum bob.

4.3.2 Friction Coefficient Dependence

The behaviour of the web tension control brake system depending on the static and dynamic friction coefficients, μ_s and μ_d respectively, between the brake drum and pad is presented below in figures 29 to 31. Additionally, figures 32 and 33 show the results of the stopping time measurements.

Figure 29 shows the general behaviour of the brake system after activation by deceleration until it reaches a full stop. Presented are the angular velocity in revolutions per minute and the contact force in newton.

Figure 30 shows the differences between a wide range of coefficients. The case $\mu_s = 0.3$, $\mu_d = 0$ is again notable for being close to the same as if the brake did not activate. For easier interpretation, the dynamic friction has been indicated adjacent to each of the lines in the zoomed-in view, figure 30b.

Figure 31 is a number of runs with constant static friction, $\mu_s = 0.3$. The difference in μ_d is here smaller in order to compare the distribution of lines to figure 30.

The dynamic friction coefficient has a bigger influence on the stopping time than the static, as seen when comparing figures 32a and 32b. Figure 32c is the stopping times for the cases when the static and dynamic friction coefficients are equal.

Once more, figure 33b implements pseudo values to show the expected behaviour while 33a does not. The reaction and swing out times were not dependent on the friction coefficients. A detailed table of all measured results can be found in the appendix, table A.2.3.

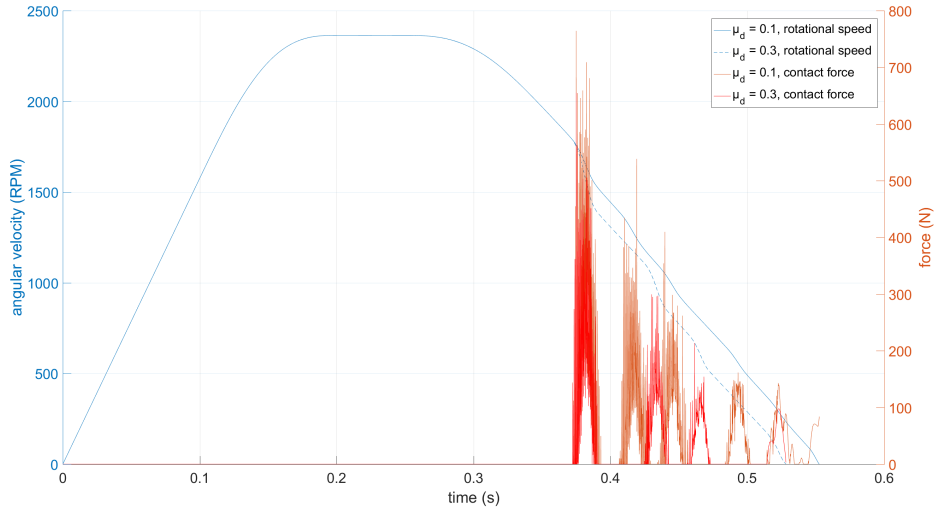

Figure 29: General behaviour of the brake system for static friction coefficient $\mu_s = 0.3$.

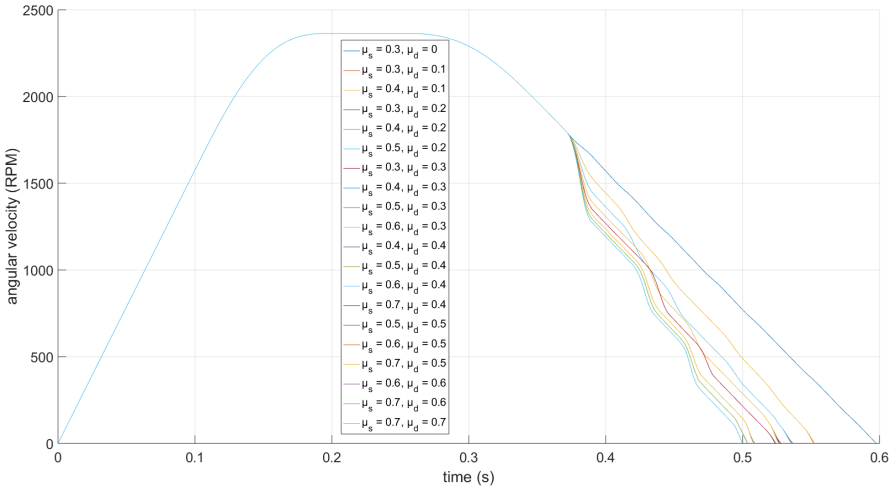

(a) Complete run.

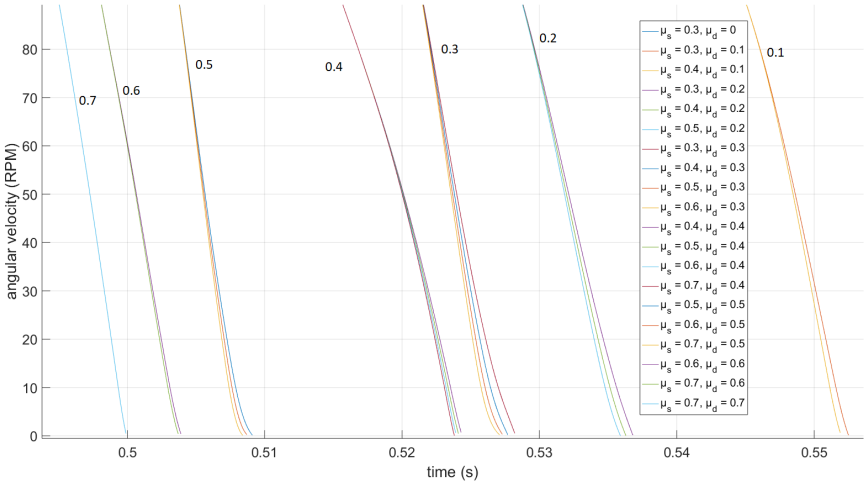

(b) Zoomed-in view.

Figure 30: Behaviour of the brake system for different friction coefficients.

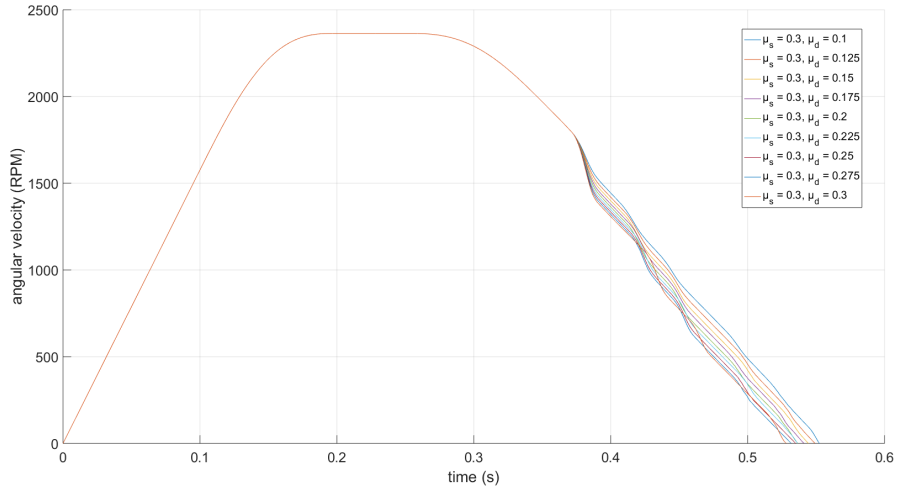

(a) Complete run.

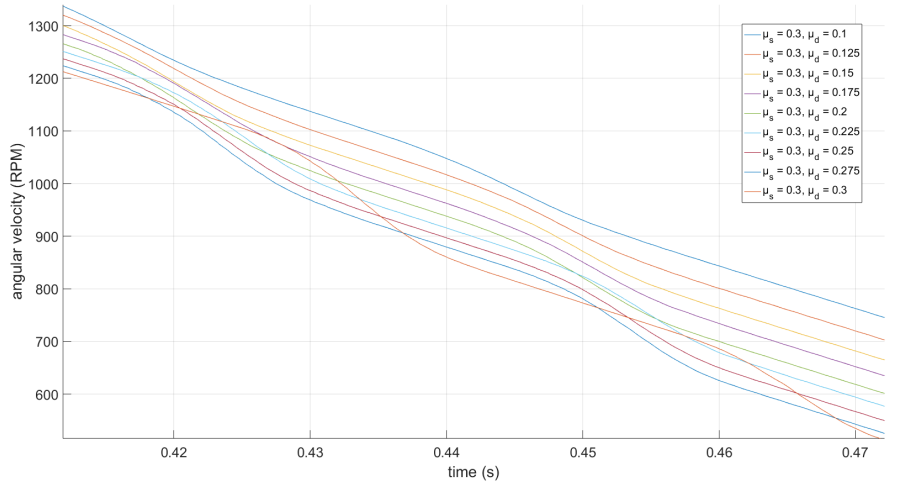

(b) Zoomed-in view.

Figure 31: Behaviour of the brake system for different dynamic friction coefficients with $\mu_s = 0.3$.

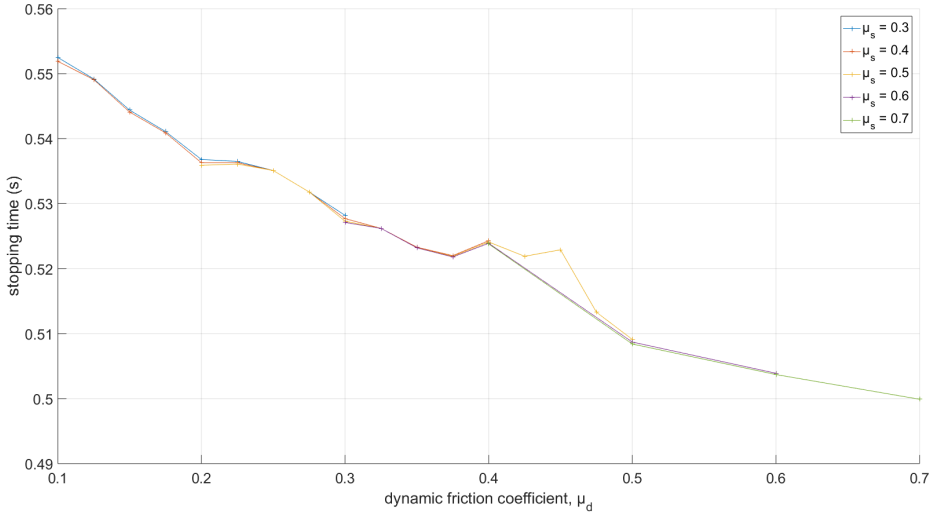

(a) μ = dynamic friction coefficient, μ_d

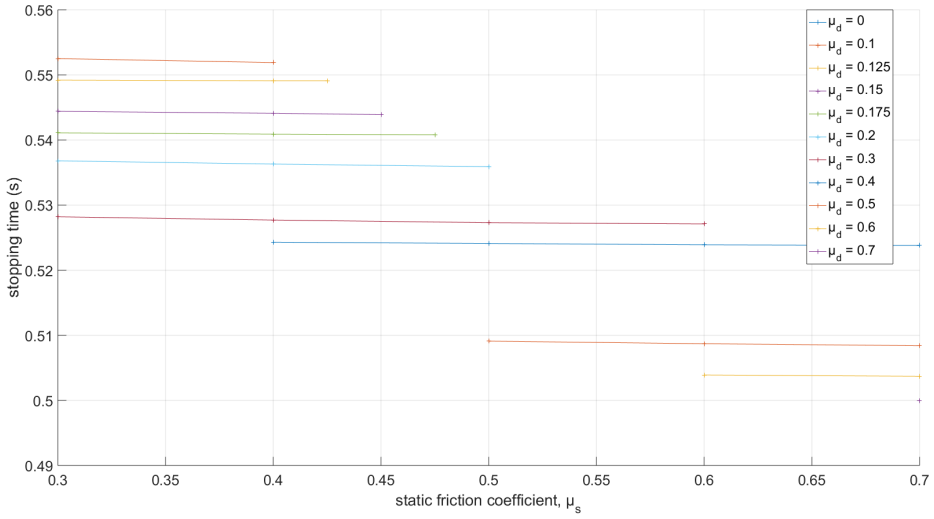

(b) μ = static friction coefficient, μ_s

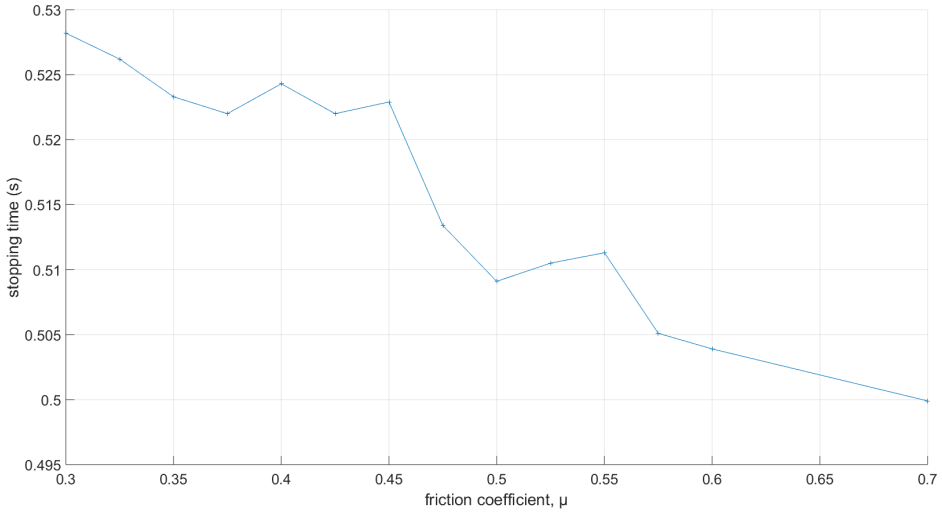

(c) When the static and dynamic friction coefficients are equal, $\mu = \mu_s = \mu_d$.

Figure 32: Stopping time as a function of friction coefficient, μ.

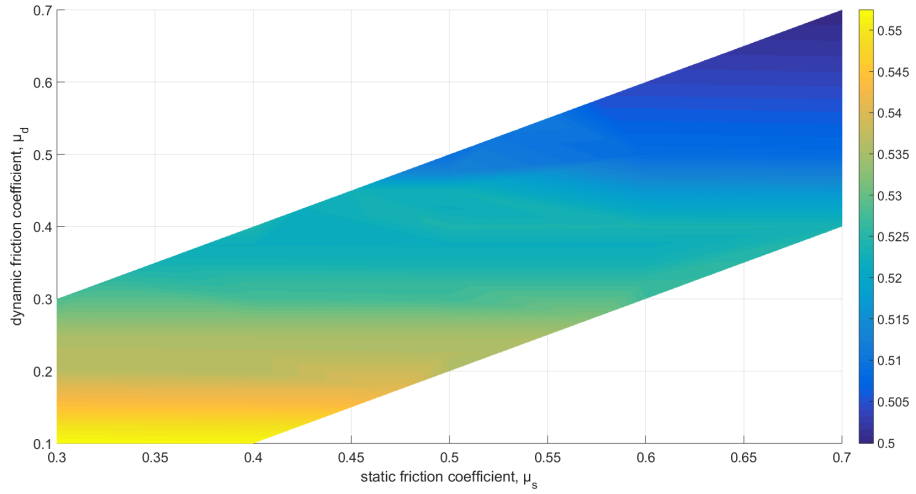

(a) Two-dimensional mesh function graph.

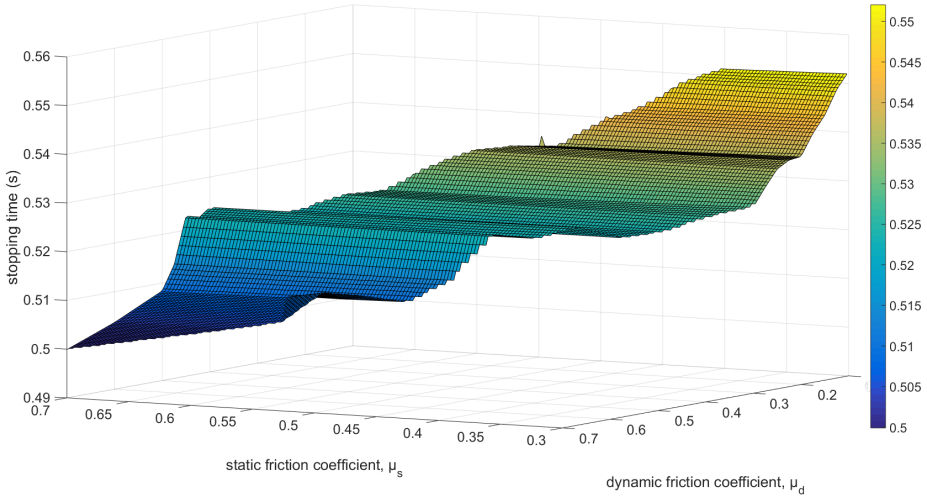

(b) Three-dimensional surf function graph.

Figure 33: Distribution of stopping times depending on the friction coefficients.

4.3.3 Spring Stiffness Dependence

The way the web tension control system behaves according to the stiffness, k, of the spring is presented below in figures 34 to 36. Additionally, figure 37 shows the results of the stopping time measurements.

Figure 34 shows the behaviour of the brake system for selected values of stiffness k. The brake system is activated by deceleration and then run until it reaches a full stop. Presented are the angular velocity in revolutions per minute and the contact force in newton.

Figure 35 shows the differences between a wide range of coefficients. Of special note is $k = 100$ N/mm which shows signs of the system failing, e.g. the brake arm hitting the brake drum. Look for the sudden increase in angular velocity around the 0.4 second mark.

Figure 36 is a number of runs with the coefficients closer in value. Upon closer examination, as in figure 36b, it is apparent that the slower the speed after the initial activation of the brake, i.e. the heavier the braking, the longer the time it takes to stop.

Figure 37 is the sole representative graph for the spring stiffness dependence of the stopping time. For high enough values, around 500 N/mm and higher, the stopping time stays pretty much the same, whereas for low enough values, in this case lower than 140 N/mm, the brake system is unstable. This is because the brake arm swung so widely, to the point of hitting the brake drum. Therefore the info is best conveyed using a logarithmic scale was used for stiffness axis.

The reaction and swing out times were consistent for most stable runs. For the cases when the pendulum hits the brake drum, with these settings $k = 130$ N/mm and below, the reaction and swing out time vary greatly. The noted measurements can be found in the appendix, table A.3.1.

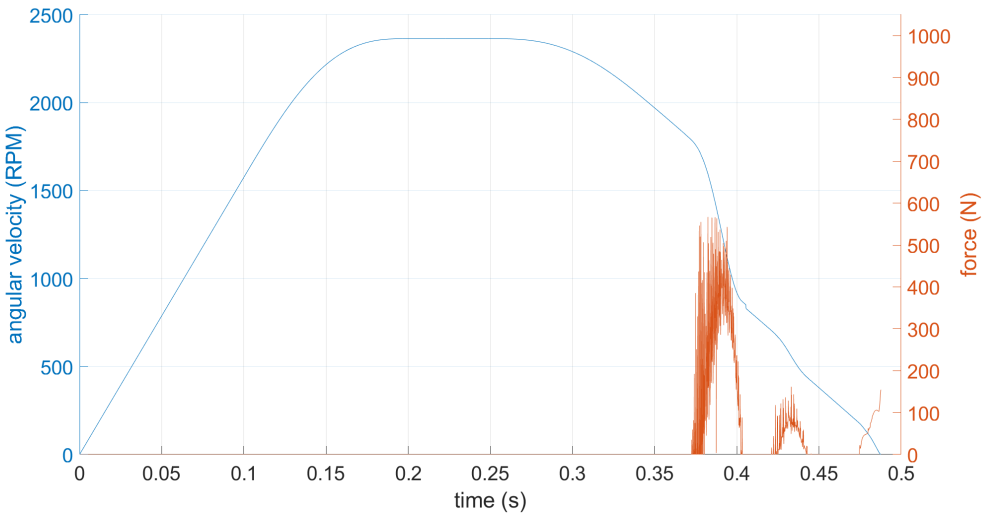

(a) $k = 200$.

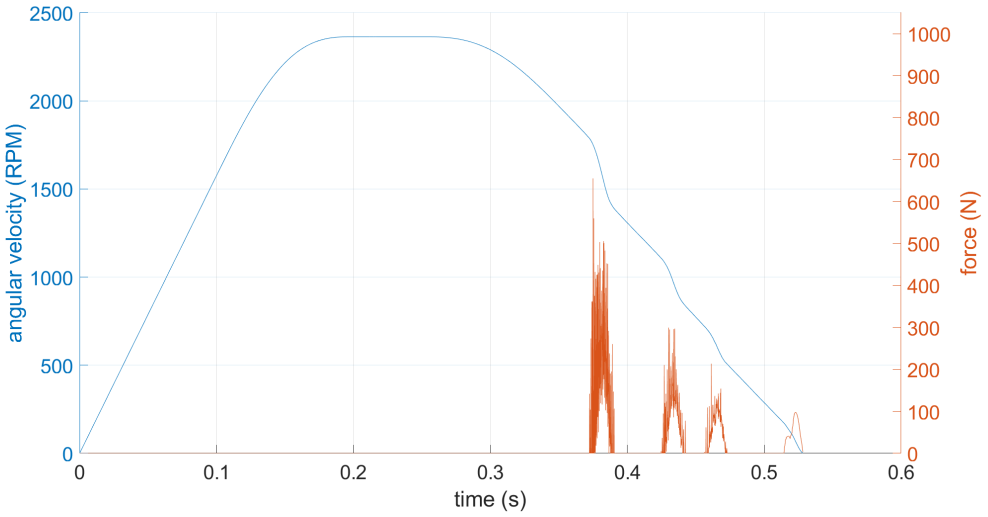

(b) $k = 500$.

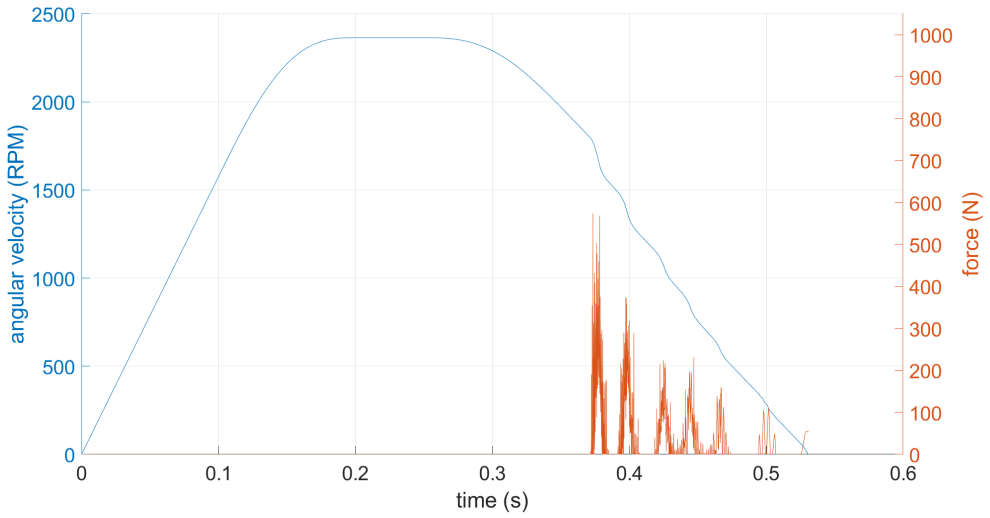

(c) $k = 2000$.

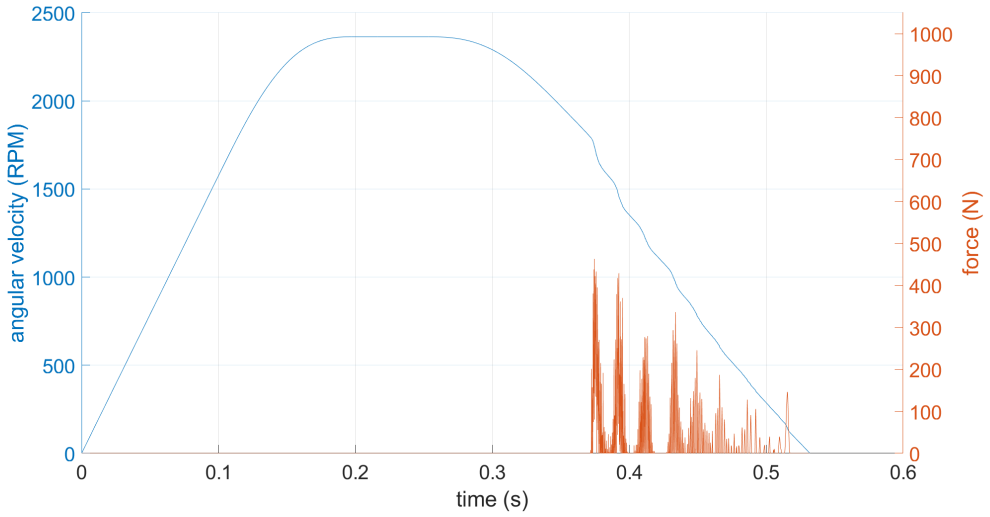

(d) $k = 7000$.

Figure 34: General behaviour of the brake system for different spring stiffness coefficients k.

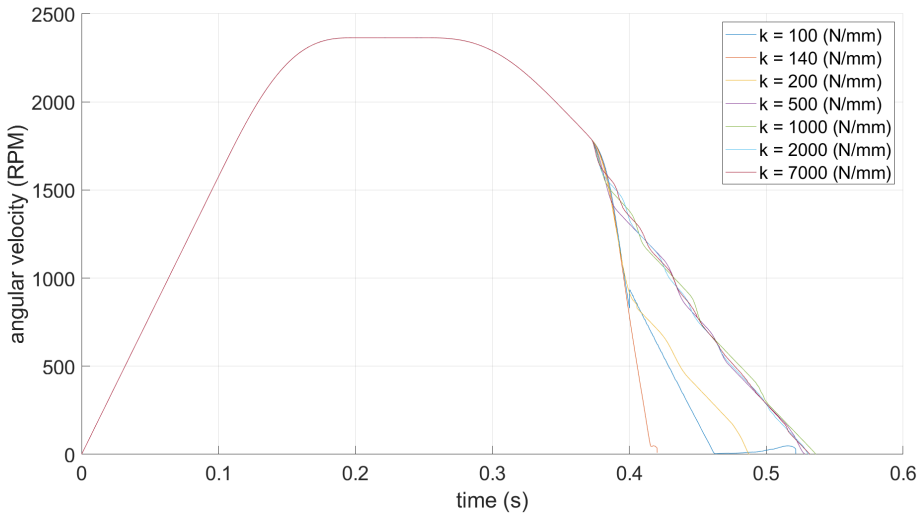

(a) Complete run.

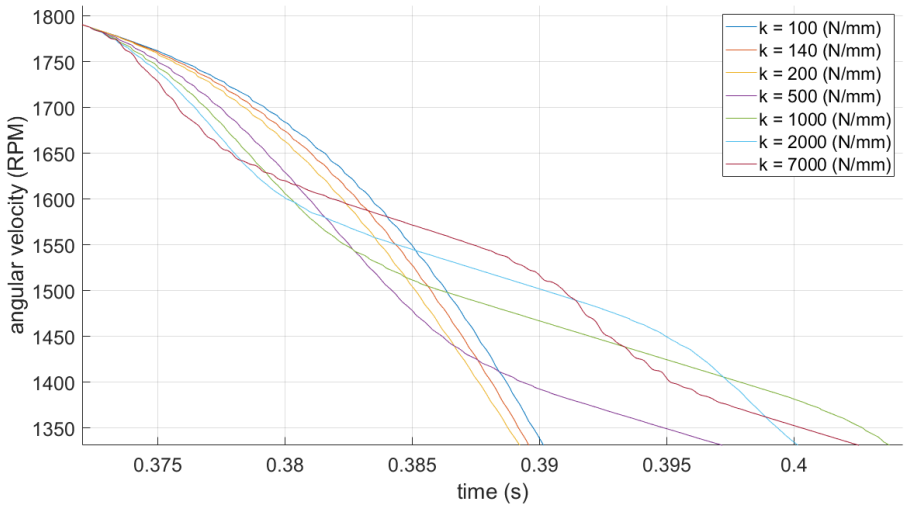

(b) Zoomed-in view.

Figure 35: Behaviour of the brake system for a large range of different spring stiffness coefficients.

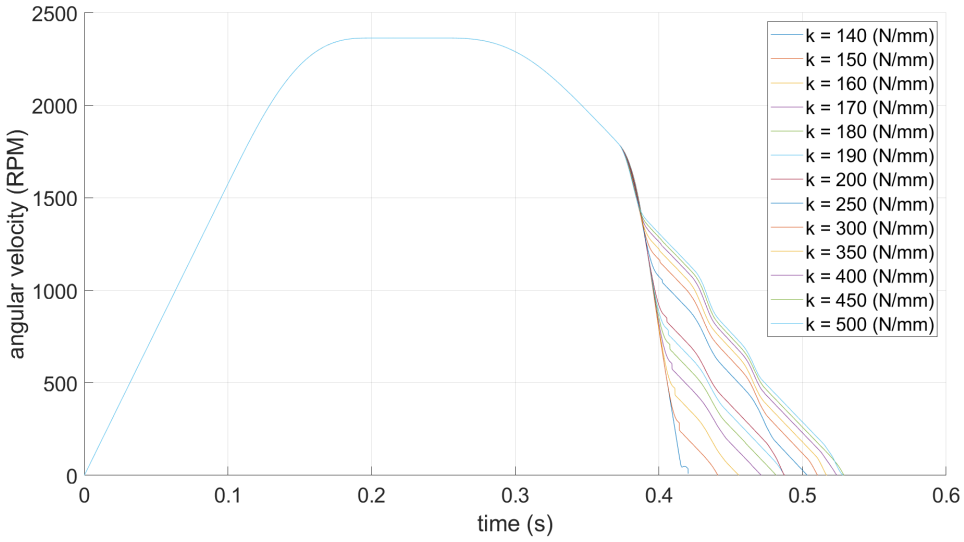

(a) Complete run.

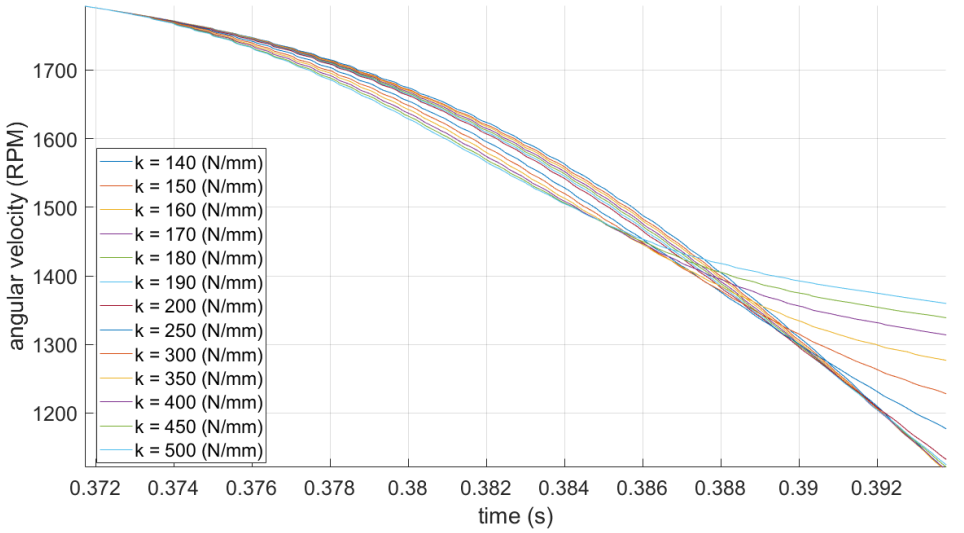

(b) Zoomed-in view.

Figure 36: Behaviour of the brake system for a small range of different spring stiffness coefficients.

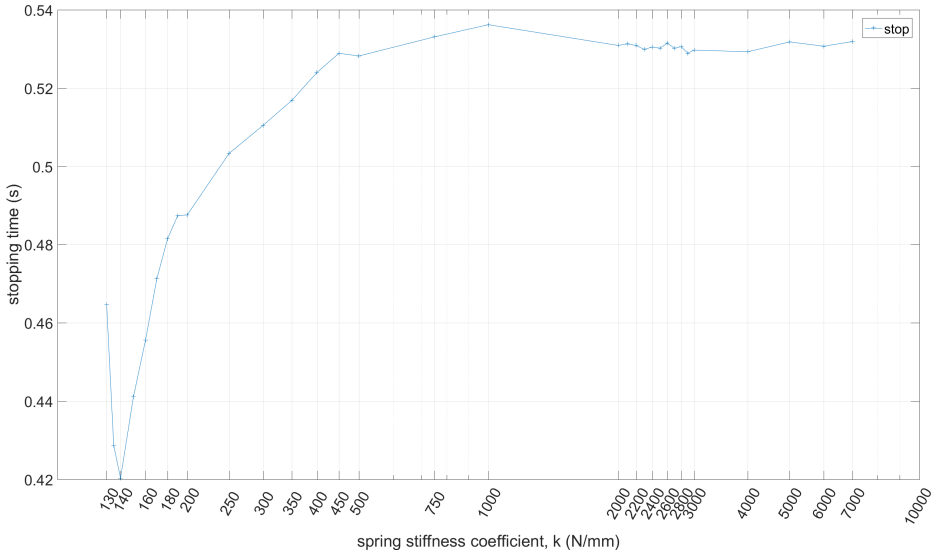

Figure 37: Stopping time as a function of spring stiffness, k.

Plots comparing the angle the arms swings out for different stiffness coefficients are seen in figure 38. The runs were evenly divided between those that periodically return all the way to the zero reference line each time they brake and those that do not. In figure 38a $k = 550$ N/mm is a borderline case where the first minimum does not reach zero.

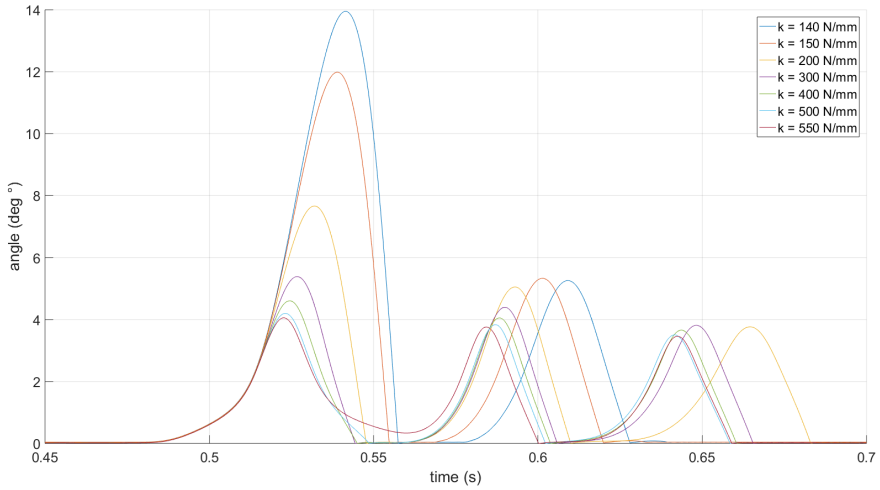

(a) Low stiffness coefficients.

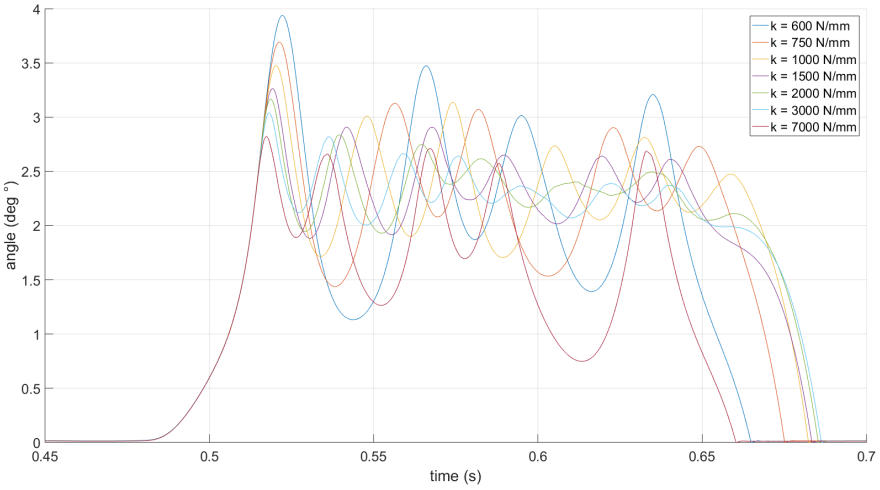

(b) High stiffness coefficients.

Figure 38: Position of the brake arm in terms of the angle swung out from the zero reference line.

4.3.4 Non-Linear Spring

Force applied on a linear spring with the stiffness 400 N/mm plotted against deformation is found in figure 39a. A sequence where the brake arm is activated and then deactivated is observed in figure 39b. The angular velocity of the brake axle and magnitude of the brake force is plotted against time.

Activation of the brake arm generates two distinct brake force peaks. The peaks have maximum magnitudes of just below 1100 and 600 newtons. The active duration is approximately 25.9 and 23.1 milliseconds. In the second peak, some values are much greater in magnitude than their neighbouring values. The angular velocity after deactivation is 1975.68 revolutions per minute.

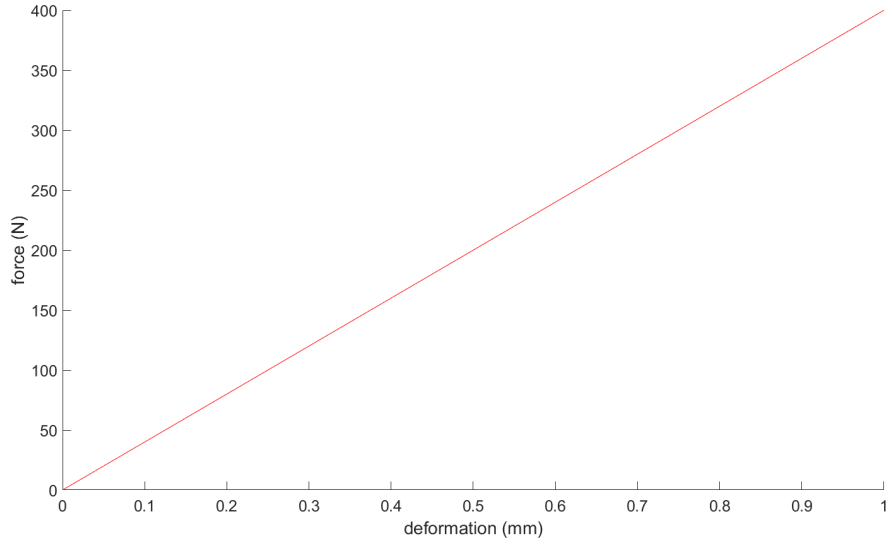

(a) Design for a linear spring

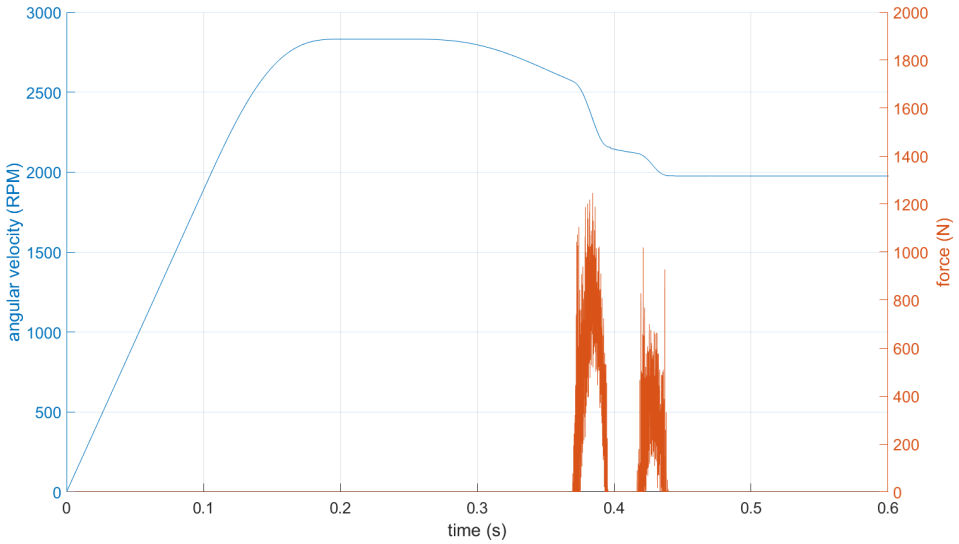

(b) A brake sequence for the spring

Figure 39: Appearance and a sequence for a linear spring.

Force applied on a logarithmic spring, with a spring stiffness comparable to the linear spring above, is plotted against deformation in figure 40a. A sequence where the brake arm is activated and then deactivated is observed in figure 40b. The angular velocity of the brake axle and magnitude of the brake force is plotted against time.

Activation of the brake arm generates three distinct peaks of the brake force magnitude. The peaks have maximum magnitudes of just above 800, 600 and 600 newtons. The active duration is approximately 17.4, 18.4 and 17.6 milliseconds. The angular velocity after deactivation is 2095.71 revolutions per minute.

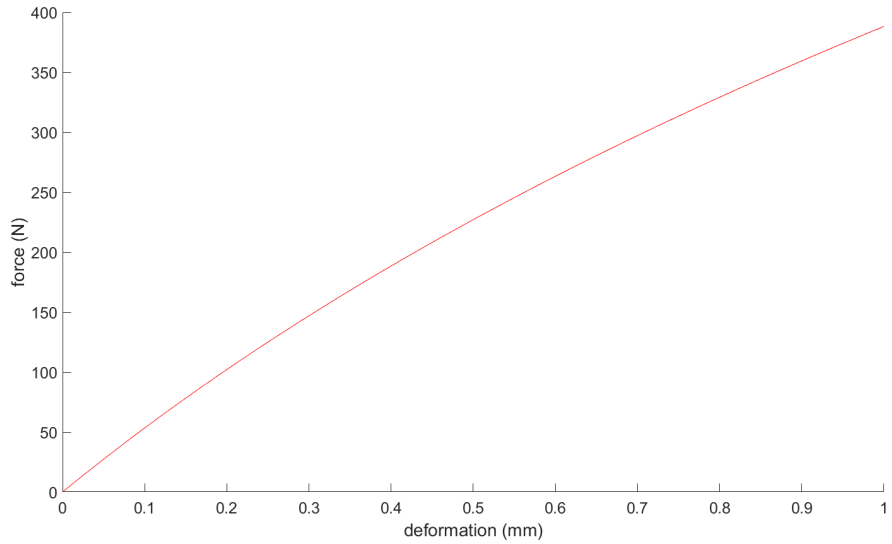

(a) Design for a logarithmic spring

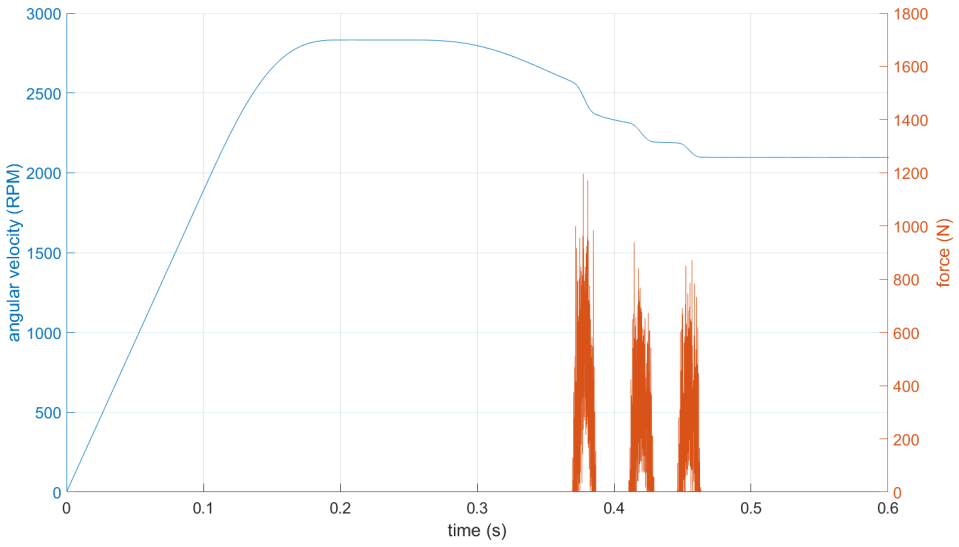

(b) A brake sequence for the spring

Figure 40: Appearance and a sequence for a logarithmic spring.

Force applied on an exponential spring, with a spring stiffness comparable to the linear spring above, is plotted against deformation in figure 41a. A sequence where the brake arm is activated and then deactivated is observed in figure 41b. The angular velocity of the brake axle and magnitude of the brake force is plotted against time.

Activation of the brake arm generates one distinct brake force peak. The peak has a maximum magnitude of just below 1200 newtons. The active duration is approximately 32.2 milliseconds. The angular velocity after deactivation is 1905.88 revolutions per minute.

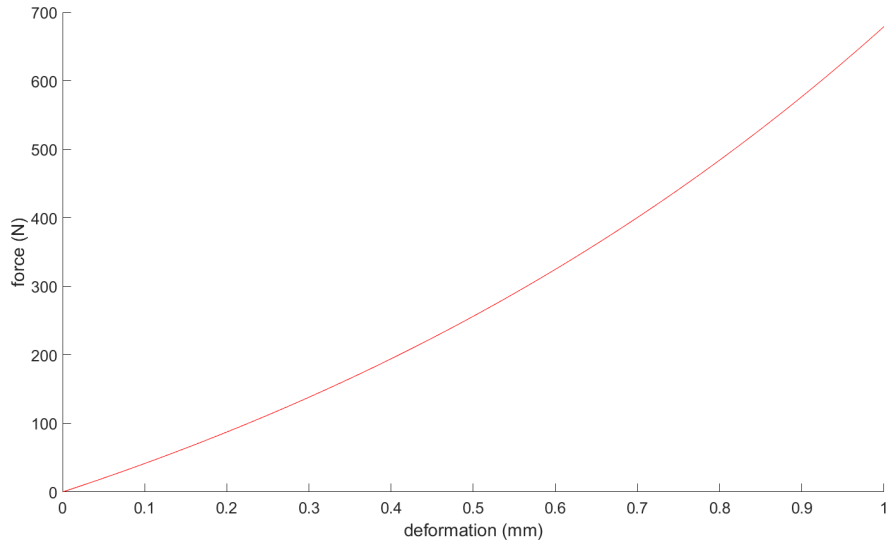

(a) Design for a exponential spring

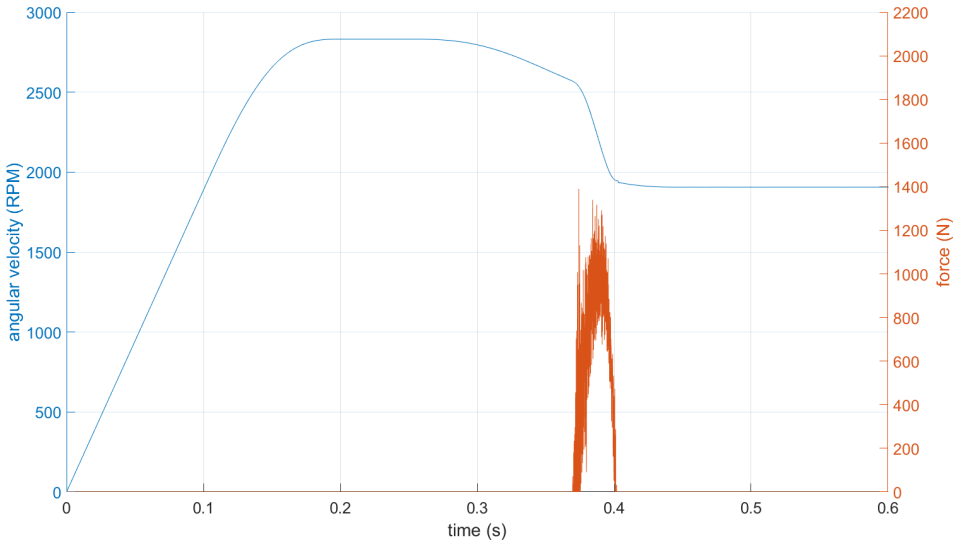

(b) A brake sequence for the spring

Figure 41: Appearance and a sequence for a exponential spring.

Figure 42a contains designs for some logarithmic springs. Applied force is plotted against deformation for each spring. A linear spring with spring stiffness 1000 N/mm is included for comparison. Stopping time for the springs are found in figure 42b. For the logarithmic springs, stopping times range from 0.5338 to 0.5364 seconds. Reaction and swing out times are determined equal for each spring.

Figure 43a contains designs for some exponential springs. Applied force is plotted against deformation for each spring. A linear spring with spring stiffness 1000 N/mm is included for comparison. Stopping times for the springs are found in figure 43b. For the exponential springs, stopping times range from 0.5340 to 0.5355 seconds. Reaction and swing out times are determined equal for each spring.

Figure 44a contains designs for additional exponential springs. Applied force is plotted against deformation for each spring. A linear spring with spring stiffness 1000 N/mm is included for comparison. Stopping times for the springs are found in figure 44b. For the exponential springs, stopping times range from 0.5123 to 0.5308 seconds. Reaction and swing out times are observed equal for each spring.

Data points for figures 42b, 43b and 44b are found in table A.3.3. The stopping time for the linear spring included for comparison is 0.5362 seconds.

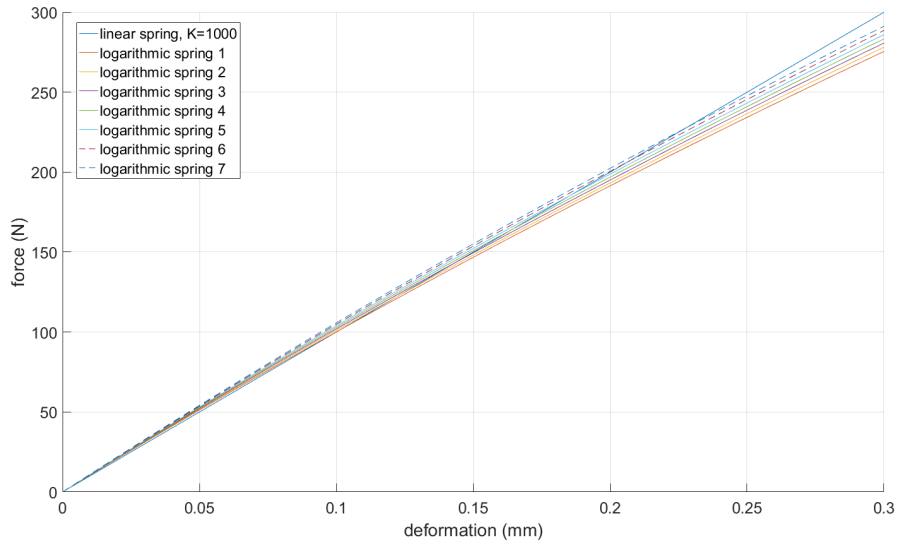

(a) Design for logarithmic springs.

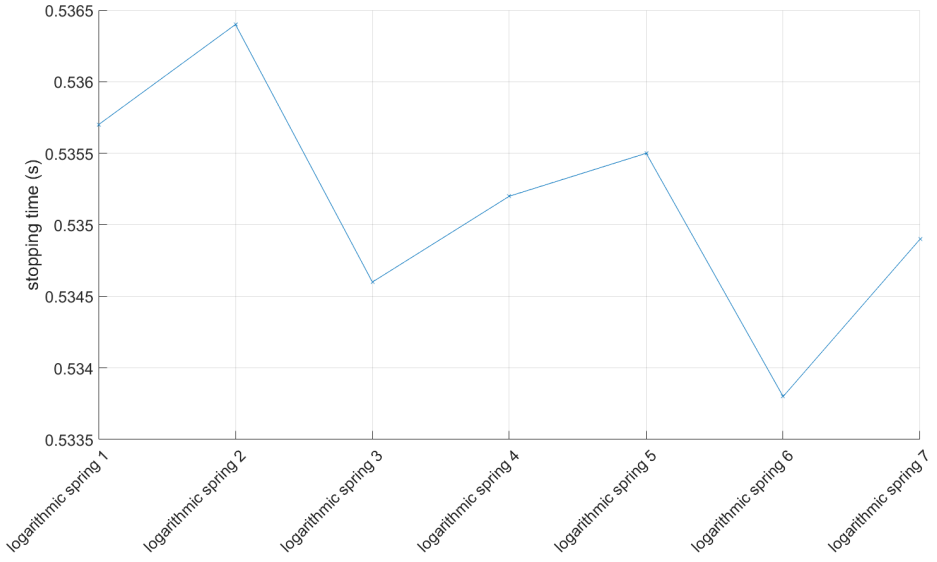

(b) Stopping time for logarithmic springs

Figure 42: Appearance and stopping time for a number of logarithmic springs.

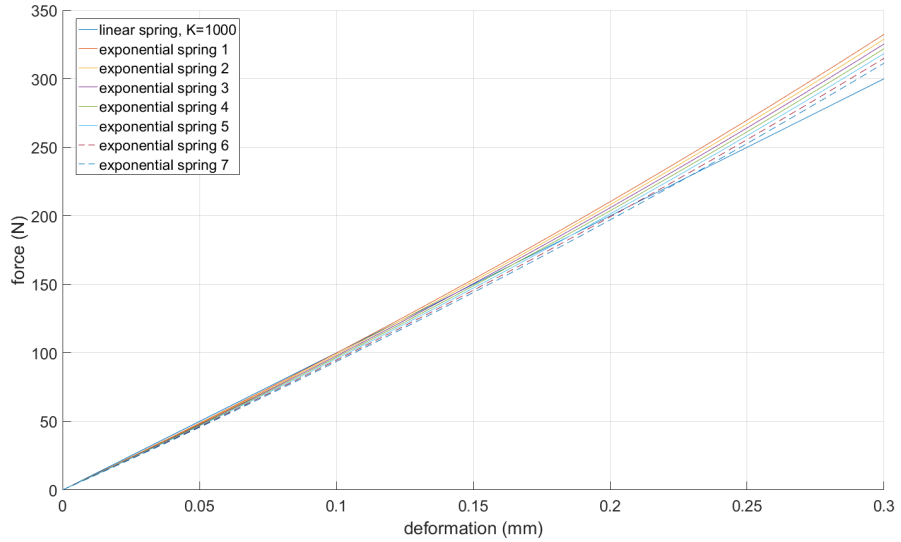

(a) Design for exponential springs.

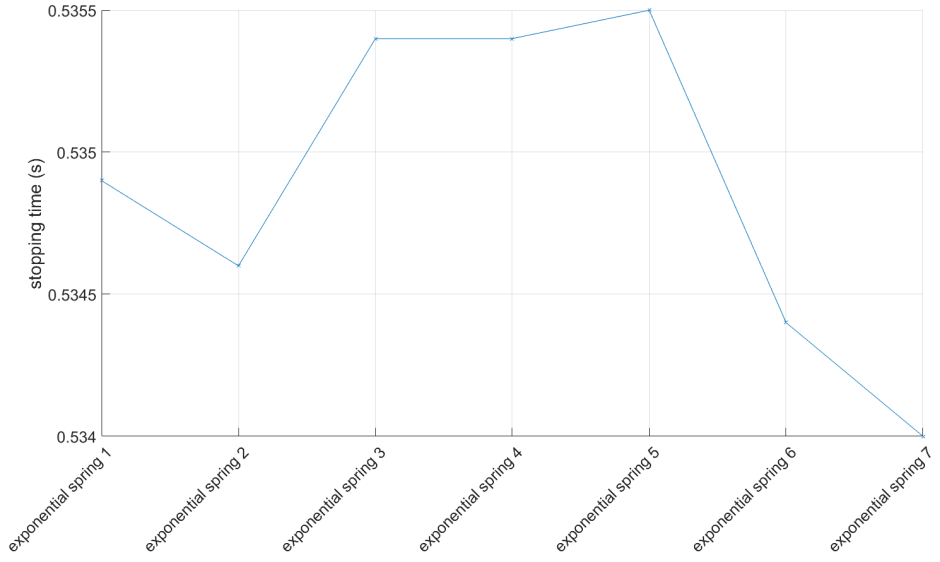

(b) Stopping time for exponential springs.

Figure 43: Appearance and stopping time for a number of exponential springs.

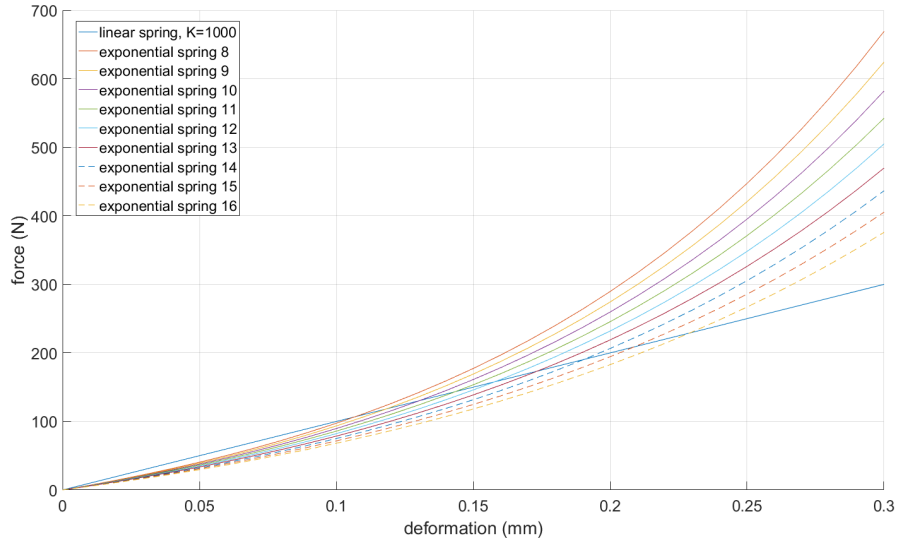

(a) Design for exponential springs.

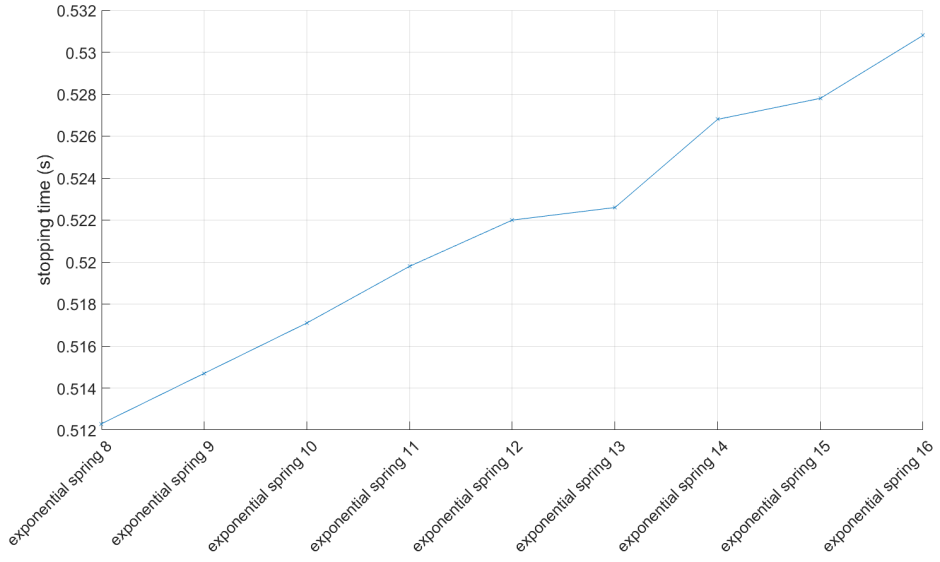

(b) Stopping time for exponential springs.

Figure 44: Appearance and stopping time for a number of exponential springs.

4.3.5 Comparison to Emergency Brake for Winch

The different results of the brake system models presented in sections 4.2.2 and 4.3.2 lend themselves to comparison in stopping time, thanks to the similarities in size and speed. Figure 45 is the stopping times in figure 33b, the web tension control for spools, subtracted with the times in figure 25b, the emergency brake for winch. Because of the nature of the results, figure 45a uses pseudo values in order to even out results.

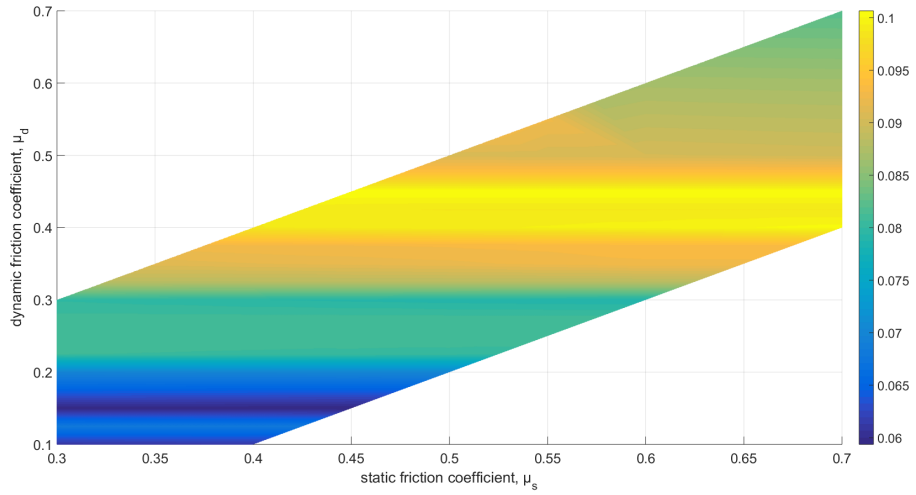

(a) Two-dimensional mesh function graph.

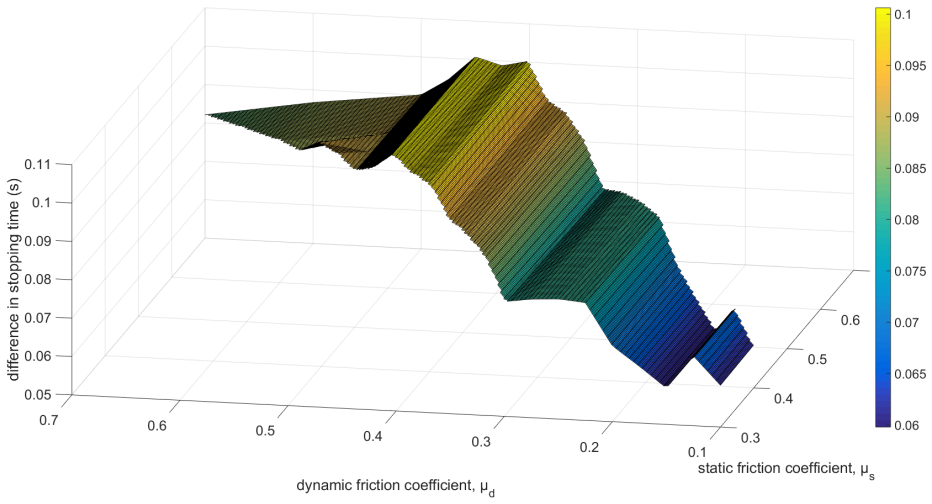

(b) Three-dimensional surf function graph.

Figure 45: Differences in the distribution of stopping times depending on the friction coefficients.

4.4 Building Sequences

Because of their similar values and in order to easily examine the behaviour in one graph, the angular velocity share axes with torque or force.

4.4.1 Torque Driven Model

The results of the torque-driven sequences are presented in figures 46 and 47. In figure 46 the brake arm does not swing back until the system has reached its target velocity. In figure 47 though, despite using the same settings for the braking, the arm swings all the way back to the zero reference line only in the middle of the third attempt.

The speed is visibly constant for the model alternating between higher speeds, but figure 46 shows the velocity eventually lowering. The first sequence also differs initially from the second in that the ball bearing friction is not sufficient to maintain that the external mass and brake axle keep the same speed.

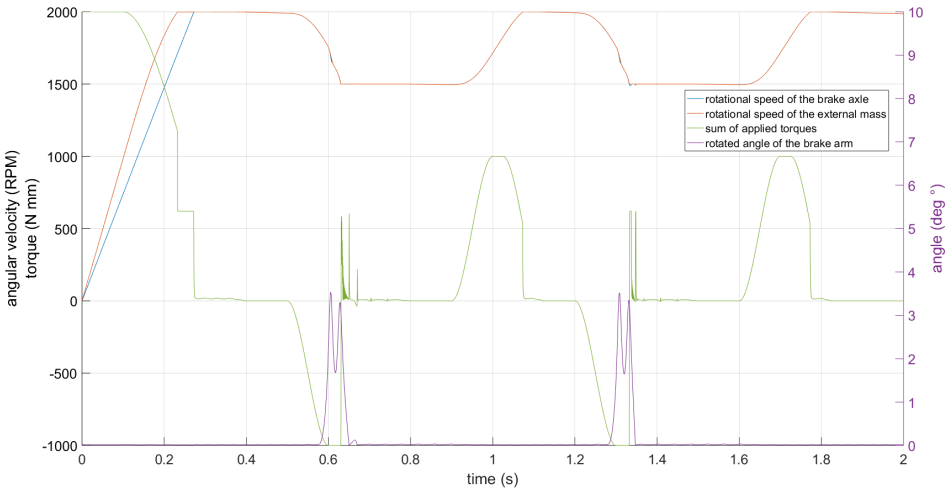

Figure 46: A simulation sequence interchanging lower speeds.

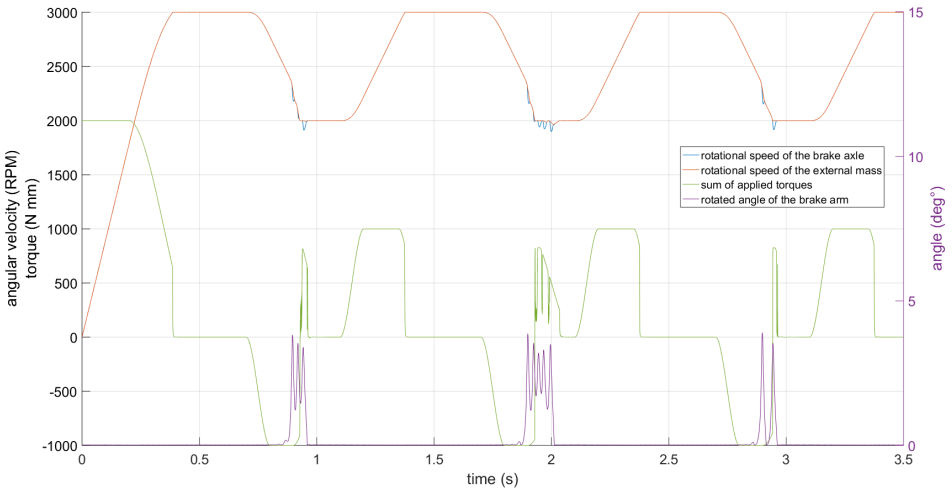

Figure 47: A simulation sequence interchanging higher speeds.

4.4.2 Angular Velocity Driven Model

In figure 48 and 49 two different sequences are found. For both, a 0.2 seconds long deceleration is applied and the spring stiffness is 2600 N/mm. The mass centre of the pendulum bob is located 0.45 and 0.43 millimetres from the zero reference line in the negative direction for figure 48 and figure 49 respectively. The friction coefficients in the revolute joint between the driving mass and the brake axle are $\mu_s = 0.5$ and $\mu_d = 0.5$ for both simulations.

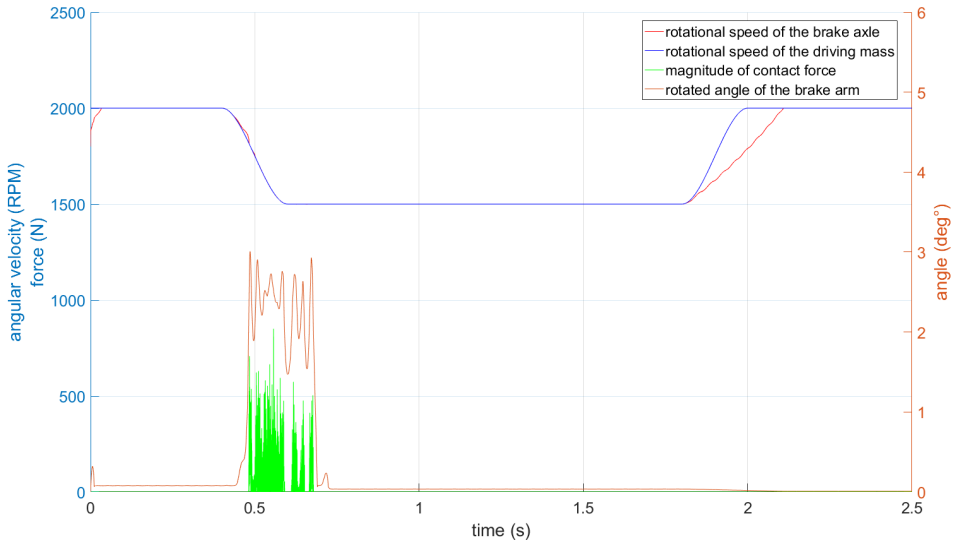

Figure 48: A simulation sequence with a 0.2 s long applied deceleration.

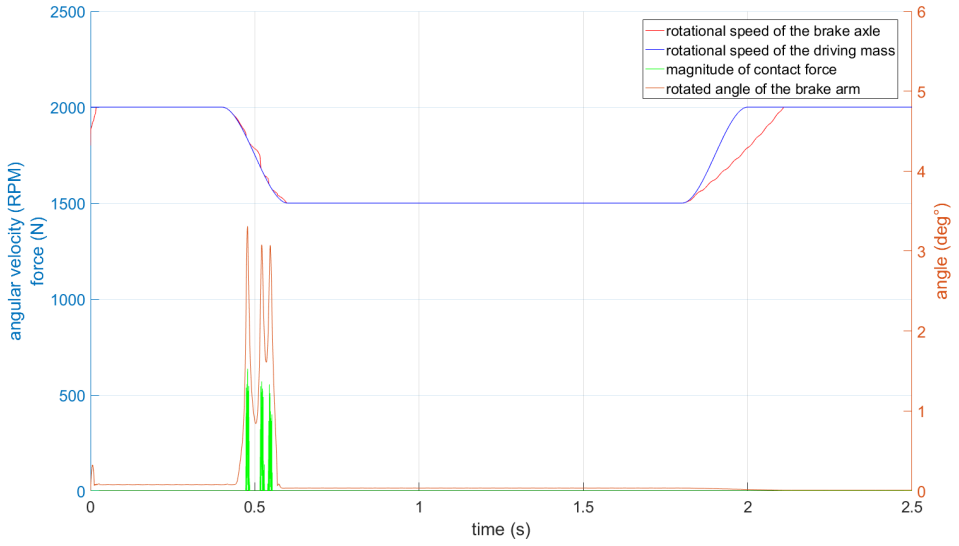

Figure 49: A simulation sequence with a 0.2 s long applied deceleration.

In figure 50, a simulation sequence with a 0.3 seconds long applied deceleration is found. The mass centre of the pendulum bob is located 0.50 millimetres from the zero reference line in the negative direction. The spring stiffness is 1000 N/mm. The friction coefficients in the revolute joint between the driving mass and the brake axle are $\mu_s = 0.5$ and $\mu_d = 0.5$.

In figure 51, a simulation sequence with a 0.6 seconds long applied deceleration is found. The mass centre of the pendulum bob is located 0.45 millimetres from the zero reference line in the negative direction. The spring stiffness is 900 N/mm. The friction coefficients in the revolute joint between the driving mass and the brake axle are $\mu_s = 0.28$ and $\mu_d = 0.28$.

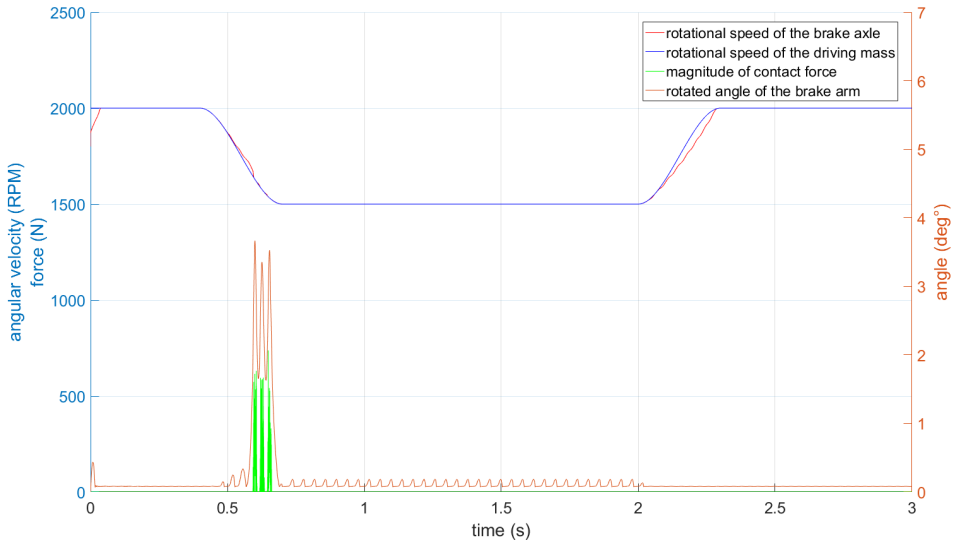

Figure 50: A simulation sequence with a 0.3s long applied deceleration.

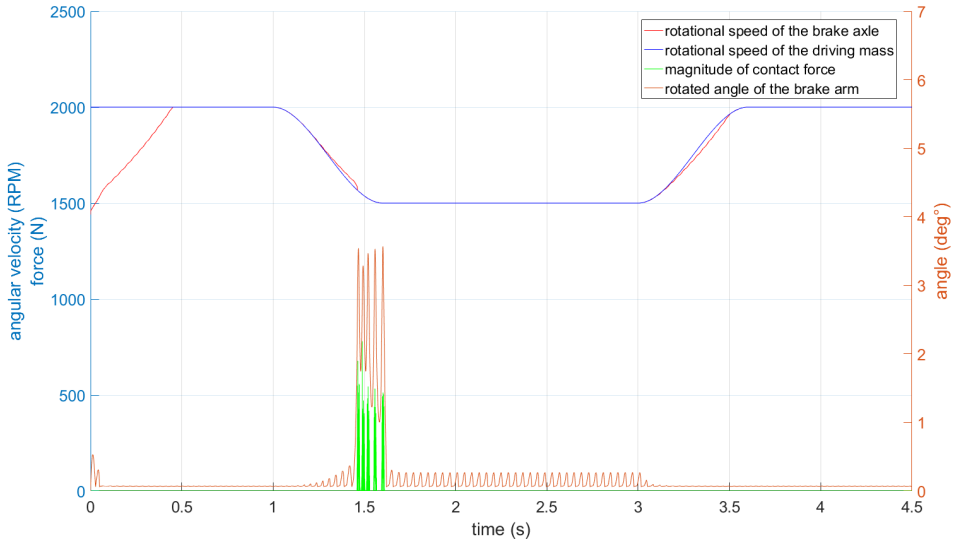

Figure 51: A simulation sequence with a 0.6s long applied deceleration.

4.5 Influence of Simulation Settings and Post Processing

Figure 52 shows the results obtained by using different simulation settings. Changed are time step size and integrator tolerance. Notice the spikes on the cruder run in figure 52b. The effect the MATLAB functions surf and mesh have on the visual representation was already brought up in section 3.3 and shown in figure 12.

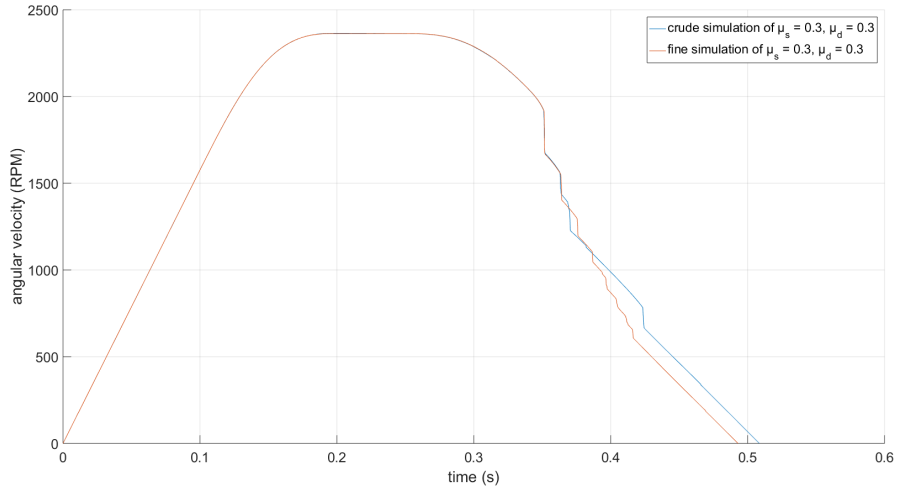

(a) Complete run.

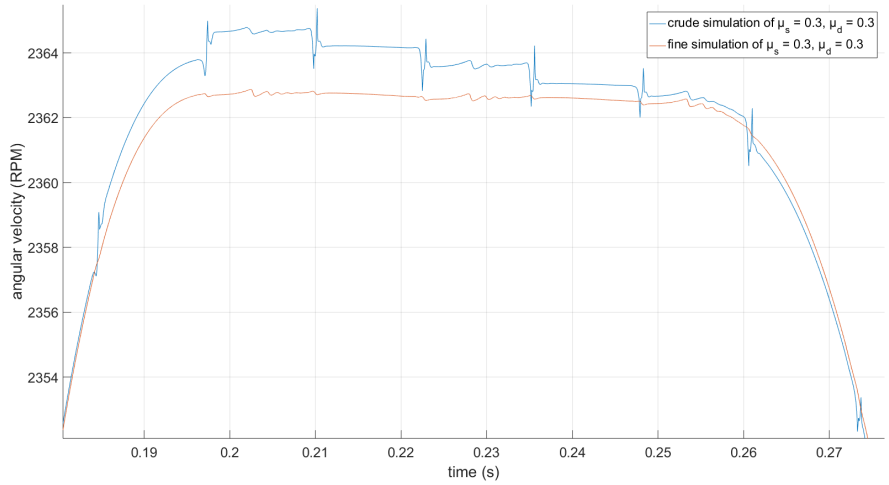

(b) Zoomed-in view.

Figure 52: Comparison between two runs, one of which uses cruder simulation settings while the other uses finer.

5 Discussion and Conclusions

5.1 Mass Body Dependence

The following is realised by observing the figures regarding mass body dependence. As the weight increases, the angular velocity needed to avoid activation of the brake arm due to gravity decreases. At the same time, the applied force needed for activation gets larger. As the pendulum bob's mass centre is translated in the negative direction of the zero reference line, the same behaviour is noted. Further away from the zero reference line, the slope gets weaker. Increased weight has the same effect as a translated mass centre, but the scope of the values is larger when alternating the mass centre. It is desired to have a constant rotational speed as low as possible to avoid activation as well as a low magnitude of deceleration needed for activation of the brake arm. As it is not possible to lower both of the parameters at the same, a trade-off between them depending on application of the brake system is needed. These conclusions hold for all models.

Regarding the web tension control for spools the mass centre of the pendulum bob was translated in the positive direction of the zero reference line to find the equilibrium point for the brake arm. This means the mass centre for the brake arm, without the pendulum bob, is located on the negative side. The brake arm is therefore not in equilibrium when the pendulum bob has not been rotated.

For the existing prototypes, adjustment of the pendulum bob mass centre is done by rotating it. To simplify the process during simulations, only translations in the x-direction were made. However, rotation of the pendulum bob also gives an altered y-coordinate but is assumed to not affect the function of the brake system. This is debatable because a longer pendulum behaves like a longer moment arm and less force is needed to get the same torque. How does this affect the moment of inertia? The distance from the zero-reference line may be a greater decisive factor, such that the effect of the pendulum arm length is unnoticeable. Simulations where only the y-coordinate was altered supports this, as only the angular velocity of the brake axle differed.

5.2 Friction Coefficient Dependence

In general during examination of the friction coefficient dependence, the contact force plot has spikes and at each of those the angular velocity decreases instantly. When the contact force is zero, the velocity decrease is the same as the benchmark but a curve can be seen just before the spikes. This is most noticeable in figure 21. For the web tension control model the spring ensures a smoother decrease in velocity and the contact force in figure 29 is not applied instantaneously but looks like a quadratic curve. It may be that the brake pad material in the other models was not flexible enough to allow for this type of braking.

The behaviour graphs for different friction coefficients in the universal brake system show that there is not quite a linear correlation for how the system behaves. The zoomed-in views on the other two models show that the runs bifurcate nicely just before the velocity reaches zero. That is because the influence of the static friction coefficient gets larger the closer the model is to stand still. Plotting the behaviour for the same static friction coefficient is a way of showing the dispersion between different μ_d values. Both types of comparison graphs show for all the models that the dependence on the dynamic coefficient impacts the behaviour significantly more than the dependence on the static. An exception is in figure 15b for $\mu_d = 0.1$ but that may be due to the somewhat coarser simulation settings.

In the behaviour graphs, the point at which the velocity reaches zero corresponds to the stopping time for each set of parameters. These times are presented for the models in 3D plots and above those are cross-sections of the plots to ease interpretation of the data. For the universal brake system in figure 17b the previously mentioned exception is apparent as the only line not to be near-horizontal. For all models these cross-section plots indicate that the static friction coefficient has nearly no influence on the stopping time. This confirms the assumption made when introducing the pseudo values to better the results from the 3D MATLAB plots. The dynamic friction coefficient in general shows a downward trend in time for higher values. Note that in for example figure 17a there appears to be a big difference between μ_s for $0.4 < \mu_d < 0.5$ but that is only due to which parameter pairs were selected to be simulated.

Comparing the stopping times for the emergency brake and the web tension control in figure 45 gives the impression that the emergency brake is the better model as it is quicker. The web tension control is increasingly much slower until $\mu_d \approx 0.4$ where the difference plateaus. However as the name implies, the behaviour shown for the emergency brake is an initial quick deceleration followed by uneven braking. The smoother web tension control for spools system is better suited for situations prone to overrun. Furthermore, as has been mentioned the difference in play are a few hundredths of a second.

All of these show that low friction coefficients, but rather not lower than $\mu = 0.1$ are the desired values to use. Stopping times for these are among the highest but the difference is negligible when talking about a few percent of a second in implementations that may take course over much larger durations. Higher friction coefficients lead to shorter stopping times, but exhibit undesirable behaviour. Too high values give too large contact forces and the rotated angle of the brake arm changes rapidly. This results in the "pulsating" behaviour of the force seen in for example figure 14. Lower values on the other hand result in smoother braking. Because of this, the stopping time will have a rather small difference when altering the friction coefficients.

5.3 Spring Stiffness Dependence

When examining the behaviour graphs for different spring stiffnesses it is apparent, by specifically looking at the force, that for higher values the number of times the arm swings in contact with the brake drum, the number of times it brakes, increases. Scale along the time axis might be misleading in figure 34a because the reaction time was the same for all measurements. Lower stiffnesses mean that the system brakes more smoothly and for a longer period of time each time. However, this also means that the decrease in velocity is not as even.

As mentioned in the results section for figure 36b, up to a certain level around $k \approx 1000$ N/mm as seen in the stopping time graph, higher values of k brake harder but then slow down less rapidly in-between. This is supported by figure 38 in which it can be seen that lower values of k swing further out from the zero reference line. Higher values of k lead to spring systems more prone to staying activated. Too low stiffness values however fail to properly brake when the spring force is insufficient to hinder the pendulum bob hitting the brake drum. Look for the sudden increase in velocity for $k = 100$ N/mm in figure 35a. The stopping time graph, figure 37, again presents the extreme value at which the brake system stops working properly.

The exact stiffness values that act as separators for behaviour are system dependent and no conclusions can be drawn as to which are the best in general. It is a trade-off between keeping the brake arm activated for high values of k, and slowing down steadily for lower values. The force according to Hooke's law, equation (7), is linearly dependent on the stiffness coefficient and if too large the brake axle will slow down so much that the arm will rotate wildly. This law also implies that the stiffness needed depends on the force with which the pendulum arm swings. Therefore it must be altered for different applications.

Regarding the simulations for a brake sequence with a non-linear spring stiffness applied, a different number of brake force peaks are observed for each type of spring. The linear spring has two peaks while the logarithmic spring has three, shorter in time, and the exponential spring has one, greater in time. It is desired to avoid too much rotation of the brake arm during a braking sequence. This corresponds to having only one brake force peak and therefore the exponential spring seems to be the better choice of design. At the same time, the angular velocity decreases greatly during the brake sequence for this spring and too powerful decelerations are not desirable. As the friction coefficients between the brake drum and brake pad are set quite high in these simulations, this problem can easily be fixed by lowering them.

There are some brake force values with very large magnitudes compared to their neighbouring values. As an example, this is noted in figure 39b. These extreme values most likely arise because of the simulation settings. If simulations with lower step size and integrator tolerance were made, they would be minimised.

When observing the logarithmic and exponential springs with a design comparable to a linear spring, there is no clear relationship between stopping time and the different designs. But when applying exponential springs less similar in design to the linear spring, a relationship is noted. The spring most similar to the linear spring, exponential spring 16, generates a stopping time greater than the rest of the springs and the design least similar to the linear spring, exponential spring 8, has the smallest stopping time.

The designs of the non-linear springs are derived in Adams from a number of data points. The software then takes these points and makes a spline function, obtaining values for the spring stiffness coefficient as a function of deformation of the spring. Because any data points may be entered, there are an endless number of opportunities regarding a non-linear spring's design. To get realistic simulation results, it is important to choose a design that is obtainable in real life.

5.4 Distance Between Brake Drum and Brake Pad

A smaller distance between the brake drum and brake pad gives a shorter reaction time. The slope gets weaker as the distance increases. As the distance approaches zero the reaction time decreases greatly, also approaching zero. This is to be expected as if there is no distance between the brake drum and brake pad there will always be a contact between them.

For the current configurations, the rotated angle of the brake arm needed for contact between the brake pad and brake drum vary greatly. The web tension control model requires a much smaller angle, 2.67 degrees, compared to the universal brake system model, 23.23 degrees, while the value for the emergency brake model lies in between the two. A smaller angle gives a shorter reaction time, which is desired. The required angle depends on the distance between the brake pad and brake drum as well as the design of the brake pad. Changing any of these parameters alters the required angle and therefore also the reaction time.

As mentioned in section 2.3.2, the friction material will exhibit wear and tear over time. This will lead to a larger distance between the brake pad and drum, affecting the function of the brake system. How great this affect will be is currently unknown and further research is to be made if it is of interest.

5.5 Building Sequences

For the torque driven sequence, in figure 46, a lowering of angular velocity is observed when it should keep constant. This is because the gravity and friction losses always lower the velocity. It does look a lot better for the sequence alternating between higher speeds. Perhaps the simulation settings were better or the centre of mass was placed further from the point at which the brake deactivates. Why the brake temporarily deactivates only during the third separate braking sequence within figure 47 may be because the initial conditions going into it differ. It could be that the brake arm was in another position.

By comparing figure 48 and 49, the influence of the pendulum bob's mass centre for the velocity driven model is obtained. When the mass centre is located closer to the zero reference line, the brake arm is activated earlier. Also, it stays activated for a longer period of time. The rotated angle of the brake arm when active is more consistent and the difference in angular velocity between the brake axle and driving mass is smaller compared to a mass centre at a further distance from the zero reference line. This is desirable when looking at an optimal brake sequence. One drawback with a pendulum bob mass centre closer to the zero reference line is the brake arm not deactivating at the desired moment in time.

When trying to find optimal brake sequences different durations were examined. In both simulations from figures 50 and 51 the angular velocity is lowered from 2000 to 1500 RPM. This means a longer duration of the sequence equals a lower magnitude of deceleration. It is most likely the reason for a later activation of the brake arm for the 0.6 seconds long applied deceleration. The location of the pendulum bob's mass centre also affects the activation. The rotated angle of the brake arm has similar behaviour, apart from a later deactivation of the brake arm for the sequence longer in time. As many of the design parameters differ between the two models, it is difficult to make conclusions about which of them should be changed for better results. More thorough testing should be done. The results when testing dependencies should be used as guidelines for appropriate values.

5.6 Other Thoughts

This thesis is the first time any simulations have been made on this brake system. No literature and only a few previously acquired results are available for comparison. Brillianze Sweden AB has made some tests, but never examined as many parameters as in this report.

None of the results were found to disprove the theory and sequence of events assumed by Brillianze Sweden AB. As will be discussed further in section 6 however, there are a lot of parameters in play. We cannot prove that these models always will work as intended because there is no way to test all of the applications and variables. The adage goes that you can never prove a hypothesis, only disprove it. For each implementation of the brake it will be needed to optimise all parameters used.

A larger mass added on the brake axle leads to a higher stopping time. If the mass is too large compared to the weight of the brake axle, deactivation of the brake arm is difficult. An acceleration, much larger than the deceleration needed for activation, must be applied for deactivation. This might be due to the increase in kinetic energy of the system.

Sometimes deactivation is not even possible, especially for the web tension control model. This may not be true for all values of spring stiffness. Maybe a non-linear spring is the solution to this problem. As simulations regarding this were only performed with linear springs, no conclusion about this can be made.

Values for the magnitude of applied force required for activation of the brake arm are difficult to interpret. The magnitude depends on where on the brake axle the force is applied. A measure that would be easier to relate to is the acceleration, expressed in mm/s^2, or even the angular acceleration, expressed in rad/s^2, of the brake axle. Even so, the correlation between the required force and an alternating weight or position of mass centre will be the same, or at least very similar, as the correlation between angular acceleration and an alternating weight or position of mass centre.

Only the brake pad material is made into a flexible body in the models. All other bodies were set as solid as converting them to flexible was deemed unnecessary. This is because the brake pad material is considered to be the body that will deform the most under a few brake sequences. If instead the lifetime of a brake system is to be looked at, wear and tear of the pendulum will be a factor to analyse.

There is always a lowest possible angular velocity that the brake axle may rotate with to avoid activating the brake arm. This can be a big problem for some possible applications of the brake system. The placement of it is originally in the vertical plane. As the problem arises due to gravity, an easy solution is to place the brake system along the horizontal plane. This is most likely not possible for all applications.

During the simulations it was also noticed when zooming in on seemingly constant angular velocities that the gravity still does have a small impact. This presented a problem during setup of the sequence models because misplacing the centre of mass meant that the brake was activated earlier due to nothing but gravity.

During the course of the whole project it was noticed that "the butterfly effect" was in play. Two simulations with almost the same parameters except for one with a very small difference could lead to two completely separate results. This was also noted when doing extended simulations with more than one brake sequence. The result would often differ for each sequence even if they were identical. If the first sequence gave a desired result, the next one would not. The reason for this is at key moments the position of the brake arm could determine activation or not, the step size could overshoot a perturbation and so on.

6 Sources of Error and Limitations

Adams is sometimes not very user-friendly. Several problems were encountered, demanding time and effort to solve. Putting together the longer sequences and getting them to run was periodically very trying. What may have been bugs that appeared during the process of saving the models eventually led to the Adams software crashing after one simulation. No progress could therefore be made. During setup of the sequences, the web tension control model with all of the simulation parameters had to be redone from the CAD files. An unlikely reason may be that the connections between bodies were made incorrectly from the beginning but that does not explain the gradual deterioration of the files. Both sequence models were after that also redone twice or thrice from a functioning web tension control model.

Problems were also encountered doing simulations for the universal brake system model. Adams often aborted the simulations or even shut down entirely. This led to a limited number of results, and also limited accuracy as the step size and integrator tolerance needed to be increased compared to the other models. This may be because the model is in a smaller scale than the others, as the integrator tolerance is unit sensitive. The difference in stopping times for this model as seen in figure 17a is most likely because of the limited accuracy.

The step size determines the precision of simulations. It should be set as small as possible, but smaller step sizes require longer times to run. As there were many simulations required for this project, the step size could not be set too low.

Regarding the integration error tolerances that must be satisfied at each integration step, it works much the same way. For larger values the error will be greater per step in the solution. According to the Adams manual, the GSTIFF integration solver "*monitors the integration errors in the displacement and state variables that the other differential equations [...] define.* [3]

Which values that work for the step size and integrator tolerance therefore depend on each other. Keeping these simulation settings constant while examining parameters, their impact can be disregarded. However, while studying the behaviour of the model, the solution can still vary greatly for different simulation settings due to certain calculations at key moments. This was suggested in the discussion section regarding the butterfly effect. All together, available computational power and available time determines how precise the simulations are.

The process of converting a body from solid to flexible may affect the results. The size of the elements, itself dependent on the number of nodes, what material was used and most of all, the other settings in Adams which we did not understand the importance of, all affect the end result. In the case of the contact forces a similar situation was encountered.

Contact force is defined as the magnitude of the exhibited force between the brake drum and brake pad. In reality, the force slowing down the brake axle is the friction force and the normal force is not of any particular interest. It was proven difficult to get the friction force from Adams and as the contact force is not a big part of the project, efforts doing this were abandoned.

When creating a contact force in Adams several parameters, such as damping and penetration depth, are available. These parameters had preset values which were not altered. We do not know how altering them may affect the results, but as they are preset they hopefully are as realistic as possible.

Each body in Adams is composed of a number of elements. Even if a circular body contains many elements, it will never be completely circular. This is noted when looking at a model's brake drum in Adams. How much it will affect the results is debatable. At most it may generate some extreme value or noise for the brake force. In that case it may be because the calculated displacement of the nodes is dependent on the angle the elements coincide in.

In Adams, simulations are made in vacuum. In reality, variables such as air streams, drag force and terminal velocity may affect the brake system, especially at higher angular velocities. Furthermore, heat will be generated during brake sequences. Thermal expansion of the brake drum may therefore be a factor when choosing its material. The same goes for fatigue but all of these factors are outside the delimitations of the thesis.

Our knowledge of Adams at the start of the project work was limited. A lot of time was spent in Adams doing things that ultimately did not end up in the report. If we had used the software more extensively in the past, creating and modifying the models would not have required nearly as much time.

7 Recommendations and Future Work

How different design parameters are affecting the brake system is examined in a general perspective in this project. Brillianze Sweden AB already has areas of use for its brake system for multiplier reels and is at this moment exploring new implementations and markets for its product. Finding more specific applications and creating more models in Adams is naturally the next step.

Brillianze Sweden AB wanted us to create a model for the universal brake system for multiplier reels where a fishing line pulled the spool, imitating a throw with a fishing rod. We did not know how to implement this and instead simplified it by only using a pulling force. It is recommended to implement desired applications with the help of experts.

Gravity is a problem for lower angular velocities as it leads to unwanted activation of the brake arm. In conjunction with the company, some ideas regarding how to remove the influence of gravity have been discussed. These ideas should be further developed to optimise the brake system, increasing the number of possible applications.

There should be further work with building sequences to get more accurate models and results.

To get better understanding of non-linear springs, further simulations should be done. Additional different types of springs may be researched, but further examination of their behaviour during a whole brake sequence is the most important part.

To help optimising shape and materials of the bodies, forces and deformations should be analysed. This could be done with finite element calculations in a engineering simulation software, such as ANSYS.

References

[1] Brillianze Sweden AB, *Brillianze - Safer motion*
`http://brillianze.com`
retrieved on 2019-05-07

[2] MathWorks, Inc., *MATLAB - MathWorks - MATLAB & Simulink*
`https://se.mathworks.com/products/matlab.html`
retrieved on 2019-05-10

[3] MSC Adams 2017.2 Instruction Manual, *Solver Settings - Dynamics*

[4] MSC Software, *Adams - The Multibody Dynamics Simulation Solution*
`http://www.mscsoftware.com/product/adams`
retrieved on 2019-05-10

[5] Nyberg, Christer, *Mekanik: Stelkroppsdynamik*. 2nd ed. Liber AB Stockholm 2014
`ISBN 978-91-47-11444-3`

[6] Ottosen, Niels Saabye and Petersson, Hans. *Introduction to the Finite Element Method* Prentice-Hall Europe 1992
`ISBN 978-0-13-473877-2`

[7] Rahul Raosaheb Pind, Prof. Swami M. C, *Analysis and Computational Investigation of Brake Disc for Composite Materials*. International Journal of Engineering Development and Research (IJEDR), ISSN:2321-9939, Volume 4, Issue 4, pp.927-946, December 2016
`http://www.ijedr.org/papers/IJEDR1604141.pdf`
retrieved on 2019-01-23

[8] SGL GROUP, *Carbon-Ceramic Brake Disks*
`http://web.archive.org/web/20181014223536/http://www.sglgroup.com:80/cms/international/products/product-groups/cc/carbon-ceramic-brake-disks/index.html?__locale=en`
page archived on 2018-10-14
retrieved on 2019-01-23

[9] Shabana, Ahmed A., *Dynamics of Multibody Systems*. 2nd ed. Cambridge University Press Cambridge 1998
`ISBN 0-521-59446-4`

[10] SVIVLO, *Svivlo - Fish Longer*
`http://svivlo.com/`
retrieved on 2019-05-07

Appendix

A Simulation Data

A.1 Mass Body Dependence

Table A.1.1: Data used for the plot in figure 13

Material	Density (g/cm^3)	Weight (g)	Lowest rotational speed possible without activation (RPM)	Magnitude of deceleration needed for activation (N)
-	5.3881	0.2583	4326.00	-
-	5.9868	0.2870	2850.84	0.164
-	6.4999	0.3116	2395.56	0.260
Cast iron	7.0800	0.3394	2059.02	0.422
-	7.4407	0.3567	1957.62	0.497
Steel	7.8010	0.3740	1843.14	0.573
Brass	8.5450	0.4096	1695.54	0.679
Copper	8.9060	0.4269	1632.42	0.736
-	9.4078	0.4510	1576.62	0.791
-	10.0065	0.4797	1505.10	0.853
-	10.6052	0.5084	1455.24	0.902
-	11.1183	0.5330	1413.60	0.936
Lead	11.3700	0.5451	1398.84	0.958
-	12.0000	0.5753	1363.14	0.996
-	13.0000	0.6232	1320.66	1.043
-	14.0000	0.6711	1277.64	1.080
-	15.0000	0.7191	1248.48	1.116
-	16.0000	0.7670	1211.70	1.144
-	17.0000	0.8150	1196.88	1.183
-	18.0000	0.8629	1182.30	1.197
Tungsten	19.2220	0.9215	1160.52	1.215
-	20.0000	0.9588	1154.16	1.236
-	21.0000	1.0067	1138.44	1.256

Table A.1.2: Data used for the plot in figure 19

Material	Density (g/cm^3)	Weight (g)	Lowest rotational speed possible without activation (RPM)	Magnitude of deceleration needed for activation (N)
Magnesium	1.7950	20.988	1281.630	12100
-	2.0526	24.000	1233.018	13300
-	2.3947	28.000	1181.136	14700
Aluminium	2.7400	32.037	1142.190	16000
-	3.1644	37.000	1104.816	17300
-	3.7631	44.000	1064.100	18400
-	4.2763	50.000	1063.440	19500
Titanium	4.8500	56.709	1013.556	20300
-	5.3881	63.000	997.152	21100
-	5.9868	70.000	980.886	21900
-	6.4999	76.000	969.186	22500
Cast iron	7.0800	82.783	957.618	23000
-	7.4407	87.000	952.608	23400
Steel	7.8010	91.213	945.984	23600
Brass	8.5450	99.912	936.930	24000
Copper	8.9060	104.133	932.568	24300
-	9.4078	110.000	925.884	24700
-	10.0065	117.001	920.772	25100
-	10.6052	124.001	915.660	25400
-	11.1183	130.000	912.198	25700
Lead	11.3700	132.943	910.470	25900
-	11.9736	140.001	905.358	26300

Table A.1.3: Data used for the plot in figure 20

The mass centre's distance from the zero reference line, negative direction (mm)	Lowest rotational speed possible without activation (RPM)	Magnitude of deceleration needed for activation (N)
0.1	3545.988	-
0.2	2426.808	2800
0.3	1956.648	5200
0.4	1684.548	7500
0.5	1501.008	9750
0.6	1347.774	11900
0.7	1260.828	14000
0.8	1177.416	16000
0.9	1109.808	17800
1.0	1045.410	19700
1.2	956.886	23200
1.25	936.930	24000
1.4	882.840	26400
1.6	824.892	29400
1.8	775.020	32200
2.0	736.386	34800
2.4	668.796	39600
2.8	620.538	44000
3.2	580.320	47900
3.6	546.534	51300
4.0	515.940	54500

Table A.1.4: Data used for the plot in figure 27

Material	Density (g/cm^3)	Weight (g)	Lowest rotational speed possible without activation (RPM)	Magnitude of deceleration needed for activation (N)
Magnesium	1.7950	18.158	1234.062	10600
-	2.0526	20.763	1211.250	11000
-	2.3947	24.251	1185.156	11450
Aluminium	2.7400	27.717	1163.922	11850
-	3.1644	32.010	1142.652	12250
-	3.7631	38.066	1116.438	12700
-	4.2763	43.257	1099.986	13050
Titanium	4.8500	49.061	1083.516	13400
-	5.3881	54.504	1071.912	13600
-	5.9868	60.560	1060.284	13850
-	6.4999	65.750	1051.938	14050
Cast iron	7.0800	71.619	1045.176	14250
-	7.4407	75.267	1040.142	14350
Steel	7.8010	78.912	1036.728	14450
Brass	8.5450	86.438	1029.888	14600
Copper	8.9060	90.090	1024.860	14800
-	9.4078	95.166	1021.380	14900
-	10.0065	101.222	1016.232	15050
-	10.6052	107.278	1012.704	15200
-	11.1183	112.468	1009.224	15300
Lead	11.3700	115.014	1009.098	15400
-	11.9736	121.120	1003,956	15550

Table A.1.5: Data used for the plot in figure 28

The mass centre's distance from the zero reference line, negative direction (mm)	Lowest rotational speed possible without activation (RPM)	Magnitude of deceleration needed for activation (N)
0.1	2423.940	1700
0.2	1994.856	3500
0.3	1717.206	5200
0.4	1533.264	6800
0.5	1399.344	8300
0.6	1292.862	9700
0.7	1207.350	11100
0.8	1139.592	12300
0.9	1079.898	13500
1.0	1029.888	14600
1.1	983.100	15700
1.2	944.388	16700
1.25	926.640	17100
1.4	878.244	18500
1.6	823.392	20200
1.8	779.868	21700
2.0	741.144	23000
2.4	678.258	25400
2.8	631.500	27600
3.2	597.654	29600
3.6	567.024	31200
4.0	542.838	32500

A.2 Friction Coefficient Dependence

Regarding the first two rows in table A.2.3: Due to the settings of the simulation, specifically the deceleration and end time, no stopping time was obtained for $\mu_d = 0$. It was decided to skip the next row due to lack of application for the behaviour.

Table A.2.1: Friction coefficient results, universal brake system for multipliers reels.

μ_s	μ_d	reaction time (s)	swing out time (s)	stopping time (s)
0.3	0	0.351	0.3314	0.5793
0.3	0.05	0.351	0.3314	0.5232
0.3	0.1	0.351	0.3314	0.5097
0.3	0.125	0.351	0.3314	0.5086
0.3	0.15	0.351	0.3314	0.5117
0.3	0.175	0.351	0.3314	0.5095
0.3	0.2	0.351	0.3314	0.5011
0.3	0.225	0.351	0.3314	0.5034
0.3	0.25	0.351	0.3314	0.4979
0.3	0.275	0.351	0.3314	0.4961
0.3	0.3	0.351	0.3314	0.5086
0.325	0.325	0.351	0.3314	0.4902
0.35	0.35	0.351	0.3314	0.4951
0.375	0.375	0.351	0.3314	0.4912
0.4	0.1	0.351	0.3314	0.5073
0.4	0.125	0.351	0.3314	0.5084
0.4	0.15	0.351	0.3314	0.5117
0.4	0.175	0.351	0.3314	0.5095
0.4	0.2	0.351	0.3314	0.5011
0.4	0.225	0.351	0.3314	0.5004
0.4	0.25	0.351	0.3314	0.4975
0.4	0.275	0.351	0.3314	0.496
0.4	0.3	0.351	0.3314	0.5086
0.4	0.325	0.351	0.3314	0.49
0.4	0.35	0.351	0.3314	0.4951
0.4	0.375	0.351	0.3314	0.4912
0.4	0.4	0.351	0.3314	0.5059
0.425	0.125	0.351	0.3314	0.5084
0.425	0.425	0.351	0.3314	0.506
0.45	0.15	0.351	0.3314	0.5117
0.45	0.45	0.351	0.3314	0.5102
0.475	0.175	0.351	0.3314	0.5095
0.475	0.475	0.351	0.3314	0.4861
0.5	0.2	0.351	0.3314	0.5011
0.5	0.225	0.351	0.3314	0.4997
0.5	0.25	0.351	0.3314	0.4972
0.5	0.275	0.351	0.3314	0.4958
0.5	0.3	0.351	0.3314	0.5086
0.5	0.325	0.351	0.3314	0.4899
0.5	0.35	0.351	0.3314	0.495
0.5	0.375	0.351	0.3314	0.4912
0.5	0.4	0.351	0.3314	0.5057
0.5	0.425	0.351	0.3314	0.5058
0.5	0.45	0.351	0.3314	0.5102
0.5	0.475	0.351	0.3314	0.486
0.5	0.5	0.351	0.3314	0.496

μ_s	μ_d	reaction time (s)	swing out time (s)	stopping time (s)
0.525	0.225	0.351	0.3314	0.4996
0.525	0.525	0.351	0.3314	0.4988
0.55	0.25	0.351	0.3314	0.4971
0.55	0.55	0.351	0.3314	0.4823
0.575	0.275	0.351	0.3314	0.4957
0.575	0.575	0.351	0.3314	0.4954
0.6	0.3	0.351	0.3314	0.5086
0.6	0.325	0.351	0.3314	0.4898
0.6	0.35	0.351	0.3314	0.495
0.6	0.375	0.351	0.3314	0.4912
0.6	0.4	0.351	0.3314	0.5053
0.6	0.5	0.351	0.3314	0.4959
0.6	0.6	0.351	0.3314	0.4929
0.7	0.4	0.351	0.3314	0.505
0.7	0.5	0.351	0.3314	0.4958
0.7	0.6	0.351	0.3314	0.4928
0.7	0.7	0.351	0.3314	0.4881

Table A.2.2: Friction coefficient results, emergency brake for winch.

μ_s	μ_d	reaction time (s)	swing out time (s)	stopping time (s)
0.3	0	0.3484	0.3151	0.5638
0.3	0.05	0.3484	0.3151	0.5109
0.3	0.1	0.3484	0.3151	0.4677
0.3	0.125	0.3484	0.3151	0.4571
0.3	0.15	0.3484	0.3151	0.461
0.3	0.175	0.3484	0.3151	0.4524
0.3	0.2	0.3484	0.3151	0.4431
0.3	0.225	0.3484	0.3151	0.4319
0.3	0.25	0.3484	0.3151	0.4299
0.3	0.275	0.3484	0.3151	0.427
0.3	0.3	0.3484	0.3151	0.4244
0.325	0.325	0.3484	0.3151	0.414
0.35	0.35	0.3484	0.3151	0.4081
0.375	0.375	0.3484	0.3151	0.4054
0.4	0.1	0.3484	0.3151	0.4668
0.4	0.125	0.3484	0.3151	0.4571
0.4	0.15	0.3484	0.3151	0.4608
0.4	0.175	0.3484	0.3151	0.4524
0.4	0.2	0.3484	0.3151	0.4424
0.4	0.225	0.3484	0.3151	0.4319
0.4	0.25	0.3484	0.3151	0.43
0.4	0.275	0.3484	0.3151	0.427
0.4	0.3	0.3484	0.3151	0.4244
0.4	0.325	0.3484	0.3151	0.414
0.4	0.35	0.3484	0.3151	0.4078
0.4	0.375	0.3484	0.3151	0.4053
0.4	0.4	0.3484	0.3151	0.4017
0.425	0.125	0.3484	0.3151	0.4571
0.425	0.425	0.3484	0.3151	0.3992
0.45	0.15	0.3484	0.3151	0.4607
0.45	0.45	0.3484	0.3151	0.3983

μ_s	μ_d	reaction time (s)	swing out time (s)	stopping time (s)
0.475	0.175	0.3484	0.3151	0.4524
0.475	0.475	0.3484	0.3151	0.3951
0.5	0.2	0.3484	0.3151	0.4419
0.5	0.225	0.3484	0.3151	0.4319
0.5	0.25	0.3484	0.3151	0.4299
0.5	0.275	0.3484	0.3151	0.427
0.5	0.3	0.3484	0.3151	0.4244
0.5	0.325	0.3484	0.3151	0.414
0.5	0.35	0.3484	0.3151	0.4072
0.5	0.375	0.3484	0.3151	0.405
0.5	0.4	0.3484	0.3151	0.401
0.5	0.425	0.3484	0.3151	0.3993
0.5	0.45	0.3484	0.3151	0.3983
0.5	0.475	0.3484	0.3151	0.395
0.5	0.5	0.3484	0.3151	0.3945
0.525	0.225	0.3484	0.3151	0.4319
0.525	0.525	0.3484	0.3151	0.3942
0.55	0.25	0.3484	0.3151	0.4299
0.55	0.55	0.3484	0.3151	0.395
0.575	0.275	0.3484	0.3151	0.427
0.575	0.575	0.3484	0.3151	0.3939
0.6	0.3	0.3484	0.3151	0.4244
0.6	0.325	0.3484	0.3151	0.414
0.6	0.35	0.3484	0.3151	0.4065
0.6	0.375	0.3484	0.3151	0.4046
0.6	0.4	0.3484	0.3151	0.4003
0.6	0.5	0.3484	0.3151	0.3944
0.6	0.6	0.3484	0.3151	0.3931
0.7	0.4	0.3484	0.3151	0.3996
0.7	0.5	0.3484	0.3151	0.3944
0.7	0.6	0.3484	0.3151	0.3931
0.7	0.7	0.3484	0.3151	0.3939

Table A.2.3: Friction coefficient results, web tension control for spools.

μ_s	μ_d	reaction time (s)	swing out time (s)	stopping time (s)
0.3	0	0.3723	0.34	-
0.3	0.05			
0.3	0.1	0.3723	0.34	0.5525
0.3	0.125	0.3723	0.34	0.5492
0.3	0.15	0.3723	0.34	0.5444
0.3	0.175	0.3723	0.34	0.5411
0.3	0.2	0.3723	0.34	0.5368
0.3	0.225	0.3723	0.34	0.5365
0.3	0.25	0.3723	0.34	0.5351
0.3	0.275	0.3723	0.34	0.5318
0.3	0.3	0.3723	0.34	0.5282
0.325	0.325	0.3723	0.34	0.5262
0.35	0.35	0.3723	0.34	0.5233
0.375	0.375	0.3723	0.34	0.522
0.4	0.1	0.3723	0.34	0.5519
0.4	0.125	0.3723	0.34	0.5491

μ_s	μ_d	reaction time (s)	swing out time (s)	stopping time (s)
0.4	0.15	0.3723	0.34	0.5441
0.4	0.175	0.3723	0.34	0.5409
0.4	0.2	0.3723	0.34	0.5363
0.4	0.225	0.3723	0.34	0.5363
0.4	0.25	0.3723	0.34	0.5351
0.4	0.275	0.3723	0.34	0.5318
0.4	0.3	0.3723	0.34	0.5277
0.4	0.325	0.3723	0.34	0.5262
0.4	0.35	0.3723	0.34	0.5233
0.4	0.375	0.3723	0.34	0.522
0.4	0.4	0.3723	0.34	0.5243
0.425	0.125	0.3723	0.34	0.5491
0.425	0.425	0.3723	0.34	0.522
0.45	0.15	0.3723	0.34	0.5439
0.45	0.45	0.3723	0.34	0.5229
0.475	0.175	0.3723	0.34	0.5408
0.475	0.475	0.3723	0.34	0.5134
0.5	0.2	0.3723	0.34	0.5359
0.5	0.225	0.3723	0.34	0.5361
0.5	0.25	0.3723	0.34	0.5351
0.5	0.275	0.3723	0.34	0.5318
0.5	0.3	0.3723	0.34	0.5273
0.5	0.325	0.3723	0.34	0.5262
0.5	0.35	0.3723	0.34	0.5232
0.5	0.375	0.3723	0.34	0.5219
0.5	0.4	0.3723	0.34	0.5241
0.5	0.425	0.3723	0.34	0.5219
0.5	0.45	0.3723	0.34	0.5229
0.5	0.475	0.3723	0.34	0.5133
0.5	0.5	0.3723	0.34	0.5091
0.525	0.225	0.3723	0.34	0.536
0.525	0.525	0.3723	0.34	0.5105
0.55	0.25	0.3723	0.34	0.5351
0.55	0.55	0.3723	0.34	0.5113
0.575	0.275	0.3723	0.34	0.5318
0.575	0.575	0.3723	0.34	0.5051
0.6	0.3	0.3723	0.34	0.5271
0.6	0.325	0.3723	0.34	0.5262
0.6	0.35	0.3723	0.34	0.5232
0.6	0.375	0.3723	0.34	0.5218
0.6	0.4	0.3723	0.34	0.5239
0.6	0.5	0.3723	0.34	0.5087
0.6	0.6	0.3723	0.34	0.5039
0.7	0.4	0.3723	0.34	0.5238
0.7	0.5	0.3723	0.34	0.5084
0.7	0.6	0.3723	0.34	0.5037
0.7	0.7	0.3723	0.34	0.4999

A.3 Spring Stiffness Dependence

Table A.3.1: Linear stiffness coefficient results.

k	reaction time (s)	swing out time (s)	stopping time (s)
0	0.212	0.2908	0.4703
50	0.3741	0.3391	0.5061
100	0.3734	0.3385	0.5216
130	0.3729	0.3403	0.4646
135	0.3728	0.3405	0.4287
140	0.3728	0.3407	0.4203
150	0.3724	0.3395	0.4411
160	0.3728	0.3403	0.4556
170	0.3723	0.3398	0.4713
180	0.3723	0.3399	0.4815
190	0.3723	0.3402	0.4874
200	0.3723	0.3401	0.4876
250	0.3723	0.34	0.5033
300	0.3723	0.34	0.5105
350	0.3723	0.34	0.5169
400	0.3723	0.34	0.524
450	0.3723	0.34	0.5289
500	0.3723	0.34	0.5282
750	0.3723	0.34	0.5331
1000	0.3722	0.34	0.5362
2000	0.3722	0.34	0.5309
2100	0.3722	0.34	0.5313
2200	0.3722	0.34	0.5309
2300	0.3722	0.34	0.5299
2400	0.3722	0.34	0.5305
2500	0.3722	0.34	0.5302
2600	0.3722	0.34	0.5315
2700	0.3722	0.34	0.5302
2800	0.3722	0.34	0.5306
2900	0.3722	0.34	0.5289
3000	0.3722	0.34	0.5297
4000	0.3722	0.34	0.5293
5000	0.3723	0.34	0.5318
6000	0.3723	0.34	0.5307
7000	0.3723	0.34	0.5319

Table A.3.2: Formula for the non-linear springs from subsection 4.3.4. For the formula: y=force applied to the spring (N), x=deformation of spring (mm).

Name	Formula	Figure number
Logarithmic spring	y=560·log(x+1)	40a
Logarithmic spring 1	y=1050·log(x+1)	42a
Logarithmic spring 2	y=1060·log(x+1)	42a
Logarithmic spring 3	y=1070·log(x+1)	42a
Logarithmic spring 4	y=1080·log(x+1)	42a
Logarithmic spring 5	y=1090·log(x+1)	42a
Logarithmic spring 6	y=1100·log(x+1)	42a
Logarithmic spring 7	y=1110·log(x+1)	42a
Exponential spring	y=395.2·(exp(x)-1)	41a
Exponential spring 1	y=950·(exp(x)-1)	43a
Exponential spring 2	y=940·(exp(x)-1)	43a
Exponential spring 3	y=930·(exp(x)-1)	43a
Exponential spring 4	y=920·(exp(x)-1)	43a
Exponential spring 5	y=910·(exp(x)-1)	43a
Exponential spring 6	y=900·(exp(x)-1)	43a
Exponential spring 7	y=890·(exp(x)-1)	43a
Exponential spring 8	y=100·((exp(x).^6.8)-1)	44a
Exponential spring 9	y=100·((exp(x).^6.6)-1)	44a
Exponential spring 10	y=100·((exp(x).^6.4)-1)	44a
Exponential spring 11	y=100·((exp(x).^6.2)-1)	44a
Exponential spring 12	y=100·((exp(x).^6.0)-1)	44a
Exponential spring 13	y=100·((exp(x).^5.8)-1)	44a
Exponential spring 14	y=100·((exp(x).^5.6)-1)	44a
Exponential spring 15	y=100·((exp(x).^5.4)-1)	44a
Exponential spring 16	y=100·((exp(x).^5.2)-1)	44a

Table A.3.3: Data used for figures 42b, 43b and 44b. Swing out time and stopping time are not included in the figures.

Name	Reaction time (s)	Swing out time (s)	Stopping time (s)
Linear spring, K=400 (N/mm)	0.3722	0.3400	0.5362
Logarithmic spring 1	0.3722	0.3400	0.5357
Logarithmic spring 2	0.3722	0.3400	0.5364
Logarithmic spring 3	0.3722	0.3400	0.5346
Logarithmic spring 4	0.3722	0.3400	0.5352
Logarithmic spring 5	0.3722	0.3400	0.5355
Logarithmic spring 6	0.3722	0.3400	0.5338
Logarithmic spring 7	0.3722	0.3400	0.5349
Exponential spring 1	0.3722	0.3400	0.5349
Exponential spring 2	0.3722	0.3400	0.5346
Exponential spring 3	0.3722	0.3400	0.5354
Exponential spring 4	0.3722	0.3400	0.5354
Exponential spring 5	0.3722	0.3400	0.5355
Exponential spring 6	0.3722	0.3400	0.5344
Exponential spring 7	0.3722	0.3400	0.5340
Exponential spring 8	0.3723	0.3400	0.5123
Exponential spring 9	0.3723	0.3400	0.5147
Exponential spring 10	0.3723	0.3400	0.5171
Exponential spring 11	0.3723	0.3400	0.5198
Exponential spring 12	0.3723	0.3400	0.5220
Exponential spring 13	0.3723	0.3400	0.5226
Exponential spring 14	0.3723	0.3400	0.5268
Exponential spring 15	0.3723	0.3400	0.5278
Exponential spring 16	0.3723	0.3400	0.5308

A.4 Distance Between Brake Drum and Brake Pad

The reason for why the reaction time is not zero for a negative distance (itself near-zero) in table A.4.1 is that the software needs to process a step to get results.

Table A.4.1: Measurements on the distance between brake drum and pad.

distance (mm)	max contact force (N)	reaction time (s)
$-2.10942 \cdot 10^{-15}$	3687.2546	$2.00 \cdot 10^{-4}$
0.05476375	8031.5906	0.0404
0.15476375	7792.7387	0.0434
0.20476375	10682.8876	0.0439
0.25476375	13690.7029	0.0445
0.30476375	9736.0008	0.0448
0.35476375	8893.3345	0.0453
0.45476375	8906.4881	0.0457
0.55476375	9138.8627	0.0461
0.65476375	8867.1198	0.0465
0.75476375	8722.9204	0.0468
0.85476375	11415.115	0.047